Replacing the Monte Carlo Simulation with the COS Method for PFE (Potential Future Exposure) Calculations

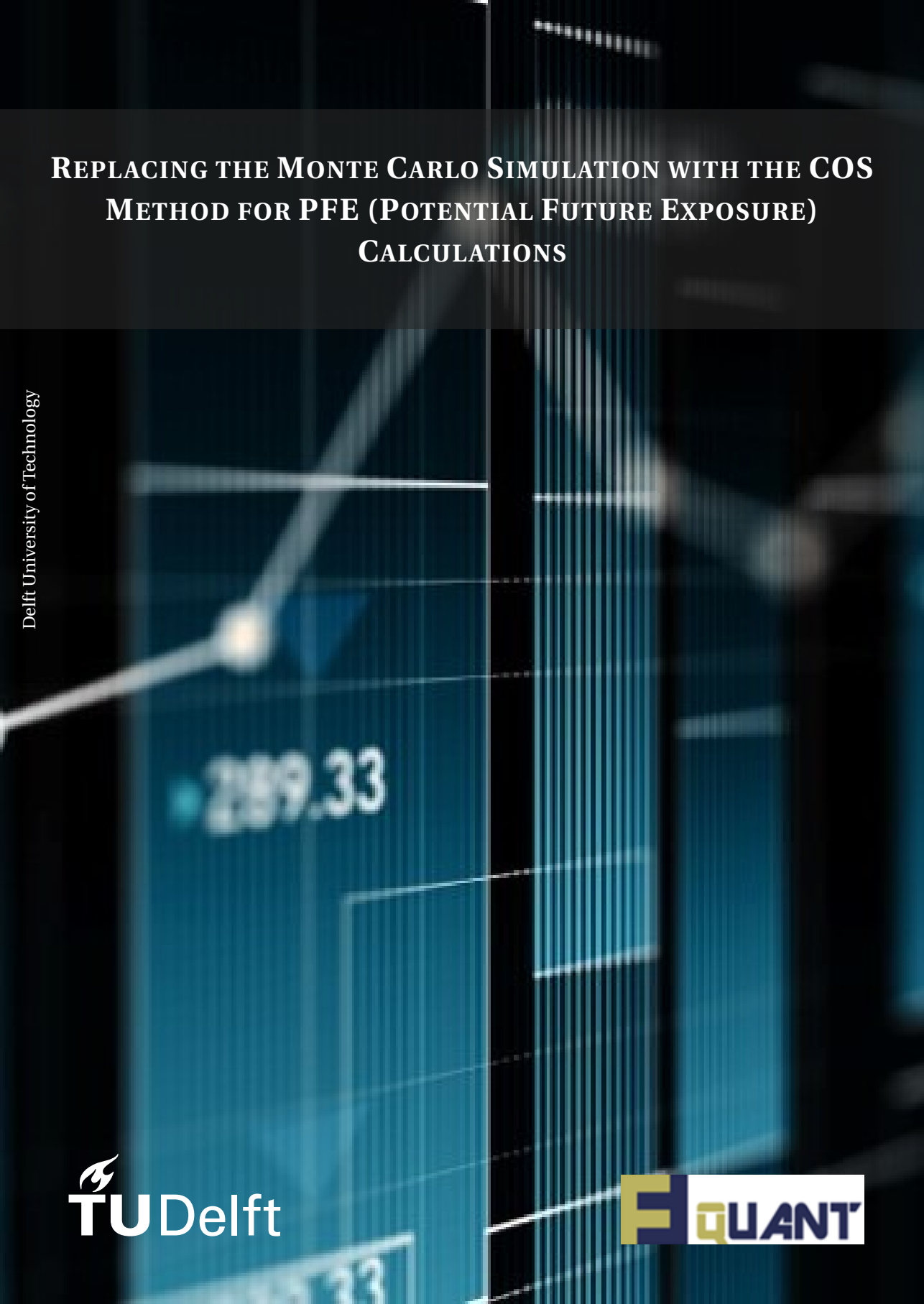

Delft University of Technology

TU Delft

FQUANT

REPLACING THE MONTE CARLO SIMULATION WITH THE COS METHOD FOR PFE (POTENTIAL FUTURE EXPOSURE) CALCULATIONS

by

Gijs MAST

to obtain the degree of Master of Science
at the Delft University of Technology,
to be defended publicly on Sep 20, 2022

Student number:	4693655	
Project duration:	Jan 17, 2022 - Sep 20, 2022	
Thesis committee:	Dr. F. Fang,	TU Delft, supervisor
	Prof.Dr.ir. C. Vuik,	TU Delft
	Prof.Dr. A. Papapantoleon,	TU Delft
	Dr. X. Shen,	FFQuant, supervisor

ABSTRACT

To fulfill the need in the industry for fast and accurate PFE calculations in practice, a new, semi-analytical method of calculating the PFE metric for CCR has been developed, tested and analyzed in this thesis. Herewith we focus on the calculation of PFEs for liquid IR and FX portfolios involving up to three correlated risk-factors: a domestic and foreign short rate and the exchange rate of this currency pair. Both netting-set level and counterparty level PFEs are covered in our research. The short rates are modelled under the one-factor Hull–White (HW1F) model and for the exchange rate we assume they follow geometric Brownian motion. The key insight is that the cumulative distribution function (CDF) can be recovered semi-analytically using Fourier-cosine expansion, whereby the series coefficients are readily available from the characteristic function of the total exposure. The characteristic function in turn can be solved numerically via quadrature rules. Risk metrics, such as the potential future exposure (PFE), can be attained once the CDF is reconstructed using the Fourier series.

Our theoretical error analysis predicts stable convergence of the COS method and observed exponential convergence of the COS method for both netting-set and counterparty level PFE calculations. For three artificial portfolios of different sizes, it was observed that the COS method is at least five times more accurate than the Monte Carlo (MC) simulation method but takes only one-tenth of the CPU time of the MC method. The advantage of the COS method becomes even more prominent when the number of derivatives in a portfolio increases. We conclude that the COS method is a much more efficient alternative for MC method for PFE calculations, at least for portfolios involving three risk factors.

Key words. counterparty credit risk, potential future exposure, Hull–White model, geometric Brownian motion model, Monte Carlo simulation, COS Method, spectral filter

CONTENTS

List of Abbreviations

Abbreviations

CCR counterparty credit risk.

CDF cumulative distribution function.

ch.f. characteristic function.

EE expected exposure.

EPE expected positive exposure.

FDMC finite difference Monte-Carlo.

FRA forward-rate agreement.

GBM geometric Brownian motion.

IRS interest rate swap.

LSMC least squares Monte-Carlo.

MCCOS Monte-Carlo COS.

MtM mark-to-market.

OTC over-the-counter.

PFE potential future exposure.

ppf per cent point function.

RFS receiver IRS.

SGBM stochastic grid bundling method.

VaR value-at-risk.

XCS cross-currency swap.

ZCB zero-coupon bond.

NOMENCLATURE

$(S_t)_{t\geq 0}$ stochastic càdlàg process adapted to filtration $(\mathscr{F}_t)_{t\geq 0}$.

$B(t)$ money-market account at time $t \geq 0$.

$C^2(\mathbb{R})$ vector space of twice differentiable functions in $\mathbb{R}$.

$G1{+}{+}$ Gaussian one-factor model.

H attainable contingent claim.

$HW1F$ Hull–White one-factor model.

L^2 vector space of square-integrable functions.

V_t value process associated with a strategy ϕ.

$W(t)$ Brownian motion.

$[S]$ the quadratic variation of S with itself also written as $[S,S]$.

Ω set of all possible events.

$\mathbb{P}$ real-world probability measure on $(\Omega, \mathscr{F})$.

$\mathbb{Q}$ risk-neutral probability measure on $(\Omega, \mathscr{F})$.

$\mathbb{Q}^d$ the domestic risk-neutral measure.

$\mathbb{Q}^f$ foreign risk-neutral measure.

$\mathscr{F}$ σ-algebra of events.

$\mathscr{M}_{loc}$ set of processes that are local martingales.

v set of processes with finite variation.

ϕ a trading strategy.

$\phi(\omega)$ characteristic function.

π_t unique price associated with a contingent claim H.

$x_d(t)$ domestic shifted short rate.

$x_f(t)$ foreign shifted short rate.

List of Figures

LIST OF TABLES

1

INTRODUCTION

The 2007 financial crisis saw banks topple and set the financial world in turmoil. Another name for this series of events is the credit crisis. The name reflects the nature of the problem that led to the economic collapse. The main problem was the counterparty credit risk (CCR), which is the loss in the to exposure with a counterparty that fails to meet its financial obligations. This risk was not new, as it was also a factor in the Asian crisis (1997), the default of Russia (1998) and the collapse of LTCM (1998, was saved). Past crises have led to the formation of the Basel Committee on Banking Supervision (BCBS), which set up capital regulations for banks to stay solvent in case of extreme adverse scenarios. However, the 2007 credit crisis made it unmistakably clear that in order to restrict excessive risk taking in the over-the-counter (OTC) derivatives market, banks needed to be subject to stricter regulations.

Interest rate derivatives make up the largest portion of the traded OTC derivatives in the financial market. According to International Swaps and Derivatives Association (ISDA), interest rate derivatives made up 80% of the total OTC notional in 2020. One-tenth of these, amounting to 46 trillion dollars, were under-collateralised [1]. The quantification of CCR is the important first step for properly managing CCR in these derivatives.

Mathematically, exposure in a trade is defined as

$$E_t(X_t) = \max\{V_t(X_t), 0\},$$

where $\mathbf{X}_t$ is the risk factor, and V_t is the mark-to-market (MtM) price of a portfolio at time t. In other words, the calculation of the exposure essentially projects the current exposure of the underlying assets into the future [2]. Because the risk factors are unknown for future time points, we need to assume appropriate stochastic models for the market variables which then lead to an exposure distribution.

The potential future exposure (PFE) is a measure that quantifies and limits the CCR in banks. It can be regarded as the worst loss over a time horizon to a certain confidence level. It is usually considered at the counterparty level and netting-set level. Note that

netting can reduce the market exposure by up to 93% [3]. An example of the PFE is shown in Figure 1.1.

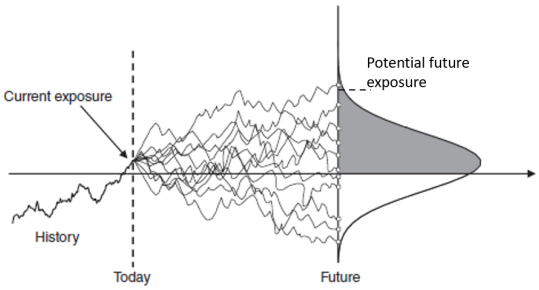

Figure 1.1: Illustration of the potential future exposure defined as a quantile of the future distribution. The grey area represents the exposure. (Source: [4])

Monte Carlo simulation is the industry-standard numerical method to simulate the risk factors according to chosen stochastic models. In a backward sweep, the generated paths are fed to the pricers to yield the MtM values of a portfolio at that future time point. By flooring all simulated MtM values by zero, one yields a distribution for the exposure of the portfolio at a future time point. Afterwards, risk measures like PFE can be calculated easily.

One can find various ways to calculate future exposures in the literature. For exotic derivatives, the most straightforward and robust method is the nested Monte Carlo (MC) method, which simulates paths using MC and another nested MC simulation is used to price the derivative for each scenario. However, due to the low convergence rate of MC, a large number of simulations is needed to acquire a high level of accuracy, making the method very time consuming.

An alternative method is the finite difference Monte-Carlo (FDMC) method proposed by Tavella [5]. This method solves the option pricing PDE given by the Feynman–Kac theorem on a chosen grid for different time points. It is accurate and can price multiple options on one grid; however, it becomes infeasible for products using more than three risk factors [6]–[8].

Furthermore, regression-based modelling techniques are popular in practice like the least squares Monte-Carlo (LSMC) [9]. The method is useful when pricing path-dependent structures like lookback or Asian options. However, the technique has high computation costs, performance in the tail of the distribution is poor, and calibration is difficult [10], [11]. The stochastic grid bundling method (SGBM) is a similar regression-based modelling technique that decreases the noise in the tail distribution [7]. The technique proposed by Oosterlee clusters paths in bundles based on their stock and variance values [12]. The bundles are assumed to have similar properties, like coefficients. Nevertheless, this method shows slower convergence results than the LSMC [13], [14].

Chebyshev polynomial interpolation is a recent promising method to calculate the PFE proposed by Glau in [15]. It approximates the option prices using basis functions on Chebyshev grid points. This method is shown to outperform the LSMC method on

accuracy and runtime [2].

Another technique involving MC path discretisation is the Monte-Carlo COS (MCCOS) method [16]. The exposure is calculated using a Fourier-cosine transform method proposed by Fang and Oosterlee in [17]. The method shows high accuracy at the cost of lower computational speed [7].

This paper proposes a potential replacement of the MC methods which is much faster and more accurate and is based on the COS method. The COS method, short name for Fourier-cosine series based method, is in essence a highly efficient method to calculate the expectation of a function defined on random variables. It was first proposed by Fang and Oosterlee for pricing options. Here in our context, instead of applying the COS method to price options for each path like the MCCOS method, the aim is to directly calculate the PFE from the cumulative distribution function (CDF). The key insight we have is that the CDF can be recovered by applying the COS method using the characteristic function solved numerically.

The next chapter covers the mathematical descriptions of the models and numerical methods used. Using the mathematical foundation, Chapter 3 explains how to obtain the PFE for portfolios involving up to three risk factors. The convergence rate of the COS method is analyzed theoretically in Chapter 4. Chapter 5 elaborates on numerical tests and analysis on the convergence rate. In addition, Chapter 5 also compares the performance of the MC simulation and the COS method for both individual trades and different netting sets.

2

MATHEMATICAL FRAMEWORK

In this chapter, we give the mathematical definition of the problem-to-solve and the notations, and prepare the mathematical toolkits needed for he quantification of CCR.

2.1. EXPOSURE QUANTIFICATION

In this section, the quantification measures used in the rest of the thesis are discussed in more detail, based on [4], [18]. To start, the definition of the exposure given in the introduction is repeated below.

Definition 2.1.1 (Exposure)**.** *The (positive) exposure, E(t), can be defined on three levels. First, we have contract-level exposure, which is defined as*

$$E_t(X_t) := \max\{V_t(X_t), 0\}, \tag{2.1}$$

where X_t is the risk factor and $V_t(X_t)$ represents the MtM value or price of a derivative contract at time t. Second, there is netting-set level exposure, which is the exposure of netting sets, the net value of multiple homogeneous contracts. The netted exposure is given by

$$E_n(t) = \max\{V_t(t) + V_2(t), 0\}. \tag{2.2}$$

Lastly, there is Counterparty-level exposure, which involves all traded derivatives with a certain counterparty. This gives

$$E_c(t) = \max\{V_1(t), 0\} + \max\{V_2(t), 0\} =: E_1(t) + E_2(t). \tag{2.3}$$

A netting set is defined in the next definition.

Definition 2.1.2 (Netting set)**.** *A netting set is a group of transactions with a single counterparty that are subject to a legally enforceable bilateral netting arrangement, which allows the offsetting of all transaction values.*

The value of a risk factor, such as interest rate or FX rate, is not known before hand, and thus, is a random variable and can be assumed to follow a certain distribution. Therefore, the exposure at any future time instance is also a random variable and follows its own distribution. A few measures are used in industry to quantify CCR, which include expected exposure (EE), potential future exposure PFE, expected positive exposure (EPE), etc.

Definition 2.1.3 (Expected exposure)**.** *Given the exposure profiles, $E_t(X_t)$, we wish to calculate the expected (positive) exposure EE at time t, which is defined as follows:*

$$\mathrm{EE}_t(X_t) = \mathbb{E}^{\mathbb{Q}}[E_t(X_t)], \quad 0 \le t \le T. \tag{2.4}$$

PFE, on the other hand, is is essence value-at-risk (VaR) metric on the distribution of the exposure. The mathematical definition is given as,

Definition 2.1.4 (Potential future exposure)**.** *The potential future exposure (PFE) at time t, as seen from time zero, is defined as*

$$\mathrm{PFE}_{\alpha,t} = \inf\{x : \mathbb{P}(E_t \le x) \ge \alpha\}, \quad 0 \le t \le T, \tag{2.5}$$

where α is the given confidence level, and $\mathbb{P}$ is the real-world measure.

If the risk factors were modelled with a deterministic function, the (future) exposure could be acquired by simply solving the equation analytically. However, as mentioned before, the risk factor at a future time point is not known beforehand. Hence, the risk factors involved in valuing interest rate derivatives, that is, the short rates, should be modeled with a level of uncertainty. The short rate is defined below.

Definition 2.1.5. *The short rate, or instantaneous spot rate, is defined as the instantaneous rate at which the bank account accrues. That is,*

$$r(t) = \lim_{T \to t^+} L(t,T), \tag{2.6}$$

where $L(t,T)$ is the simply-compounded spot interest rate as defined in definition 2.4.3.

A formal definition of the bank account is given in definition 2.4.1.

The next section is devoted to the mathematical definitions needed to understand the stochastic modelling framework, followed by the derivative pricing theory.

2.2. STOCHASTIC CALCULUS DEFINITIONS AND NOTATION

The definitions and notation used in the field of stochastic calculus are adapted from the books [18]–[20] by Morters and Peres, Le Gall and Oosterlee and Grzelach, respectively. These definitions are needed or the derivation of the derivative pricing theory in Section 2.3.

We consider a probability space $(\Omega, \mathscr{F}, \mathbb{P})$ where Ω is the sample space, $\mathscr{F}$ is the event space, and $\mathbb{P}$ is the probability measure.

Definition 2.2.1 (Filtration). *A filtration on* $(\Omega, \mathscr{F}, \mathbb{P})$ *is a collection* $(\mathscr{F}_t)_{0\le t\le\infty}$ *indexed by* $[0,\infty]$ *of sub-*σ*-fields of* $\mathscr{F}$*, such that* $\mathscr{F}_s \subset \mathscr{F}_t$ *for every* $s \le t \le \infty$.

Definition 2.2.2 (Brownian motion). *A real-valued process* $\{W(t) : t \ge 0\}$ *is called a Brownian motion if*

1. *Starting at 0: W(0)=0.*
2. *Normally distributed increments:* $\forall s, t$ *such that* $0 \le s \le t, W(t) - W(s) \simeq N(0, t-s)$.
3. *Independent increments: For* $0 \le t_0 < t_1 < \ldots < t_n$*, the random variables* $Y_i := W(t_i) - W(t_{i-1})$*,* $i = 1, \ldots, n$ *are independent.*
4. *Continuous trajectories: The map* $t \mapsto W(t)$ *is continuous.*

For Brownian motions, we will usually consider the filtration defined as

$$\mathscr{F}_t = \sigma(W_s,\ 0 \le s \le t).$$

Definition 2.2.3 (Martingale). *We say that the process* $\{M_t : t \ge 0\}$ *is a* $\{\mathscr{F}_t, t \ge 0$ *martingale if*

1. *Adapted:* M_t *is* $\mathscr{F}_t$ *measurable for all* $t \ge 0$.
2. *Integrable:* M_t *is integrable for all* $t \ge 0$.
3. *Martingale property:* $\forall s, t$ *such that* $0 \le s \le t$:

$$\mathbb{E}(M_t \mid \mathscr{F}_s) = M_s. \tag{2.7}$$

Similar to a martingale, we will also define a semimartingale, as this definition is often used.

Definition 2.2.4 (Semimartingale). *A semimartingale* $S = (S_t)_{t\ge0}$ *is a càdlàg, adapted process of the form*

$$S_t = S_0 + M_t + A_t \quad (t \ge 0),$$

for a finite and $\mathscr{F}_0$ *measurable* S_0*, a local martingale* $(M_t)_{t\ge0}$ *with* $M_0 = 0$ *and a process with finite variation* $(A_t)_{t\ge0}$ *with* $A_0 = 0$*. The definition of these last two can be found in Appendix A.0.1 and Appendix A.0.2, respectively.*

Definition 2.2.5 (Itô integral). *For any square-integrable adapted process f(t) with continuous sample paths, we can define the stochastic integral, also known as the Itô integral, by*

$$I(T) \overset{\text{def}}{=} \int_0^T f(s)dW(s) = \lim_{n\to\infty} I_n(T),\ \text{in } L^2. \tag{2.8}$$

Here $I_m(T) = \int_0^T f_m(s)dW(s)$ *for some elementary process* $f(t) = \sum_{j=0}^{n-1} \eta_j \left(W(t_{j+1} - W(t_j)\right)$ *satisfying*

$$\lim_{n\to\infty} \mathbb{E}\left[\int_0^T (f_m(s) - f(s))^2 ds\right] = 0. \tag{2.9}$$

In the above equations, η_j *is* $\mathscr{F}_{t_j}$ *measurable for all* $j = 0, 1, \ldots, n-1$ *and square integrable.*

A very useful property of the Itô integral is that it is a martingale with respect to filtration $\mathscr{F}_t$.

Theorem 2.2.6 (Itô's formula)**.** *Let $f \in C^2(\mathbb{R})$ and consider a continuous semimartingale $S = M + A$ with $M \in \mathscr{M}_{loc}$ and $A \in \mathcal{V}$. Then $f(S_t))_{t\geq 0}$ is also a semimartingale, and it holds*

$$f(S_t) = f(S_0) + \int_0^t \frac{\partial f}{\partial s}(S_u)dS_u + \frac{1}{2}\int_0^t \frac{\partial^2 f}{\partial s^2}(S_u)d[S]_u, \tag{2.10}$$

where the first and second partial derivatives are with respect to the considered semimartingale. The last operator $[S]$ signifies the quadratic variation of the stochastic process $(S_t)_{t\geq 0}$.

2.3. DERIVATIVE PRICING

The definitions and theorems needed for pricing derivatives as found in [21] are summarized in this section. Throughout the remaining sections, we will use $S = S_t : 0 \leq t \leq T$ to denote an adapted semimartingale to model the price process of a security. To be more specific, S is multi-dimensional, allowing for a security to be dependent on multiple assets. The general convention is that asset 0, denoted by S^0, is the money-market account as defined in definition 2.4.1. This allows us to define the value V_t of a trading strategy ϕ.

Definition 2.3.1. *A trading strategy is a process $\phi = \{\phi_t : 0 \leq t \leq T\}$, whose components are locally bounded and predictable. The value process associated with a strategy ϕ is defined by*

$$V_t(\phi) = \phi_t S_t = \sum_{k=0}^{K} \phi_t^k S_t^k, \quad 0 \leq t \leq T.$$

where ϕ_t^k is the k-th component of the strategy ϕ at time t.

This allows us to define one of the most fundamental concepts in financial mathematics, which is the notion of arbitrage.

Definition 2.3.2 (Arbitrage)**.** *An arbitrage opportunity is defined as a self-financing strategy (see Appendix A.0.3), such that $V_0(\phi) = 0$, but $\mathbb{Q}\{V_T(\phi) > 0\} > 0$.*

In the absence of arbitrage, Harrison and Pliska proved the fundamental proposition that every attainable contingent claim H has a unique price π_t [22].

Proposition 2.3.3. *Assume there exists an equivalent martingale measure $\mathbb{Q}$ and let H be an attainable contingent claim. Then, for each time t, $0 \leq t \leq T$, there exists a unique price π_t associated with H, that is,*

$$\pi_t = \mathbb{E}^{\mathbb{Q}}\left(\frac{B(t)}{B(T)}H \mid \mathscr{F}_t\right). \tag{2.11}$$

The risk-neutral measure is often a natural choice for an equivalent martingale measure (Appendix A.0.4). However, the risk-neutral measure is not necessarily the best choice for pricing a contingent claim. Sometimes, real-world risk should be considered in pricing an option. When considering a foreign and domestic currency, it may be more convenient to consider the foreign currency in the domestic measure [23]. Geman et al. formulated the following proposition to switch between measures [24].

Proposition 2.3.4. *Assume there exist a numeraire N and a probability measure $\mathbb{Q}^N$, equivalent to the initial $\mathbb{Q}_0$, such that the price of any traded asset X (without intermediate payments) relative to N is a martingale under $\mathbb{Q}^N$; that is,*

$$\frac{X_t}{N_t} = \mathbb{E}^N \left\{ \frac{X_T}{N_T} \mid \mathscr{F}_t \right\} \quad 0 \le t \le T. \tag{2.12}$$

Let U be an arbitrary numeraire. Then there exists a probability measure $\mathbb{Q}^U$, equivalent to the initial $\mathbb{Q}_0$, such that the price of any attainable claim Y normalised by U is a martingale under $\mathbb{Q}^U$; that is,

$$\frac{Y_t}{U_t} = \mathbb{E}^U \left\{ \frac{Y_T}{U_T} \mid \mathscr{F}_t \right\} \quad 0 \le t \le T. \tag{2.13}$$

Moreover, the Radon–Nikodym derivative defining the measure $\mathbb{Q}^U$ is given by

$$\frac{d\mathbb{Q}^U}{d\mathbb{Q}^N} = \frac{U_T N_0}{U_0 N_T}. \tag{2.14}$$

The numeraire in this proposition is any positive non-dividend-paying asset [21]. Switching from the original measure will result in an additional drift term in the considered dynamics. The additional drift term can be calculated with the help of Girsanov's theorem,

Theorem 2.3.5 (Girsanov's Theorem)**.** *Consider a Wiener process W_t on the probability space $\{\Omega, \mathscr{F}, \mathbb{P}\}$. Let X_t be a measurable process adapted to natural filtration. We define a process Z_t such that*

$$Z_t = \mathscr{E}(X)_t,$$

where $\mathscr{E}(X)$ is the Doléans–Dade exponential, better known as stochastic exponential, of X with respect to the Wiener process W. The exponential is given by

$$\mathscr{E}(X)_t = e^{X_t - \frac{1}{2}[X]_t}. \tag{2.15}$$

If Z_t is a martingale, then a probability measure $\mathbb{Q}$ can be defined such that the Radon–Nikodym derivative is equal to Z_t; that is,

$$\left.\frac{d\mathbb{Q}}{d\mathbb{P}}\right|_{\mathscr{F}_t} = Z_t = \mathscr{E}(X)_t. \tag{2.16}$$

In addition, if X_t is a continuous process, and W_t is a Brownian motion under measure $\mathbb{P}$, then the Brownian motion under the new measure $\mathbb{Q}$ is given by

$$\tilde{W}_t = W_t - [W, X]_t. \tag{2.17}$$

2.4. INTEREST RATE DERIVATIVES

This section will elaborate on the mathematical foundation of several important interest rate derivatives. Additionally, the pricing of such derivatives will be discussed. All definitions and theorems can be found in [21].

We start by defining the money-market account, which is the riskless investment of putting money in your savings account continuously accruing the instantaneous (spot) rate. Also known as the short rate, this is the continuously compounded interest rate at which one can borrow money over an infinitesimally small time horizon.

Definition 2.4.1 (Money-market account)**.** *$B(t)$ is the value of the bank account at time $t \geq 0$. We assume $B(0) = 1$ such that we get*

$$B(t) = e^{\int_0^t r_s ds}, \tag{2.18}$$

where r_s is the instantaneous rate.

Definition 2.4.2 (Zero-coupon bond)**.** *A T-maturity zero-coupon bond (ZCB) is a contract that guarantees its holder the payment of one unit of currency at time T, with no intermediate payments. The contract value at time $t < T$ is denoted by $P(t,T)$ and is given as*

$$P(t,T) = \mathbb{E}^{\mathbb{Q}}\left[\frac{B(t)}{B(T)} P(T,T) \mid \mathscr{F}_t\right] = \mathbb{E}^{\mathbb{Q}}\left[e^{\int_t^T r(s)ds} \mid \mathscr{F}_t\right], \tag{2.19}$$

where we used the definition of the ZCB, P(T,T)=1 and proposition 2.3.3. Furthermore, the superscript $\mathbb{Q}$ denotes that the expectation is taken in the risk-neutral probability measure.

Different from the earlier mentioned continuous compounded interest rate, simple compounding is used to define interbank rates like the LIBOR.

Definition 2.4.3 (Simply-compounded spot interest rate)**.** *The simply compounded spot interest rate prevailing at time t for the maturity T is denoted by L(t,T) and is the constant rate at which an investment must be made to produce an amount of one unit of currency at maturity, starting from P(t,T) unit of currency at time t, when accruing occurs proportionally to the investment time. This can be given in formulas as*

$$L(t,T) := \frac{1 - P(t,T)}{\tau(t,T)P(t,T)}, \tag{2.20}$$

where P(t,T) is the ZCB at time t with maturity T, and $\tau(t,T)$ is the year fraction according to the day-count convention, usually Act365.

Forward rates are similar to the previously discussed interest rates. Forward rates are used to lock in an interest rate over a future time period. Therefore, forward rates depend on three time points, the current time t, the expiry time T and the maturity S. Forward rates are agreed upon in a forward-rate agreement (FRA), which sees the exchange of a fixed rate K at maturity S against a floating rate $L(T,S)$ resetting in T. The payoff of an FRA is given by

$$\begin{aligned} V^{FRA}(t,T,S,\tau(T,S),N,K) &= N\tau(T,S)\,(K - L(T,S)) \\ &= N\left[P(t,S)\tau(T,S)K - P(t,T) + P(t,S)\right]. \end{aligned} \tag{2.21}$$

As stated before, K is a constant interest rate that is exchanged for the floating rate, τ is the year fraction, $P(t,T)$ is the ZCB at time t with maturity T and N is the notional amount of the transaction. It is clear from the payoff formula of an FRA that there exists a K for which the payoff is zero at each time t. This results in the simply-compounded forward interest rate defined below.

Definition 2.4.4 (Simply-compounded forward interest rate)**.** *The simply-compounded forward interest rate prevailing at time t for the expiry $T > t$ and maturity $S > T$ is denoted by $F(t;T,S)$ and is defined by*

$$F(t;T,S) := \frac{1}{\tau(T,S)}\left(\frac{P(t,T)}{P(t,S)} - 1\right). \tag{2.22}$$

It is the value of the fixed rate in a prototypical FRA with expiry T and maturity S that renders the FRA a fair contract at time t.

If we let the maturity date S get infinitely close to the expiry date T, we can define the instantaneous forward interest rate. This forward rate will be of importance in the calibration of the interest rate model to the observed market, discussed in Subsection **??**.

Definition 2.4.5 (Instantaneous forward interest rate)**.** *The instantaneous forward interest rate prevailing at time t for the maturity $T > t$ is denoted by $f(t,T)$ and is defined as*

$$f(t,T) := \lim_{S \to T^+} F(t;T,S) = -\frac{\partial \ln\left(P(t,T)\right)}{\partial T}. \tag{2.23}$$

In the same way that the FRA was defined, we can also define the interest rate swap (IRS). An IRS is a derivative exchanging two different legs, usually a fixed and a floating leg. The fixed and floating legs pay coupons during a period divided into terms with their agreed interest rates, a fixed amount K for the fixed leg and a forward rate for the floating leg. The forward rate depends on the reset and maturity date, where we will assume that they overlap with the coupon payment dates, instead of the industry standard $T+2$, for mathematical readability. Additionally, we will use the convention that the interest rate resets at T_{i-1} over the coupon period $[T_i, T_{i+1}]$ throughout this thesis. The MtM, or price of an IRS, is its discounted payoff. Hence, the MtM value of an IRS can be calculated by discounting the net cashflows of the fixed and floating legs using the zero-coupon curve. A formula of the receiver IRS (RFS)[1] for $t < T_\alpha$ is given below and shows the relationship to the previously stated FRA.

[1] A RFS receives the fixed leg and pays the floating leg.

$$
\begin{aligned}
V^{RFS}(t,\mathcal{T},\tau,N,K) &= \sum_{i=\alpha+1}^{\beta} V^{FRA}(t,T_{i-1},T_i,\tau_i,N,K) \\
&= N\sum_{i=\alpha+1}^{\beta} \tau_i P(t,T_i)\,(K - F(t;T_{i-1},T_i) \\
&= -NP(t,T_\alpha) + NP(t,T_\beta) + N\sum_{i=\alpha+1}^{\beta} \tau_i K P(t,T_i),
\end{aligned}
\tag{2.24}
$$

where N is the notional amount of the RFS, K is the fixed rate, $\mathcal{T}$ is the set of dates $\{T_\alpha,\ldots,T_\beta\}$, and $\tau := \{\tau_{\alpha+1},\ldots,\tau_\beta\}$ the set of year fractions.

2.5. FX DERIVATIVES

In addition to interest rate derivatives, dependent on only one interest rate, FX derivatives are prominently traded products. As the name suggests, they are contracts involving the exchange of two currencies. This brings forth another risk factor, the spot exchange rate X connecting the two currencies. Throughout the literature, the spot rate is defined as the amount of domestic currency needed to buy one unit of foreign currency. Domestic and foreign merely distinguish between the numeraire currencies used to value the trading leg. The names domestic and foreign currency are often replaced by quote and base currency [25]. However, there is ambiguity in this naming convention, as domestic is sometimes also called the base currency [26]. In practice, these ambiguities disappear because of the default quotations for currency pairs. For example, the convention in trading is to quote the spot rate of the currency pair of euros and US dollars as EUR-USD, meaning the amount of USD exchanged for one euro.

To evaluate the MtM value of an FX derivative, one needs to compare the value of the different cashflows in one valuation currency. This does not necessarily have to be one of the currencies of the traded cashflows, although, for analytical tractability, it will be assumed that the valuation currency is the domestic currency in the rest of this thesis. This means that the cashflows of the trade leg in the foreign currency must be converted to the domestic (valuation) currency. Due to the absence of arbitrage, it does not matter whether the cashflows are first discounted using the foreign money-market account and thereafter converted to the domestic currency or whether the cashflows are first converted to the domestic currency and then discounted using the domestic money-market account.

A simple and common FX derivative is the FX forward contract. The contract is an agreement to exchange a certain amount of currency for another currency at a fixed exchange rate on a specified day in the future. Suppose one wants to exchange an amount of domestic currency N^d for an amount of foreign currency N^f at time $t = T$. At the time of the agreement, the two parties agree on the spot FX rate $X(0)$ to make the exchange at time $t = T$ fair. The value of the FX forward contract at a time $t \le T$ is given by

$$\begin{aligned} V_{FX}(t) &= N^f P^f(t,T) X(t) - N^d P^d(t,T) \\ &= N^d \left[P^f(t,T) \frac{X(t)}{X(0)} - P^d(t,T) \right], \end{aligned} \tag{2.25}$$

where the superscripts d and f specify the currency. Note that although mathematically correct, the last expression in Equation 2.25 is not used in practice. It is impossible to know the exact time at which parties enter the contract beforehand, which would be of importance for the continuously changing spot rate. Therefore, the parties will agree to the exchange of notional based on the spot rate.

The FX forward rate $X_F(t,T)$ is defined similarly to the simply-compounded forward interest rate. It renders the FX forward agreement a fair contract.

Definition 2.5.1 (FX forward rate)**.** *The FX forward rate prevailing at time t for the maturity $T > t$ is denoted by $X_F(t;T)$ and is defined by*

$$X_F(t;T) = \frac{P^d(t,T)}{P^f(t,T)} X(t). \tag{2.26}$$

Here, P^d, P^f are the ZCBs in the domestic and foreign currencies, respectively. $X(t)$ is the exchange rate at time t defined as the number of units in domestic currency for one unit of foreign currency. X_F is the value of the FX exchange rate in an FX forward agreement with maturity T that renders the FX forward a fair contract at time t.

Another very liquid FX derivative is the cross-currency swap (XCS). A cross-currency swap is a contract agreeing on the exchange of two currencies. There are fixed-for-fixed, fixed-for-floating and floating-for-floating currency swaps, indicating the fixed or floating types of the traded legs. The value of a fixed-for-floating currency swap in which one receives the fixed foreign currency and pays the domestic floating currency can be valued as

$$\begin{aligned} V_{XCS}(t) &= \sum_{i=\alpha+1}^{\beta} \left[N^f X(t) K \tau_i P^f(t,T_i) - N^d L^d(t;T_{i-1},T_i) \tau_i P^d(t,T_i) \right], \\ &= N^d \left[X(0) \sum_{i=\alpha+1}^{\beta} \tau_i K X(t) P^f(t,T_i) - P^d(t,T_\alpha) + P^d(t,T_\beta) \right]. \end{aligned} \tag{2.27}$$

Here, N^d is the notional given in domestic currency τ_i corresponds to the days according to the day-count convention, K is the fixed rate, $X(t)$ is the exchange rate defined as the number of units of domestic currency for one unit foreign currency, and $P^f(t,T)$, $P^d(t,T)$ are the foreign and domestic ZCBs. $\mathcal{T}$ is the set of dates $\{T_\alpha, \ldots, T_\beta\}$, and $\tau := \{\tau_{\alpha+1}, \ldots, \tau_\beta\}$ is the set of year fractions.

Additionally, it is common for cross-currency swaps to include a notional exchange. This is the upfront borrowing of funds that will be returned at the maturity of the swap. The discounted value of the notional exchange for both the domestic and foreign leg given in domestic currency is added to the swap value and given by

$$
\begin{aligned}
V^d_{exchange} &= N^d P^d(t, T_\beta) - N^d P^d(t, T_0) \\
V^f_{exchange} &= X(t)\left[N^f P^f(t, T_\beta) - N^f P^f(0, T_0)\right].
\end{aligned}
\tag{2.28}
$$

2.6. INTEREST RATE MODELS

The choice of an interest rate model forms the basis for acquiring the potential future exposure distribution. There are many different stochastic interest rate models that simulate the path of the short rate over time. The short rate is the interest rate over money borrowed for an infinitesimally small period of time. The early models by Vasicek (1977), Dothan (1978) and CIR (1985) had success in the analytical pricing of interest rate derivatives. However, they were endogenous [27]–[29]. This means that the resulting term structure is dependent on the calibration of the input variables to the real world instead of being imposed on the model [4]. Hull and White extended the Vasicek model using the same mean-reverting characteristic but making the constant drift and volatility deterministic functions of time [30]. This enabled the reproduction of the initial interest rate curve, making it exogenous.

This section will discuss the general affine term-structure models, followed by the Hull–White model and the equivalent $G1{+}{+}$ model adapted from [21], [30], [31], respectively.

2.6.1. AFFINE TERM-STRUCTURE MODELS

Affine term-term structure models are a general class of stochastic models where the drift $\mu(t, r(t))$ and volatility $\sigma(t, r(t))$ are of the affine form. Thus, an affine term-structure model has short-rate dynamics of the form,

$$
dr(t) = \mu(t, r(t))\,dt + \sigma(t, r(t))\,dW^{\mathbb{Q}}(t), \tag{2.29}
$$

where the drift and volatility parameters are both of the affine form, respectively satisfying,

$$
\mu(t, r(t)) = a_0 + a_1 r(t), \tag{2.30a}
$$

$$
\sigma^2(t, r(t)) = b_0 + b_1 r(t). \tag{2.30b}
$$

Here, all coefficients a_0, a_1, b_0 and b_1 are deterministic functions of time.

It is highly desirable for a term-structure model to be an affine process because affine processes have a convenient relationship with the ZCB. That is, the ZCB can be written as

$$
P(t, T) = A(t, T)e^{-B(t,T)r(t)}. \tag{2.31}
$$

The coefficients A, B depend on the term-structure model and can be obtained using the Ricatti differential equations. The Ricatti equations are given by

$$
\frac{\partial}{\partial t}B(t, T) + a_1 B(t, T) - \frac{1}{2}b_1 B(t, T)^2 + 1 = 0, \quad B(T, T) = 0, \tag{2.32a}
$$

$$\frac{\partial}{\partial t}\left[\ln\left(A(t,T)\right)\right] - a_0 B(t,T) + \frac{1}{2} b_0 B(t,T)^2 = 0, \quad A(T,T) = 1. \tag{2.32b}$$

Here a_0, a_1, b_0, b_1 are the coefficients from the affine drift and volatility parameters, and the boundary conditions follow from the definition of a ZCB, $P(T,T) = 1$.

2.6.2. THE HULL–WHITE MODEL

The Hull–White one-factor model ($HW1F$) falls into the affine term structure class [30]. In addition to being affine, the Hull–White model is mean-reverting, meaning that in the long term, the process will revert to a mean. The Hull–White model is an extension of the Vasicek model using deterministic time-dependent parameters. This thesis will consider the Hull–White dynamics of the form,

$$dr(t) = [\theta(t) - ar(t)]\,dt + \sigma dW^{\mathbb{Q}}(t), \tag{2.33}$$

where the speed of mean-reversion is a, the volatility σ are positive constants and $\theta(t)$ is a deterministic function of time used to calibrate the model to the observed market. To calibrate the model to fit the observed market, the drift $\theta(t)$ can be calculated analytically [21]. The derivation can be found in A.0.7, and the expression for $\theta(t)$ is given by

$$\theta(t) = \frac{\partial f^M(0,t)}{\partial T} + a f^M(0,t) + \frac{\sigma^2}{2a}\left(1 - e^{-2at}\right). \tag{2.34}$$

The market instantaneous forward rate f^m is defined as a function of the price of a ZCB observed in the market P^M,

$$f^M(0,T) = \frac{-\partial \ln\left(P^M(0,T)\right)}{\partial T}. \tag{2.35}$$

Integrating the Hull–White dynamics shown in Equation 2.33 yields the solution,

$$r(t) = r(s)e^{-a(t-s)} + \int_s^t e^{-a(t-u)}\theta(u)du + \sigma\int_s^t e^{-a(t-u)}dW(u). \tag{2.36}$$

This representation shows that $r(t)$ contains a deterministic part and an Itô integral. From Section 2.2, it is known that an Itô integral is a martingale. It is easily proven that $r(t)$ conditional on $\mathcal{F}_s$ is normally distributed. The proof is given in A.0.6. The mean and variance of $r(t)$ can be found from Equation 2.36,

$$\mathbb{E}^{\mathbb{Q}}\left(r(t)\,|\,\mathcal{F}_s\right) = r(s)e^{-a(t-s)} + \int_s^t e^{-(t-u)}\theta(u)du \tag{2.37a}$$

$$\mathrm{Var}\left(r(t)|\mathcal{F}_s\right) = \frac{\sigma^2}{2a}\left[1 - e^{-2a(t-s)}\right]. \tag{2.37b}$$

Due to the affinity of the Hull–White model, we know that the ZCB can be written in an expression of the form of Equation 2.31. A derivation uses the fact that the short rate $r(t)$ conditional on $\mathcal{F}_t$ is normally distributed. Notice that $\int_t^T r(u)du|\mathcal{F}_t$ is also normally distributed. Using the moment generating function for a normal distribution, the final expression is obtained, which is of the form,

$$P(t,T) = A(t,T)e^{-B(t,T)r(t)},$$

with parameters

$$B(t,T) = \frac{1}{a}\left[1 - e^{-a(T-t)}\right], \tag{2.38a}$$

$$A(t,T) = \frac{P^M(0,T)}{P^M(0,t)} \exp\left\{B(t,T) f^M(0,t) - \frac{\sigma^2}{4a}(1 - e^{-2at}) B(t,T)^2\right\}. \tag{2.38b}$$

Notice that the above expression is dependent on the market instantaneous forward rate. However, the value of the market instantaneous forward rate cannot be observed because it cannot be traded. To use the above expression to calculate the ZCB, one would have to use the relation between the market instantaneous forward rate and the observed ZCB price, as shown in Equation 2.35. However, taking the derivative of the ZCB price observed in the market with respect to the maturity T is a problem. Even though the price of a ZCB can be observed in the market because it is traded, it is only traded for specific maturities. This means that it is a discrete function of maturity T. To take the derivative, one would first need to interpolate between the known ZCB prices and then take the derivative with respect to maturity to get the market instantaneous forward rate. Doing this would severely impact the accuracy of the results. To solve this problem, we shall look at the $G1{+}{+}$ model, which is equivalent to the Hull–White model.

2.6.3. THE G1++ MODEL

The Gaussian one-factor model ($G1{+}{+}$) is equivalent to the Hull–White model. It assumes that the dynamics of the short rate r(t) are given by

$$r(t) = x(t) + \beta(t), \tag{2.39}$$

where $x(t)$, hereafter also referred to as 'shifted short rate', is modelled using an Ornstein–Uhlenbeck process satisfying the stochastic differential equation,

$$\begin{aligned} dx(t) &= -ax(t)dt + \sigma dW(t), \\ x(0) &= 0. \end{aligned} \tag{2.40}$$

In the Ornstein–Uhlenbeck dynamics, the mean-reversion constant a and the volatility σ are the same as in the Hull–White model. The $\beta(t)$ is a deterministic function of time that can be acquired by fitting the process to the term structure observed in the market, similar to what was done for the drift $\theta(t)$ in the Hull–White model. The relationship between the parameters of the different models is

$$\theta(t) = a\beta(t) + \frac{\partial \beta(t)}{\partial t}. \tag{2.41}$$

The process $x(t)$ from the driftless Ornstein–Uhlenbeck process 2.40 is known to be normally distributed with zero mean μ_X and variance $\sigma_X^2(t)$ given by

$$\sigma_X^2(t) = \frac{\sigma^2}{2a}\left(1 - e^{-2at}\right). \tag{2.42}$$

Analogous to what was done for the Hull–White model, integrating the Ornstein–Uhlenbeck dynamics and adding the deterministic function $\beta(t)$ gives us

$$r(t) = x(s)e^{-a(t-u)} + \sigma \int_s^t e^{-a(t-u)} dW(u) + \beta(t). \tag{2.43}$$

This again shows that $r(t)$ conditional on $\mathscr{F}_t$ is normally distributed with the mean and variance given by

$$\mathbb{E}^{\mathbb{Q}}(r(t) \mid \mathscr{F}_s) = x(s)e^{-a(t-s)} + \beta(t) \tag{2.44a}$$

$$\mathrm{Var}(r(t)|\mathscr{F}_s) = \frac{\sigma^2}{2a}\left[1 - e^{-2a(t-s)}\right]. \tag{2.44b}$$

As a result of the equivalence of the models, we indeed see that the variance is the same. The expectation will also be the same whenever $\beta(t)$ is chosen to satisfy the relation given in Equation 2.41. Whenever the $G1{+}{+}$ model is calibrated to fit the market data, we find

$$\beta(t) = f^M(0,t) + \frac{\sigma^2}{2a^2}\left(1 - e^{-at}\right)^2. \tag{2.45}$$

The proof of this expression is an intermediate result in Appendix A.0.8.
In the previous section about the Hull–White model a ZCB pricing formula is presented. It was explained that the inclusion of the market instantaneous forward rate is inconvenient in practice, which brings the need for another formulation of the ZCB price. A derivation of the ZCB price under the $G1{+}{+}$ model is shown below. A proof is given in Appendix A.0.8 adapted from the work of Francesco [31].

$$P(t,T) = A(t,T)e^{-B(t,T)X(t)}, \tag{2.46}$$

where

$$B(t,T) = \frac{1}{a}\left[1 - e^{-a(T-t)}\right], \tag{2.47a}$$

$$A(t,T) = \frac{P^M(0,T)}{P^M(0,t)} e^{1/2[V(t,T) - V(0,T) + V(0,t)]}. \tag{2.47b}$$

Here, $V(t,T)$ is the variance of $\int_t^T x(s)$ conditional on $\mathscr{F}_t$ given by

$$V(t,T) = \frac{\sigma^2}{a^2}\left(T - t - 2\frac{1 - e^{-a(T-t)}}{a} + \frac{1 - e^{-2a(T-t)}}{2a}\right).$$

Notice that the expression 2.46 only needs the market discount curve and the process $x(t)$, which only depends on the mean-reversion coefficient a and the volatility coefficient σ. This makes the expression more convenient than the earlier expression of the ZCB found with the HW1F model with coefficients given in 2.38. Equation 2.46 with the corresponding coefficients is very important in simulation because all other rates are derived from this expression.

2.6.4. THE GBM MODEL

The geometric Brownian motion (GBM) model is the stochastic model popular in industry to model the foreign exchange rate. It is described by the dynamics

$$dX(t) = \mu X(t)dt + \sigma_X X(t)dW_X^{\mathbb{P}}, \tag{2.48}$$

where $X(t)$ defines the units of domestic currency exchanged for one unit of foreign currency, μ is the drift, and σ_X is the volatility. The subscript $\mathbb{P}$ in the Brownian motion indicates the real-world measure. Under the domestic risk-neutral measure $\mathbb{Q}^d$, the dynamics of Equation 2.48 are transformed to

$$dX(t) = \big(r_d(t) - r_f(t)\big)X(t)dt + \sigma_X X(t)dW_X^{\mathbb{Q}^d}. \tag{2.49}$$

A derivation is shown in Appendix A.0.10. Here, it is also reasoned that the dynamics of the FX rate under the foreign risk-neutral measure are the same as Equation 2.49 with the subscripts d and f flipped.

2.7. SOLVERS

This thesis will consider two methods of calculating the potential future exposure of a portfolio containing basic interest rate derivatives. These two methods are the MC simulation framework and the COS method. The former serves as a benchmark, employing stochastic models for the interest and cross currency rate, and the latter is an innovative numerical method to calculate the PFE based on earlier work by Fang and Oosterlee, who applied the same method to price options [17]. The theoretical framework of both methods will be discussed in this section.

2.7.1. MONTE CARLO

Throughout the literature, there is an extensive framework about the use of Monte Carlo simulation for stochastic term-structure models. The theory on the application of the MC simulation to price options is based on the paper by Boyle et al. [32]. This subsection will discuss the basic principles of the Monte Carlo simulation. Its application in acquiring the potential future exposure will be discussed in Chapter 3.

In this thesis, we focus on the calculation of PFE for netting sets that concern three risk factors. Two are short rates in two currencies, and the other is the exchange rate X_t. These risk factors are modelled using the Hull–White or $G1{+}{+}$ models and the GBM model, respectively. Because the risk factors are stochastic, an inherent uncertainty must be modelled. This uncertainty originates from the Itô integral as shown by the dynamics of the Hull–White model 2.33 with its solution 2.36 in Subsection 2.6.2.

Analysis of the short rate shows that it can be split into a Riemann integral over a deterministic function and an Itô integral as defined in 2.2.5. For the Riemann integral, we can use the stochastic Euler scheme as a numerical integration method. On a uniform grid $0 = t_0 < t_1 < \ldots < t_N = T$, this gives the approximation

$$\int_0^T f(t)dt = \lim_{m\to\infty} \sum_{i=0}^{m-1} f(t_i)(t_{i+1} - t_i). \tag{2.50}$$

We cannot do this for the Itô integral, but we use a similar way of evaluating the integral. Instead of the Riemann integral, the Stratonovich integral is used to compute the Itô integral. That is,

$$\int_0^T g(t)dW(t) = \lim_{m\to\infty} \sum_{i=0}^{m-1} g(t_i)\left(W(t_{i+1}) - W(t_i)\right), \tag{2.51}$$

where the increments of the Brownian motion can be simulated using the relation,

$$W(t_{i+1}) - W(t_i) = Z\sqrt{\Delta t}, \text{ with } Z \sim \mathcal{N}(0,1). \tag{2.52}$$

Here, Z is the standard normal distribution, and we use $\Delta t = t_{i+1} - t_i$. Relation 2.52 follows from the definition of a Brownian motion, which says that every increment is normally distributed.

Combining the two numerical integration methods, we get the following recursion step, known as the Euler discretization:

$$r(t_{i+1}) = r(t_i) + (\theta(t_i) - ar(t_i))\,\Delta t + \sigma\sqrt{\Delta t}Z(t_i). \tag{2.53}$$

Here, $\theta(t_i)$ is a deterministic function calibrated to the observed market as defined in 2.34, a is the coefficient of mean-reversion obtained from market data, σ is the volatility and $Z(t_i)$ is a random draw from the standard normal distribution at time t_i.

Taking a random draw from $Z(t_i)$ gives us a possibility of the solution for the short rate r_{t_i}. We call this a path. The Monte Carlo simulation finds its essence in the law of large numbers, which states that the sample average converges almost surely to the expected value. By simulating many different paths and taking the average, we find an approximation to the expected value of the short rate r_t.

2.7.2. FOURIER-COSINE SERIES EXPANSION

Earlier work by Fang and Oosterlee [17], [33] showed that the COS method is an alternative method to price options. The method makes use of the relation between the weights of the Fourier-cosine expansion and the characteristic function (ch.f.). The latter is often easier to obtain; hence, the convenience of the method. This subsection will show the basic theory behind the COS method; the next chapter will use apply theory in calculating the PFE for portfolios of interest rate derivatives. The COS method finds its roots in the (inverse) Fourier transform shown below,

$$\phi(\omega) = \int_{\mathbb{R}} e^{ix\omega} f(x)dx, \tag{2.54a}$$

$$f(x) = \frac{1}{2\pi}\int_{\mathbb{R}} e^{-i\omega x}\phi(\omega)d\omega. \tag{2.54b}$$

Here, $\phi(\omega)$ is the characteristic function, $f(x)$ is the probability density function and i is the imaginary unit.

PDF RECOVERY

The Fourier-cosine series expansion is used to recover the probability density function $f(x)$. For a function supported on the interval $[a,b]$, the cosine expansion is given by[2],

$$f(x) = \sum_{k=0}^{\infty}{}' A_K \cdot \cos\left(k\pi \frac{x-a}{b-a}\right), \tag{2.55a}$$

$$A_k = \frac{2}{b-a}\int_a^b f(x)\cos\left(k\pi\frac{x-a}{b-a}\right)dx, \tag{2.55b}$$

where $\sum'$ indicates that the first term is multiplied by half. The cosine expansion exists for any real function with finite support. Additionally, it gives the optimal approximation on a finite support as well [34]. This is important because the ch.f. is often only known on an infinite domain, as shown in Equation 2.54b. Equation 2.55b, on the other hand, shows that the cosine series coefficients are defined for a finitely supported function $f(x)$. If we consider a truncated characteristic function on a finite domain, we can rewrite Equation 2.55b to

$$A_k \equiv \frac{2}{b-a}\text{Re}\left\{\phi_1\left(\frac{k\pi}{b-a}\right)\cdot e^{-i\frac{ka\pi}{b-a}}\right\}, \tag{2.56}$$

with $\phi_1(\omega) := \int_a^b e^{i\omega x} f(x)dx$ being the ch.f. of a probability density with finite support. The Fourier-cosine expansion is only an accurate approximation whenever the truncated characteristic function is a close approximation to the original ch.f. This must be true because the assumption of the existence of the ch.f. implies that it decays to zero at $\pm\infty$. Truncating the characteristic function in the tails will give a close approximation to the infinite characteristic function. Using the known ch.f. on an infinite instead of the finitely supported one has a similar expression for the cosine coefficients as Expression 2.55b,

$$A_k \approx F_k \equiv \frac{2}{b-a}\text{Re}\left\{\phi\left(\frac{k\pi}{b-a}\right)\cdot e^{-i\frac{ka\pi}{b-a}}\right\}, \tag{2.57}$$

where ϕ is now the characteristic function with infinite support. The probability density function can be approximated using the COS method with the following formula:

$$f_1(x) = \sum_{k=0}^{N}{}' F_k \cos\left(k\pi\frac{x-a}{b-a}\right). \tag{2.58}$$

This approximation of the probability density function has two main sources of errors. The first error originates from the use of the ch.f. on an infinite domain in the calculation of the cosine coefficients. The second error is introduced by the need to truncate the series summation given in Equation 2.55a to a finite amount of expansion terms N. An error analysis of the COS method approximation will be given in Chapter 4.

[2] A derivation is given in A.0.9

CDF RECOVERY

As a result of the relation of the PDF and the cumulative density function CDF, it is also possible to use the COS method to approximate the CDF. This is easily shown by considering that the CDF is defined as the integral of the probability density function $f_X(x)$,

$$F_X(x) = \int_{-\infty}^{x} f_X(t)\,dt \approx \int_{a}^{x} f_X(t)\,dt. \tag{2.59}$$

Approximating the CDF using the COS method requires the integration of Equation 2.55a. First, the integration range is truncated to $[a,x]$. The order of integration and summation is also interchanged. This is allowed by Fubini's theorem as both the density function and the cosine basis functions are bounded. This gives

$$F_X(x) \approx \frac{A_0}{2}\cdot(x-a) + \sum_{k=1}^{\infty} A_k \frac{b-a}{k\pi}\sin\left(k\pi\frac{x-a}{b-a}\right), \tag{2.60}$$

where A_k are the same coefficients as defined in 2.55b. The approximation is, in actuality, a Fourier-sine expansion but will hereafter also be referred to as the COS approximation to be in line with the literature. To approximate the CDF using the COS method, the series coefficients, the domain of support and the summation must again be finite. Therefore, 2.60 becomes

$$\tilde{F}_X(x) \approx \frac{F_0}{2}\cdot(x-a) + \sum_{k=1}^{N} F_k \frac{b-a}{k\pi}\sin\left(k\pi\frac{x-a}{b-a}\right), \tag{2.61}$$

where F_k are the coefficients defined in 2.57.

2.7.3. NUMERIC INTEGRATION

As we will see in the next section, it is not always possible to get a (semi)-analytical expression for an integral like the ch.f. Another way to evaluate an integral is by using numerical integration. The numeric integration quadrature that will be considered throughout this thesis is the Clenshaw–Curtis quadrature. This quadrature ensures the periodicity of the considered function, thereby warranting exponential convergence of the integration method [35]. Discretisation of an integral using the Clenshaw–Curtis quadrature gives us

$$I_f = \int_0^{\pi} f(\cos(\theta))\sin(\theta)\,d\theta \approx a_0 + \sum_{\substack{\nu=1 \\ \nu \text{ even}}}^{N} \frac{2a_\nu}{1-\nu^2}, \tag{2.62}$$

where the coefficients a_k are given by

$$a_k \approx \frac{2}{N}\left[\frac{f(1)}{2} + \frac{f(-1)}{2}(-1)^k + \sum_{n=1}^{N-1} f(\cos(n\pi/N))\cos(nk\pi/N)\right]. \tag{2.63}$$

In these equations, N is the number of quadrature points. Also, we notice that Expression 2.63 for the coefficients of the Clenshaw–Curtis quadrature is very similar to discrete cosine transform Type 1. For this reason, we can use the fast Fourier transform

implementation from Python to efficiently calculate these coefficients. Numeric integration can only consider finite integration ranges. The calculation of the ch.f. requires the evaluation of an infinite integral; therefore, an error will be introduced. There is an additional numeric integration error from the Clenshaw–Curtis quadrature itself. Both these errors are propagated to the approximation using the Fourier-cosine expansion. The analysis of these errors will be discussed in more detail in Chapter 4.

3

METHODOLOGY

The definitions and theorems given in the previous chapter are essential for us to formulate the calculation of the potential future exposure for interest rate derivatives mathematically. In this chapter, we will develop a new method based on Fourier-cosine series expansion to calculate PFEs of small liquid portfolios, i.e. involving up to 3 risk factors. We refer to this method as the COS method to align with [17], because the it is an extension to the original COS method from derivative pricing to portfolio level risk quantification. The Monte Carlo simulation framework is also built up, which is to serve as a benchmark to our innovative COS method.

In the beginning of this chapter, the calculation of PFE for a single trade is detailed, involving only one risk factor, the short rate r_t. As the literature revolving around the industry standard Monte Carlo (MC) simulation is large, the discussion regarding MC method will only be brief. The application of the COS method for PFE calculations will be discussed in detail, starting with a convergence analysis on a simple log-normal distribution, followed by the approximation of the distribution of a ZCB, IRS and the exposure of an IRS.

Next, the complexity will be increased to a small IR portfolio typically involving three correlated risk factors: a domestic and foreign short rate and the exchange rate of this currency pair. Again, the Monte Carlo simulation will be briefly recapped, followed by a sensitivity analysis of the COS method for a case of which the analytical solution of the PFE exists.

Thereafter, the COS method is extended to approximate the CDF of a FX Forward, a Cross-currency Swap, and a netting set of IR, FX and cross-currency trades. Finally, we will tackle the counterparty level PFE calculation using the COS method.

3.1. ONE-DIMENSIONAL MONTE CARLO

The methodology of Monte Carlo simulation to calculate thePFE of an interest rate derivative with only one risk factor is quite straightforward. The time interval over which the trade is evaluated is first discretised. For each of the discretized time points, many scenarios of the short rate are generated using Expression 2.53, whereby each scenario is

drawn from the standard normal distribution $Z(t_i)$. The next step is to calculate the MtM value of an interest rate derivative at each point in time for each possible short-rate path. Exposure is then the positive part of the MtM price, as given in Definition 2.1.1. When we get a vector with exposures for each point in time, we can directly obtain the PFE, which is VaR at 97.5% quantile.

A pseudo code for the one-dimensional Monte Carlo algorithm is given below.

Algorithm 1: 1D Monte Carlo algorithm

Start : Initialise model parameters a and σ, choose number of paths N_p and time points N_t
Generate shifted short rate paths x:
Randomly sample standard normal distribution **Z for** $i=1,\ldots,N_t$ **do**
    Compute the Brownian Motion W_i using 2.52;
    Compute shifted short rate using the model dynamics 2.40;
end
Calculate the exposure of the portfolio:
for $i=1,\ldots,N_t$ **do**
    Compute the MtM value of the portfolio for each path;
    Floor the MtM values for each path to find the exposure;
    Find the 97.5% quantile to obtain the PFE;
end

3.2. ONE-DIMENSIONAL COS METHOD

The application of the COS method to the potential future exposure calculation rests on the idea that the distribution of the MtM prices of interest rate derivatives at future points in time can be recovered directly with the help of the COS method.. As described in Section 2.7.2 of the previous chapter, the COS method can be used to approximate the CDF, from which one can immediately retrieve the 97.5% quantile from the cumulative distribution.

3.2.1. LOG-NORMAL DISTRIBUTION

As we will see later, the distribution of the interest rate derivatives has no analytic expression. To test the accuracy of the approximations with the COS method, a sensitivity analysis is conducted.

An implementation of Expressions 2.57, 2.58 is needed to approximate the density function of a log-normal variable using the COS method. These expressions indicate that two parameters that control the accuracy of the approximation, namely the number of COS terms N and the interval on which the COS method is supported, or in other words, the function is approximated by the COS method, say $[a,b]$.

The ch.f. of a log-normal distribution has no closed-form expression, but another

key insight is that, it can be calculated via numeric integration. The definition of the characteristic function reads:

$$\phi(\omega) = \int_{-\infty}^{\infty} e^{i\omega \exp(x)} \cdot \frac{1}{\sqrt{2\pi}\sigma_X} e^{-\frac{(x-\mu_X)^2}{2\sigma_X^2}} dx, \tag{3.1}$$

where μ_X and σ_X are the mean and standard deviation of the log-normal distribution. The characteristic function is approximated by applying an advanced quadrature rule on 3.1 after we truncate the integration range. In this thesis, we employ Clenshaw–Curtis quadrature rule, but other higher order integration methods are also applicable.

Worth mentioning that, this step of calculating ch.f. numerically already introduces two types of errors: integration range truncation error and the numerical integration error. Errors originating from the computation of the characteristic function using numeric integration will resonate with the approximation of the density function. For this reason, the integration range and the number of quadrature points are two important parameters that need to be studied in the sensitivity analysis and analyzed theoretically in the error analysis section. Only this way, we could fully understand the method and know how to set the parameter values properly.

Note that the convergence test is meant to check whether a regular error convergence rate can be observed in the experiments. A regular convergence is crucial to the stability of any numerical method. To achieve this goal, we have to segregate the combined impact from different error sources, by means of suppressing other errors than the targeted one we want to examine to a much lower level, or, even better, to a negligible level. For example, to analyse the convergence of the COS method in the number of cosine terms, or in other words, the impact of increasing the number of COS expansion terms on the accuracy, we fix the following parameters, at conservative levels, that jointly control the error resulted from characteristic function approximation: the number of Clenshaw–Curtis quadrature points N_q, the domain on which the COS method is supported $[a, b]$ and the integration range for the Clenshaw–Curtis quadrature $[l, u]$.

Below we elaborate on how to define the truncation ranges that occur in different places. The chosen domain for the COS method and the integration range for the quadrature both impact the accuracy of the recovered distribution function. Both ranges can be chosen precisely according to a pre-defined error tolerance level, thanks to prior information contained in the integral form of the characteristic and density functions, respectively. The characteristic function is defined as a complex integral on an infinite domain, as shown in Expression 3.1. The integrand is a complex exponential multiplied the density of the normal distribution. The density of the normal distribution causes the integrand to go to zero exponentially fast far from the mean μ. This ensures that the approximation of the truncated characteristic function is still accurate. Additionally, it enables us to choose the integration range in a smart way. As the normal distribution is known, the truncated integration range can be chosen precisely by using the per cent point function (ppf), i.e. the inverse CDF function, of the normal distribution with a

chosen tolerance. The ppf of a normal distribution is given by

$$\text{PPF}_{\text{normal}}(p) = \mu + \sigma\sqrt{2}\,\text{erf}^{-1}(2p-1), \tag{3.2}$$

where μ, σ are the mean and standard deviation of the normal distribution, respectively, and p is the quantile level at the tails of the Normal distribution, such as $1e-12$.

Similarly, the density function of a log-normal variable is to be recovered and is, therefore, known. The support of the COS method can be chosen as the ppf of the log-normal distribution with a chosen tolerance such that it covers the desired domain. Since the exponential function is monotonic, the ppf of a log-normal distribution is the exponent of the ppf of a normal distribution:

$$\text{PPF}_{\text{log-normal}}(p) = e^{\mu+\sqrt{2\sigma^2}\,\text{erf}^{-1}(2p-1))}. \tag{3.3}$$

3.2.2. RECOVERING THE CDF AND PFE

In this section, the COS method is applied to approximate the CDF of the MtM price of an interest rate derivative at any future point in time. To build up the complexity step by step, the MtM distribution of a ZCB is recovered first using the COS method. This special case is chosen because the analytical solution of the CDF exists and we can directly measure the error from the COS method. This is then followed by the extension of the COS method to approximate the MtM distribution of an RFS.

ZERO-COUPON BOND

A ZCB modelled under a Gaussian one-factor model, the equivalent of a Hull–White model, is described by Equation 2.46. Furthermore, the shifted short rate $x(t)$ is normally distributed. Rewriting Expression 2.46 one can see that the MtM of a ZCB is log-normally distributed. That is

$$\begin{aligned} P(t,T) &= A(t,T)e^{-B(t,T)x(t)} \\ &= e^{\log(A(t,T))-B(t,T)x(t)}. \end{aligned}$$

The above expression shows that a ZCB is log-normally distributed with mean $\log(A(t,T))$ and variance $B(t,T)^2\sigma_X^2$. Here $A(t,T)$ and $B(t,T)$ are defined in 2.47, μ_X, σ_X are, respectively, the mean and standard-deviation of the shifted short-rate process $x(t)$.

Because a ZCB is log-normally distributed, a convergence test can be done in the same way as in the last chapter. Since the ZCB is used in the definitions of all interest rate derivatives, as discussed in section 2.4, it is important to check the convergence of the approximated CDF. The convergence test is meant to check whether a regular error convergence rate can be observed whenever the quadrature points and number of expansion terms are increased. The expression of the characteristic function that needs to be solved using numeric integration is

$$\phi(\omega) = \int_{-\infty}^{\infty} e^{i\omega A(t,T)\exp(-B(t,T)x)} \cdot \frac{1}{\sqrt{2\pi}\sigma_X} e^{-\frac{1}{2}\left(\frac{x-\mu_X}{\sigma_X^2}\right)^2} dx. \tag{3.4}$$

Notice that this expression of the characteristic function is very similar to the one of a simple log-normal distribution given in 3.1. Hence, the same way of defining the integration range can be used. The ppf used for the COS support can be written as a function of $A(t,T), B(t,T)$ using the same form as 3.3.

After evaluating the characteristic function using numeric integration, Expressions 2.57, 2.61 can be used directly to recover the CDF of the MtM price. The PFE is then obtained by employing a root-finding algorithm to the difference between the quantile of the approximated CDF at different values of the MtM prices and the 97.5% quantile.

INTEREST RATE SWAP

Equation 2.24 shows that the MtM price of a single receiver interest rate swap can be given as a linear combination of ZCBs $P(t,T_i)$. Therefore, the probability distribution of an IRS is a linear combination of log-normal variables, which unfortunately has no closed-form expression. However, a key insight here is that the characteristic function can be solved numerically, which means, in turn, the CDF can be recovered using the Fourier-sine expansion.

The integral form of the characteristic function is given by

$$\phi(\omega) = \int_{-\infty}^{\infty} e^{i\omega V_{IRS}(x)} \cdot \frac{1}{\sqrt{2\pi}\sigma_X} e^{-\frac{1}{2}\left(\frac{x-\mu_X}{\sigma_X^2}\right)^2} dx, \tag{3.5}$$

where $V_{IRS}(x)$ is the function defined as

$$V_{IRS}(x) = -NA(t,T_\alpha)e^{B(t,T_\alpha)x} + NA(t,T_\beta)e^{B(t,T_\beta)x} + \sum_{i=\alpha+1}^{\beta} \tau_i K A(t,T_i) e^{B(t,T_i)x}. \tag{3.6}$$

It is important to note that the x parameter in Expression 3.6 is the integration parameter and not the shifted short rate. $A(t,T_i), B(t,T_i)$ are defined in 2.47 with T_i representing the maturity, whereby the subscripts α, β denote the first and last date, respectively. The same is true for the year-fractions τ_i. Additionally, N denotes the notional, and K denotes the fixed rate.

Because the integration again concerns the normal distribution of the shifted short rate, the ppf of the normal distribution is used to specify the truncated integration range. As mentioned before, the MtM price of the RFS is a linear combination of log-normal variables. For this reason, there is no closed-form representation of the distribution of the MtM price of the RFS, making it not straight forward to accurately define the COS support based on the a priori knowledge about its distribution. The COS support should be chosen in such a way that the lower and upper bounds include all relevant information of the CDF. As a rule of thumb, one could use $[a,b] = [\pm\frac{N}{2}]$ as a COS support, where N represents the notional. However, a possibility for future research is the finding of a more accurate rule of thumb.

The PFE term structure of an IRS looks as follows: it first rises rapidly due to the uncertainty that comes with time, and, as time approaches maturity, more coupon payment

dates have passed, causing the PFE to decrease again and reaches zero at maturity. At maturity, the PFE of the IRS should be 0 again as all payment dates have passed. An illustration of the PFE term structure of an IRS is given in Figure 3.1. The PFE near maturity is low compared to other evaluation times. In other words, the distribution of the MtM price (and thus that of the exposure) is the widest somewhere in the middle of the life time of the trade and is much narrower close to maturity. It is therefore not a good idea to use an uniform truncation range of the MtM price distributions, i.e. the COS support, for different points in time: when this truncation range is too wide, we need to include more cosine terms in the Fourier-cosine series expansion. One could dynamically change the COS support depending on the evaluation time.

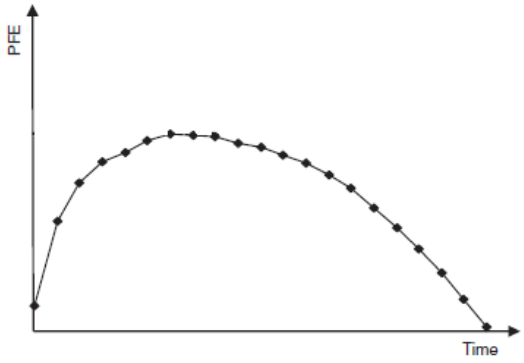

Figure 3.1: Illustration of the PFE term structure of an IRS [4].

Using the calculated characteristic function for the MtM of an RFS, the expressions for the Fourier-sine expansion given in 2.7.2 can be used to obtain an approximation of the CDF. The PFE is found by searching for the value of the input parameter of the CDF function that returns the quantile at 97.5%.

A pseudo code for the one-dimensional COS method is given in Algorithm 2.

EXPOSURE

In the previous subsection, we discussed the methodology of using the COS method to recover the CDF of the MtM of an RFS. However, we are interested in the exposure of an RFS in the context of CCR. Here we explain how to recover the CDF of the exposure using the COS method.

For a single RFS, the exposure is defined as $\mathrm{E}_t(X_t) := \max\{V_t(X_t, 0\}$ following Definition 2.1.1. The maximum operator yields a jump in the CDF of the exposure of an RFS at where the MtM price equals 0. The discontinuity gives rise to the Gibbs phenomenon around the jump when we use Fourier series to reconstruct the exposure function directly. It is still possible, as we will show later in counterparty level PFE calculation, to follow the same methodology as set out earlier, but with a filter added, to recover the CDF of the exposure. In that case the ch.f. we need to calculate using the quadrature

Algorithm 2: 1D COS method

Input : Initialise model parameters a and σ, choose number of expansion terms N_e, quadrature points N_q and time points N_t;
Set the integration range $[l,\ u]$ and COS support $[a,\ b]$;
Find the PFE:
for *i=1,...,N_t* **do**
Use numeric integration to calculate the characteristic function, having a form as in 3.5, using the Clenshaw–Curtis quadrature ;
Calculate the Fourier-cosine coefficients using the numerically integrated characteristic function;
Multiply the Fourier-cosine coefficients with the sine basis functions to obtain the CDF as in 2.61;
Use transformation 3.8 to find the CDF of the exposure;
Use root finding algorithm to find the PFE;
end

rule is the following:

$$\phi(\omega) = \int_{-\infty}^{\infty} e^{i\omega \max\{V_{IRS}(x),0\}} \cdot \frac{1}{\sqrt{2\pi}\sigma_X} e^{-\frac{1}{2}\left(\frac{x-\mu_X}{\sigma_X^2}\right)^2} dx. \tag{3.7}$$

There is, however, an alternative way to recover the CDF of the exposure highly efficiently, despite of the presence of the jump. It is done as follows.

One can observe that the distribution of the exposure is the same as the distribution of the MtM of an RFS, when the MtM price is larger than 0. This means we can first approximate the CDF of the smooth MtM of an RFS and then use a transformation to get the CDF of the exposure. More specifically, we use

$$F_X(x>0) = \begin{cases} 0 & \text{if } x \le 0, \\ F_X(x) & \text{if } x > 0. \end{cases} \tag{3.8}$$

This gives the desired CDF of the exposure where $F_X(x) = 0$ for $x \le 0$, and $F_X(x)$ for $x > 0$. This transformation ensures that the COS method is still applied to a smooth function because the discontinuity at zero is omitted. This ensures a convergence rate.

3.3. THREE-DIMENSIONAL DYNAMICS

To extend the COS method developed in the previous section to FX derivatives, we need to involve two more risk factors, and thus, two more dimensions to the problem-to-solve.

The interest rate swap discussed in the previous section exchanges the floating leg for the fixed leg when both legs have the same currency. However, the legs can also be of different currencies.

We start with Gaussian one-factor shifted short-rate processes $x_d(t)$ and $x_f(t)$ under their respective risk-neutral measures $\mathbb{Q}^d$ and $\mathbb{Q}^f$. The subscripts d and f indicate the domestic and foreign interest rates, respectively. The FX rate $X(t)$ is modelled using a geometric Brownian motion under the domestic risk-neutral measure, as commonly seen in literature, such as [36]–[38]. The dynamics are given by

$$dx_d(t) = -a_d x_d(t)dt + \sigma_d dW_d^{\mathbb{Q}^d}, \tag{3.9a}$$

$$dx_f(t) = -a_f x_f(t)dt + \sigma_f dW_f^{\mathbb{Q}^f}, \tag{3.9b}$$

$$dX(t) = \left(r_d(t) - r_f(t)\right) X(t)dt + \sigma_X X(t) dW_X^{\mathbb{Q}^d}. \tag{3.9c}$$

Here, a_d and a_f are the speed of mean reversion for each currency, and σ_d, σ_f and σ_X are the volatilities of the respective models. The short rates $r_d(t)$ and $r_f(t)$ in the dynamics of the exchange rate are required for the absence of arbitrage A.0.10. The short rates in the dynamics of the exchange-rate are acquired using the relation $r_i(t) = x_i(t) + \beta_i(t)$, where $\beta_i(t)$ is a deterministic function, and the subscript i can be d or f.

Notice that the foreign shifted short rate is given in the foreign risk-neutral measure. The dynamics of the foreign short rate must be converted to the domestic measure to be able to combine the dynamics in one model. Using Girsanov's theorem, Equation 3.9b becomes

$$dx_f(t) = \left[-a_f x_f(t) + \sigma_f \sigma_X \rho_{fX}\right] dt + \sigma_f dW_f^{\mathbb{Q}^d}, \tag{3.10}$$

where ρ_{fx} is the correlation between the FX rate and the foreign interest rate. A derivation is given in Appendix A.0.11.

For risk management purposes like calculating the potential future exposure, we need to consider the dynamics in the real-world measure $\mathbb{P}$. The change to the real-world measure relaxes the no-arbitrage restriction of the exchange-rate drift. Another way of looking at this is that in practice the theoretical triangle relation between the interest rates and the FX rate does not hold, which suggests that we can relax the relation between the drift terms.

In the real-world measure, the dynamics of the exchange rate are given by

$$dX(t) = \mu X(t)dt + \sigma X(t) dW^{\mathbb{P}^d}(t). \tag{3.11}$$

The change in dynamics for the shifted short rates from the domestic risk-neutral measure, as in Equation 3.9, to the domestic real-world measure is entirely captured in the choice of coefficients $a_d, a_f, \sigma_d, \sigma_f$ and σ_X. The solutions to the processes in the domestic real-world measure are then given by

$$\begin{aligned}
x_d(t) &= x_d(0)e^{-a_d t} + \sigma_d \int_0^t e^{-a_d(t-s)} dW_d(s), \\
x_f(t) &= x_f(0)e^{-a_f t} + \frac{\sigma_f \sigma_X \rho_{fX}}{a_f}\left(1 - e^{-a_f t}\right) + \sigma_f \int_0^t e^{-a_f(t-s)} dW_f(s), \\
\log(X(t)) &= \log(X(0)) + \left(\mu - \frac{1}{2}\sigma_X^2\right) t + \sigma_X W_X(t).
\end{aligned} \tag{3.12}$$

3.4. THREE-DIMENSIONAL MONTE CARLO

To obtain the potential future exposure using Monte Carlo simulation for a portfolio involving three risk factors, paths for each risk factor need to be generated first. The path generation of each risk factor is done in the same way as the one-dimensional case. However, an extra step is needed to incorporate the correlations between the three risk factors, which are fully determined by the correlations of the Brownian motions of the respective dynamics. The usual way of simulating correlated random Normal variables is to apply Cholesky decomposition on the correlation matrix, i.e.

$$d\mathbf{W}d\mathbf{W}^T = \begin{bmatrix} 1 & \rho_{df} & \rho_{dX} \\ \rho_{df} & 1 & \rho_{fX} \\ \rho_{dX} & \rho_{fX} & 1 \end{bmatrix} dt. \tag{3.13}$$

The Cholesky decomposition decomposes the above matrix using a lower triangular matrix $\mathbf{L}$ such that $\mathbf{W} = \mathbf{L} \cdot \tilde{\mathbf{W}}$, where

$$\mathbf{L} = \begin{bmatrix} 1 & 0 & 0 \\ \rho_{df} & \sqrt{1-\rho_{df}^2} & 0 \\ \rho_{dX} & \dfrac{\rho_{fX}-\rho_{df}\rho_{dX}}{\sqrt{1-\rho_{df}^2}} & \sqrt{\dfrac{\rho_{df}^2 - 2\rho_{df}\rho_{dX}\rho_{fX}^2 + \rho_{dX}^2 + \rho_{fX}^4 - 1}{\rho_{df}^2 - 1}} \end{bmatrix}. \tag{3.14}$$

The computer generates a system of independent Brownian motions, and the correlation is incorporated by multiplying the lower triangular matrix shown above. Afterwards, the same steps as for the 1D case are followed to yield the paths for the short rates and the exchange rate.

Once the scenarios are generated for all risk factors at each discretised time point, the MtM price or exposure scenarios can be calculated for each time point. The PFE is then again obtained by finding the 97.5%-quantile from the distribution at each time point.

A pseudo code for the three-dimensional Monte Carlo algorithm is given in Algorithm 3.

3.5. THREE-DIMENSIONAL COS METHOD

Here we extend the COS method to calculate PFEs of a trade involving three risk factors. The COS method in the case of three risk factors is similar to the case of one risk factor, i.e. one dimension. The difference purely lies in the calculation of the characteristic function.

The characteristic function is an integral over its state variables. In the 1D case, we could replace the short-rate process by the state variable x multiplied by the probability density of a normal distribution with the mean and variance matching the short-rate process. In the case of three risk factors, the dynamics are given in Equation 3.12, and the substitution of the processes by their state variables is more complex. Equation 3.12 shows that all processes consist of a deterministic part and a stochastic part. The stochastic part of the processes contain the random variables, which will hereafter be

Algorithm 3: 3D Monte Carlo algorithm

Start : Initialise model parameters a_d, a_f, σ_d, σ_f σ_x,σ_X, μ_x, ρ_{xd}, ρ_{xf}, ρ_{df} and X_0, and choose number of paths N_p and time points N_t;
Calculate the Cholesky decomposition matrix L;
Generate paths for the risk-factor $x_{d,i}$, $x_{f,i}$ and X_i:
Randomly sample standard normal distribution **Z for** *i=1,...,N_t* **do**
  Compute the Brownian Motion W_i using 2.52;
  Compute the correlated Brownian Motion $\tilde{W}_i = L \cdot W_i$;
  Compute the shifted short rates using the model dynamics 2.40 taking into account the change of measure from 3.10 Compute the exchange rate using the GBM dynamics 3.11
end
Calculate the exposure of the portfolio:
for *i=1,...,N_t* **do**
  Compute the MtM value of the portfolio for each path;
  Floor the MtM values for each path to find the exposure;
  Find the 97.5% quantile to obtain the PFE
end

referred to as the state variables $Z_d(t)$, $Z_f(t)$, $Z_X(t)$. We then write

$$\begin{aligned} x_d(t) &= x_d(0)e^{-a_d t} + \sigma_d Z_d(t), \\ x_f(t) &= x_f(0)e^{-a_f t} + \frac{\sigma_f \sigma_X \rho_{fX}}{a_f}\left(1 - e^{-a_f t}\right) + \sigma_f Z_f(t), \\ \log(X(t)) &= \log(X(0)) + \left(\mu - \frac{1}{2}\sigma_X^2\right) t + \sigma_X Z_X(t), \end{aligned} \tag{3.15}$$

with the state variables

$$\begin{aligned} Z_d(t) &= \int_0^t e^{-a_d(t-s)} dW_d(s), \\ Z_f(t) &= \int_0^t e^{-a_f(t-s)} dW_f(s), \\ Z_X(t) &= W_X(t). \end{aligned} \tag{3.16}$$

Normalising these state variables gives $Z_d(t) = \sigma_{z_d}\hat{Z}_d(t)$, $Z_f(t) = \sigma_{z_f}\hat{Z}_f(t)$ and $Z_X(t) = \sigma_{z_X}\hat{Z}_X(t)$ where $\hat{Z}_d, \hat{Z}_f, \hat{Z}_X$ are standard normally distributed. These state variables are correlated due to the correlation of the Brownian motions as shown in Equation 3.13. For numerical integration, it is required to rewrite the correlated state variables as a linear combination of independent state variables.

Note that, to solve the ch.f. numerically, we have to apply a multi-dimensional quadrature rule. To reduce the computational complexity there, a separation of the variables is desired. Even though it is difficult to fully separate the variables in the integrand of the ch.f. definition, we could employ Cholesky decomposition to do it partially.

Using the Cholesky decomposition of the correlation matrix $\boldsymbol{\Sigma}$ of variables $\hat{Z}_d, \hat{Z}_f, \hat{Z}_X$, we find a lower triangular matrix $\mathbf{L}$ such that $\hat{\mathbf{Z}} = \mathbf{L} \cdot \tilde{\mathbf{Z}}$, where $\tilde{\mathbf{Z}} = [\tilde{Z}_d \ \tilde{Z}_f \ \tilde{Z}_X]^T$ is a vector of independent standard normally distributed variables. The correlation matrix $\boldsymbol{\Sigma}$ is defined as

$$\boldsymbol{\Sigma} = \begin{bmatrix} 1 & \text{Cor}(\hat{Z}_d, \hat{Z}_f) & \text{Cor}(\hat{Z}_d, \hat{Z}_X) \\ \text{Cor}(\hat{Z}_f, \hat{Z}_d) & 1 & \text{Cor}(\hat{Z}_f, \hat{Z}_X) \\ \text{Cor}(\hat{Z}_X, \hat{Z}_d) & \text{Cor}(\hat{Z}_X, \hat{Z}_f) & 1 \end{bmatrix}, \tag{3.17}$$

where the entries of the correlation matrix can be calculated using Itô's isometry and the fact that all processes Z_d, Z_f, Z_x have zero mean. The entries are given below:

$$\text{Cor}(\hat{Z}_d, \hat{Z}_f) = \frac{\frac{\rho_{df}}{a_d + a_f}(1 - e^{-(a_d+a_f)t})}{\sqrt{\frac{1}{2a_d}(1 - e^{-2a_d t})}\sqrt{\frac{1}{2a_f}(1 - e^{-2a_f t})}}, \tag{3.18a}$$

$$\text{Cor}(\hat{Z}_d, \hat{Z}_X) = \frac{\frac{\rho_{dX}}{a_d}(1 - e^{-a_d t})}{\sqrt{\frac{1}{2a_d}(1 - e^{-2a_d t})}\sqrt{t}}, \tag{3.18b}$$

$$\text{Cor}(\hat{Z}_f, \hat{Z}_X) = \frac{\frac{\rho_{fX}}{a_f}(1 - e^{-a_f t})}{\sqrt{\frac{1}{2a_f}(1 - e^{-2a_f t})}\sqrt{t}}. \tag{3.18c}$$

Note that the correlation matrix is a positive definite matrix. This allows us to use the Cholesky decomposition $\boldsymbol{\Sigma} = \mathbf{L}\mathbf{L}^T$ with $\mathbf{L}$ acquired by calculating

$$\mathbf{L} = \begin{bmatrix} \sqrt{\Sigma_{11}} & 0 & 0 \\ \Sigma_{21}/L_{11} & \sqrt{\Sigma_{22} - L_{21}^2} & 0 \\ \Sigma_{31}/L_{11} & (\Sigma_{32} - L_{31}L_{21})/L_{22} & \sqrt{\Sigma_{33} - L_{31}^2 - L_{32}^2}. \end{bmatrix} \tag{3.19}$$

The complex exponent in the characteristic function now contains the processes from 3.15 multiplied corrected for correlation using the lower triangular matrix. The complex exponential is then multiplied by three standard normal distributions for each standard normal state variable $\tilde{Z}_i$. This integral is then solved using the three-dimensional Clenshaw–Curtis quadrature. Whenever the characteristic function is obtained, the cosine coefficients from Expression 2.57 can then be used in Expression 2.61 to obtain the CDF.

3.5.1. LOG-NORMAL DISTRIBUTION

In Subsection 3.2.1, it was explained that there were four parameters influencing the overall accuracy of approximation using the Fourier-cosine expansion. The analysis below mainly focuses on the effect of the number of quadrature points on the error of the COS method.

The number of quadrature points is the only parameter of which the value needs to be adjusted to cope with a three-dimensional quadrature to calculate the characteristic function. Increasing the number of quadrature points increases the accuracy of the characteristic function and thus of the approximation of the CDF. However, the drawback is the increase in computational costs. This drawback becomes especially significant considering three state variables, discretization of which form a three-dimensional matrix. For this reason, it is essential to balance the accuracy and computation time.

To get an indication of the effect of the number of quadrature points on the accuracy in a three-dimensional case, we analyse a function of which the distribution is known. Section 2.5 shows that the MtM values of an FX Forward or XCS have closed-form distribution functions because they are linear combinations of log-normally distributed variables, that is, both ZCBs and the exchange rate. However, we observe that omitting the subtraction of the domestic part in the expression of an FX Forward gives a distribution that can be evaluated analytically. The expression with analytical distribution is

$$V_t = N^f P^f(t,T) X(t). \tag{3.20}$$

Both the foreign ZCB and the exchange rate are log-normally distributed, and thus, their product is as well. In Equation 3.21, the distribution of both the foreign ZCB and the exchange rate are given along with the distribution of the entire expression of Equation 3.20. The distributions are as follows:

$$\begin{aligned}
\ln\left(P^f(z_f,t,T)\right) &\sim \mathcal{N}\left(\log\left(A_f(t,T)\right) - B_f(t,T)\gamma(t), B_f^2(t,T)\sigma_f^2\sigma_{z_f}^2\right),\\
\ln\left(X(z_x,t)\right) &\sim \mathcal{N}\left(\log(X_0) + \left(\mu - \frac{\sigma_X^2}{2}\right)t, \sigma_X^2\sigma_{z_x}^2\right),\\
\ln\left(N_f P^f(z_f,t,T)X(z_x,t)\right) &\sim \mathcal{N}\left(\log\left(N_f A_f(t,T)X_0\right) - B_f(t,T)\gamma(t) + \left(\mu - \frac{\sigma_X^2}{2}\right)t,\right.\\
&\quad \left\{\left(\sigma_X\sigma_{z_x}L[2,0] - B_f(t,T)\sigma_f\sigma_{z_f}L[1,0]\right)^2\right.\\
&\quad + \left(\sigma_X\sigma_{z_x}L[2,1] - B_f(t,T)\sigma_f\sigma_{z_f}L[1,1]\right)^2\\
&\quad \left.\left. + \left(\sigma_X\sigma_{z_x}L[2,2]\right)^2\right\}^{\frac{1}{2}}\right).
\end{aligned} \tag{3.21}$$

In these expressions, $A_f(t,T), B_f(t,T)$ are the parameters from the definition of a ZCB as given in Equation 2.47. The subscripts denote that the parameters use the coefficients corresponding to the foreign $G1++$ model. L is the lower triangular Cholesky-decomposition matrix, which is needed to incorporate the correlation of the state variables. For the sake of notation, we define

$$\gamma(t) = \frac{\sigma_f\sigma_X\rho_{fX}}{a_f}\left(1 - e^{-a_f t}\right).$$

In the previous section, it was shown how to rewrite the correlated risk factors as a linear combination of independent risk factors. The independence of the variables is

used to calculate the characteristic function of the MtM of our analytic case. That is,

$$\begin{aligned}\phi(\omega) &= \mathbb{E}\left(e^{i\omega V_t}\right) = \mathbb{E}\left(e^{i\omega\left[N^f P^f(z_f,t,T)X(z_X,t)\right]}\right)\\ &= \mathbb{E}\left(e^{i\omega g(\tilde{Z}_d,\tilde{Z}_f,\tilde{Z}_X)}\right) = \iiint_{\mathbb{R}^3} e^{i\omega g(\tilde{z}_d,\tilde{z}_f,\tilde{z}_X)} f(\tilde{z}_d,\tilde{z}_f,\tilde{z}_X)d\tilde{z}_d\, d\tilde{z}_f\, d\tilde{z}_X\\ &= \iiint_{\mathbb{R}^3} e^{i\omega g(\tilde{z}_d,\tilde{z}_f,\tilde{z}_X)} f(\tilde{z}_d)f(\tilde{z}_f)f(\tilde{z}_X)d\tilde{z}_d\, d\tilde{z}_f\, d\tilde{z}_X.\end{aligned} \tag{3.22}$$

Notice that in the third equality, we transformed the equation to a linear combination of independent, uncorrelated random variables denoted by a $\tilde{Z}$. The expression after the fourth equality shows the characteristic function is a function of the independent, uncorrelated state variables. Consequently, the joint probability density can be split into $f(\tilde{z}_d)$, $f(\tilde{z}_f)$, $f(\tilde{z}_X)$, which are all independent standard normal variables. The function $g(\tilde{z}_d,\tilde{z}_f,\tilde{z}_X)$ is the multiplication of the foreign notional N^f and the parts

$$\begin{aligned}P^f(z_f,t,T) &= A^f(t,T)e^{-B^f(t,T)\left(\gamma(t)+\sigma_f\sigma_{z_f}\left\{L[1,0]\tilde{z}_d+L[1,1]\tilde{z}_f\right\}\right)},\\ X(z_x,t) &= X_0 e^{(\mu-\sigma_X^2\backslash 2)t+\sigma_X\sigma_{z_X}\left\{L[2,0]\tilde{z}_d+L[2,1]\tilde{z}_f+L[2,2]\tilde{z}_X\right\}},\end{aligned} \tag{3.23}$$

with $\gamma(t)$ defined as before.

The integration range for each state variable can be chosen in the same way as in the one-dimensional case. Because state variables are all normalised, their density functions are standard normal distributions. The integration range for each state variable is, therefore, chosen using the per cent point function of a standard normal distribution with a chosen tolerance as given in Equation 3.2. By virtue of analysing an expression with a known distribution, the COS support can be chosen using the prior knowledge of the log-normal distribution given in 3.21. The COS support can, therefore, be chosen as the per cent point function of the log-normal distribution from 3.21 using Equation 3.3. The sensitivity analysis is then performed by changing the number of quadrature points while leaving the number of expansion terms, the integration ranges and the COS support the same, while looking at the difference between the analytical log-normal distribution and the approximation using the COS method. The results are presented in section 5.1

A pseudo code for the three-dimensional COS method is given in Algorithm 4.

3.5.2. RECOVERING THE CDF AND PFE OF A LIQUID PORTFOLIO

Below, the methodology for calculating the CDF and PFE using the COS method is further extended to FX Forwards, cross-currency swaps, a netting set including both types of products and a higher level portfolio (such as counterparty level).

FX FORWARD

The methodology of recovering the CDF of the MtM price and the PFE of an FX Forward trade remains exactly the same as in the previous section. The MtM of an FX Forward is given by

$$V_{FX} = N^f P^f(t,T)X(t) - N^d P^d(t,T). \tag{3.24}$$

Algorithm 4: 3D COS method

Start : Initialise model parameters a_d, a_f, σ_d, σ_f σ_x,σ_X, μ_x, ρ_{xd}, ρ_{xf}, ρ_{df} and X_0, and choose number of paths N_p and time points N_t;
Set the integration ranges $[l_i,\ u_i]$ and COS support $[a,\ b]$;
Find the PFE:
for *i=1,...,N_t* **do**
  Calculate the Cholesky decomposition L of 3.17;
  Use numeric integration to calculate the characteristic function, having a form as in 3.25, using the Clenshaw–Curtis quadrature ;
  Calculate the Fourier-cosine coefficients using the numerically integrated characteristic function;
  if *Considering counterparty-level exposure* **then**
    Multiply the Fourier-cosine coefficients with the spectral filter (described in Subsection 3.5.2);
    Multiply the above with the sine basis functions to obtain the CDF as in 3.31b
  else
    Multiply the Fourier-cosine coefficients with the sine basis functions to obtain the CDF as in 2.61;
  end
  Use transformation 3.8 to find the CDF of the exposure;
  Use root finding algorithm to find the PFE;
end

The first part is log-normally distributed, as was explained in the previous subsection. The domestic ZCB is also log-normally distributed. Hence, the distribution of the MtM of an FX Forward is a linear combination of log-normal variables, which has no closed-form distribution; therefore, we cannot choose the COS support using information about the distribution. The characteristic function is given by

$$\begin{aligned}\phi(\omega) &= \mathbb{E}\left(e^{i\omega V_{FX}}\right) = \mathbb{E}\left(e^{i\omega\left[N^f P^f(z_f,t,T)X(z_X,t) - N^d P^d(z_d,t,T)\right]}\right) \\ &= \mathbb{E}\left(e^{i\omega V_{FX}(\tilde{Z}_d,\tilde{Z}_f,\tilde{Z}_X)}\right) = \iiint_{\mathbb{R}^3} e^{i\omega V_{FX}(\tilde{z}_d,\tilde{z}_f,\tilde{z}_X)} f(\tilde{z}_d) f(\tilde{z}_f) f(\tilde{z}_X) d\tilde{z}_d\, d\tilde{z}_f\, d\tilde{z}_X.\end{aligned} \tag{3.25}$$

In the above equations $V_{FX}(\tilde{z}_d, \tilde{z}_f, \tilde{z}_X)$ is a function dependent on state variables, not to be confused with the distribution given in Expression 3.24. It is composed of the parts

$$\begin{aligned} P^d(\tilde{z}_d, t, T) &= A^d(t,T) e^{-B^d(t,T)\sigma_d \sigma_{z_d} \tilde{z}_d}, \\ P^f(\tilde{z}_d, \tilde{z}_f, t, T) &= A^f(t,T) e^{-B^f(t,T)\left(\gamma(t) + \sigma_f \sigma_{z_f}\left\{L[1,0]\tilde{z}_d + L[1,1]\tilde{z}_f\right\}\right)}, \\ X(\tilde{z}_d, \tilde{z}_f, \tilde{z}_X, t) &= X_0 e^{(\mu - 1\backslash 2\sigma_X^2)t + \sigma_X \sigma_{z_X}\left\{L[2,0]\tilde{z}_d + L[2,1]\tilde{z}_f + L[2,2]\tilde{z}_X\right\}}. \end{aligned} \tag{3.26}$$

The integration ranges for each state variable are set as the ppf of the standard normal distributions in the same way as was done in the analytical case. The COS support cannot be chosen in the same way because there is no a priori information about

the approximated distribution. It has to be chosen wide enough such that the CDF is well represented within the range or, more mathematically, the error in the COS method stemming from the truncation of the distribution is negligible. Therefore, it is better to choose the COS support too wide instead of too narrow. As a rule of thumb, we again set the COS support as $[a,b] = [\pm N^d]$ with the note that more research needs to be done to improve this choice.

Using the three-dimensional Clenshaw–Curtis quadrature, we obtain an approximation of the CDF based on Equations 2.57 and 2.61. The PFE is then again found via a root-finding algorithm.

CROSS-CURRENCY SWAP (XCS)

Again, the methodology to acquire the PFE profile of a cross-currency swap is exactly the same as we have seen in the previous sections. A XCS is defined in such a way that one receives the constant foreign rate and pays the floating domestic rate (and sometimes with reset of the Notional in the fixed leg). From Subsection 2.5, we know that the MtM price of an XCS is given by

$$V_{XCS} = N^d \left[X(0) \sum_{i=\alpha+1}^{\beta} \tau_i K X(t) P^f(t,T_i) - P^d(t,T_\alpha) + P^d(t,T_\beta) \right].$$

The characteristic function corresponding with the cross-currency swap is calculated in the same way as before, again requiring a transformation to independent, uncorrelated state variables using the Cholesky decomposition. Thus the characteristic function is calculated by applying the three-dimensional Clenshaw–Curtis algorithm to the integral shown below:

$$\begin{aligned} \phi(\omega) &= \mathbb{E}\left(e^{i\omega V_{XCS}}\right) = \mathbb{E}\left(e^{i\omega\left[N^d\left[X(0)\sum_{i=\alpha+1}^{\beta}\tau_i K X(z_X,t)P^f(z_f,t,T_i) - P^d(z_d,t,T_\alpha) + P^d(z_d,t,T_\beta)\right]\right]}\right) \\ &= \mathbb{E}\left(e^{i\omega V_{XCS}(\tilde{Z}_d,\tilde{Z}_f,\tilde{Z}_X)}\right) = \iiint_{\mathbb{R}^3} e^{i\omega V_{XCS}(\tilde{z}_d,\tilde{z}_f,\tilde{z}_X)} f(\tilde{z}_d) f(\tilde{z}_f) f(\tilde{z}_X) d\tilde{z}_d \, d\tilde{z}_f \, d\tilde{z}_X, \end{aligned} \tag{3.27}$$

where the functions making up $V_{XCS}(\tilde{z}_d,\tilde{z}_f,\tilde{z}_X)$ are of the same form as the functions in Equation 3.26. As a rule of thumb, the COS support is chosen as half of the notional $\frac{N}{2}$. The integration range is chosen in the same way as for the FX Forward, and the procedure to approximate the CDF and PFE using the calculated characteristic function is the same as well. However, similar to the one-dimensional case of the IRS, it is necessary to define the COS support dynamically for the sake of efficiency. The COS support that is wide enough for a high PFE value may be too wide for the calculation of PFE near maturity using the same number of cosine terms.

NETTING-SET-LEVEL EXPOSURE

The recovery of the individual derivatives, IRS, FX Forward and XCS, has already been discussed. The next step is to recover the PFE of a netting set consisting of multiple derivatives.

In the beginning of Chapter 2 in Definition 2.1.1, the netting-set-level exposure was defined. It is the maximum between the summation of the MtM value of all derivatives

and 0. In Subsection 3.2.2, a transformation was discussed such that we can approximate the CDF of the MtM of the netting set instead of approximating the CDF of the exposure of the netting set. This transformation ensured that a high accuracy around the discontinuity at 0 can be achieved in the absence of a jump at the origin.

The methodology of calculating the PFE for a netting set is exactly the same as the previous cases which deal with three risk factors.

For testing purposes, we generate an artificial portfolio as follows. Using a Python script, a portfolio is generated with different derivatives having random currency, fixed rate, tenor and maturity. An MS Excel file containing the used portfolio will be attached in Appendix C. For replicability, the file shows year-count fractions where Act360 is used as the day-count convention instead of dates.

The netted MtM price of the portfolio is calculated by adding up the value of each derivative. Therefore, the characteristic function becomes

$$\begin{aligned}\phi(\omega) &= \mathbb{E}\left(e^{i\omega V_{net}}\right) = \mathbb{E}\left(e^{i\omega V_{net}(\tilde{Z}_d,\tilde{Z}_f,\tilde{Z}_X)}\right) \\ &= \iiint_{\mathbb{R}^3} e^{i\omega V_{net}(\tilde{z}_d,\tilde{z}_f,\tilde{z}_X)} f(\tilde{z}_d) f(\tilde{z}_f) f(\tilde{z}_X) d\tilde{z}_d \, d\tilde{z}_f \, d\tilde{z}_X,\end{aligned} \tag{3.28}$$

where V_{net} is the sum of all derivatives in the portfolio. After we evaluate the ch.f. using numerical integration, we can calculate the CDF of the total MtM price of the netting set using Equations 2.57 and 2.61. The PFE is obtained using a root-finding algorithm similar to the other cases discussed.

The integration range for the state variables of the netted portfolio is the per cent point function of a standard normal distribution like in the previous cases. The COS support must be chosen large enough such that the error from the COS method (that particularly originated from truncating the density function) is suppressed to an ignorable level and is suggested to be updated dynamically for the balance between accuracy and speed. The dynamic updating is needed because as time increases, more and more derivatives will have matured, thereby lowering the PFE value. In this thesis we will not give a rule of thumb for choosing the COS support but assume that an accurate choice of the COS support is known by observing the PFE term structure acquired using the MC simulation. Among others, one future research topic is to define the COS support properly.

COUNTERPARTY-LEVEL EXPOSURE

In addition to the netting-set-level PFE quantification, it is also of interest to calculate the PFE on counterparty-level. Counterparty-level exposure is the total exposure with one counterparty, from multiple netting sets, often based on product type, as per Definition 2.1.1. Therefore the only change needs to be made, comparing to the netting-set-level exposure is in the definition of the characteristic function. For the exposure of a single derivative or of a netting set, Definition 2.1.1 shows that the exposure is the maximum between the MtM value of the derivative(s) and zero and it is thus possible to re-use the CDF for MtM price to resemble the CDF for the exposure, as we explained before. For counterparty-level exposure, however, a maximum is taken for every added netting set with a counterparty, and it is not possible to use the transformation of Equation 3.8 to retrieve the CDF of the counterparty-level exposure of a portfolio from that of the MtM

price. Approximating the CDF with a discontinuity at 0 using the COS method without any adjustment would give rise to the Gibbs phenomenon near the discontinuity. Below two methods are discussed to which preserve the accuracy of the COS approximation of a piecewise smooth CDF.

The first method is to rewrite the CDF of the counterparty-level exposure into an expression only involving netting-set-level exposure. This would allow the use of Transformation 3.8 and thus prevent any jumps in the CDF, thereby upholding accuracy. The second method is to utilize a spectral filter, a method well studied in the field of Engineering to reduce the Gibbs phenomenon and of which the main idea is to decrease the weights of high frequencies in the Fourier domain [39].

We will first analyse the possibility of rewriting the CDF of counterparty-level exposure into an expression involving netting-set-level exposure for two netting sets, both having one risk factor. The counterparty exposure in this situation is written as

$$E_c(x) = \max\{V_1(x), 0\} + \max\{V_2(x), 0\}, \tag{3.29}$$

where $V_1(x)$, $V_2(x)$ specify the first and second netting set, respectively, and the variable x denotes the shifted short rate. The CDF of the counterparty-level exposure is defined as $\mathbb{P}\left(E_c(x) \leq y\right)$. From the pricing functions given in Subsections 2.4 and 2.5, we can safely assume the pricing functions to be decreasing for increasing interest rate x because of the negative exponential relation in the ZCB formula. We assume that $V_2^{-1}(0) > V_1^{-1}(0)$. Using this and the fact that both netting sets are decreasing for increasing x, we can rewrite the CDF of the counterparty-level exposure as follows:

$$\mathbb{P}\left(E_c(x) \leq y\right) = \begin{cases} 0 & \text{whenever } y < 0, \\ \mathbb{P}\left(V_2(x) \leq y\right) & \text{whenever } 0 \leq y \leq V_2(V_1^{-1}(0)), \\ \mathbb{P}\left(V_1(x_+ V_2(x) \leq y\right) & \text{whenever } y > V_2(V_1^{-1}(0)). \end{cases} \tag{3.30}$$

This theoretically predicted behaviour is replicated using two netting sets, both consisting of only one interest-rate swap as shown in Figure 3.2.

Figure 3.2a shows that the pricing functions are monotonic decreasing functions with respect to the interest rate x. Figure 3.2 shows the CDFs of the MtM value of two different netting sets consisting of only one interest-rate swap. Additionally, the CDF of the total netting-set-level exposure and the counterparty-level exposure are compared. From Figure 3.2a, we can find the point $V_2(V_1^{-1}(0))$. This matches the point in Figure 3.2 where the CDF of netting set 2 and the total netting-set-level exposure intersect. This is predicted by Equation 3.30 because the CDF of a continuous random variable must be continuous, and at $y = V_2(V_1^{-1}(0))$, we must have $\mathbb{P}\left(V_2(x) \leq y\right) = \mathbb{P}\left(V_1(x_+ V_2(x) \leq y\right)$. Moreover, the graph shows that the CDF of the counterparty-level exposure follows the CDF of the exposure of netting set 2 for $0 \leq y \leq V_2(V_1^{-1}(0))$ and the total netting-set level thereafter.

The same method cannot, however, be applied to a situation in which the pricing functions depend on multiple risk factors. Suppose the MtM values of two netting sets

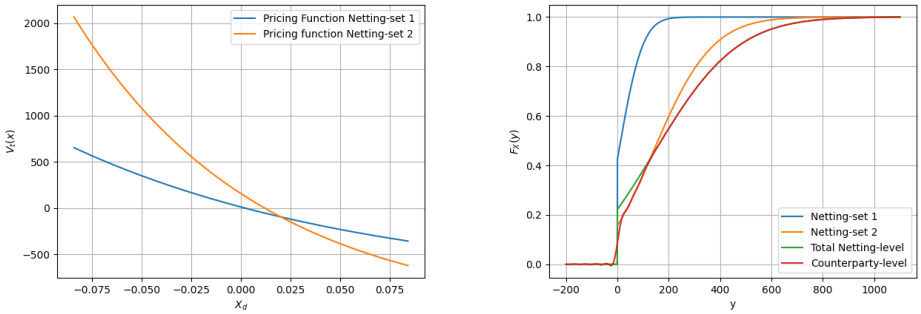

(a) Pricing functions of two netting sets, both consisting of one IRS

(b) A comparison between the CDFs of different exposure levels.

Figure 3.2: A graphic representation of rewriting the counterparty-level exposure into netting-set-level exposure. The considered netting sets contain one IRS each.

depend on two risk factors. The pricing functions would form a plane in space instead of the lines in the case of one risk factor. Two planes in space have an intersection line instead of an intersection point. The intersection line can either be constant in the MtM value of the netting sets or decreasing. The method of rewriting the counterparty-level exposure into netting-level exposure is not easily generalised for multiple risk factors. As the intersection line is decreasing, there is no simple region for y where the counterparty-level exposure can be split into netting-set-level exposure. Because this idea is not easily generalised to pricing functions depending on multiple risk factors, it was not further researched. Figure 3.3 shows that the idea used for one risk factor does not work for three risk factors. The CDF of the counterparty-level exposure does not follow any of the other plotted CDFs.

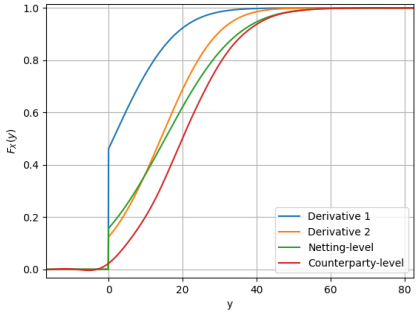

Figure 3.3: A comparison between the CDFs of different exposure levels depending on three risk factors.

The second method of alleviating the problem of the Gibbs phenomenon in the CDF of the counterparty-level exposure of a portfolio is the use of a spectral filter. A spec-

tral filter is applied in the Fourier domain, that is, the series coefficients are multiplied by a decreasing function in k. It is straightforward to include in the COS method without extra computational costs. The Fourier-cosine expansion of the PDF and CDF from Equations 2.58, 2.61 with added spectral filter become, respectively,

$$f_X^{\sigma}(x) \approx \sum_{k=0}^{N}{}' F_k \, \sigma(\frac{k}{N}) \cos\Big(k\pi \frac{x-a}{b-a}\Big), \tag{3.31a}$$

$$F_X^{\sigma}(x) \approx \frac{F_0}{2} \cdot (x-a) + \sum_{k=1}^{N} F_k \, \sigma(\frac{k}{N}) \, \frac{b-a}{k\pi} \, \sin\Big(k\pi \frac{x-a}{b-a}\Big). \tag{3.31b}$$

The Gibbs phenomenon plays an important role whenever there is a high probability of the exposure being negative, causing the CDF to make a jump at 0. If the CDF makes a large jump at 0, the PFE will not be far from the jump. For these situations, a low-order filter is desirable [39]. In this research, we use an exponential filter with $p = 2$ from [40], which is $\sigma(\eta) = \exp\left(-\alpha\eta^p\right)$ where p must be even, $\alpha = -\log(\epsilon_m)$, and ϵ_m is the machine precision. Research by Ruijter et al. [39] shows that the approximation is smoothed when a spectral filter is used and that the absolute error is dependent on the distance from the discontinuity. This behaviour is indeed observed when plotting the convergence rate in the L^1-norm for both the EE and the PFE, as shown in 5.16. The convergence rate at the discontinuity will not improve. The smoothing of the approximation increases the reliability of the result because any rapid fluctuations at the PFE will be smoothed out. The fluctuations are problematic for the root-finding algorithm used to recover the PFE.

Figure 3.4 shows the effect of adding a second-order exponential filter to acquire the CDF of the counterparty-level exposure of a portfolio with 100 derivatives. Because the CDF is evaluated at $t = 14$ years, only three derivatives have not matured and add to the exposure. The three derivatives have a low exposure and a high probability of negative exposure, as shown by the Gibbs phenomenon around 0. The exponential filter reduces the high-frequency fluctuations and becomes more accurate further from the jump, as expected.

Because there is no intelligent way to rewrite the counterparty-level exposure, the characteristic function is defined using the definition directly. This is shown in the equation below:

$$\begin{aligned}\phi(\omega) &= \mathbb{E}\left(e^{i\omega \mathrm{E}_c(V_t)}\right) = \mathbb{E}\left(e^{i\omega \mathrm{E}_c(V_t(\tilde{Z}_d,\tilde{Z}_f,\tilde{Z}_X))}\right) \\ &= \iiint_{\mathbb{R}^3} e^{i\omega \mathrm{E}_c(V_t(\tilde{z}_d,\tilde{z}_f,\tilde{z}_X))} f(\tilde{z}_d) f(\tilde{z}_f) f(\tilde{z}_X) d\tilde{z}_d \, d\tilde{z}_f \, d\tilde{z}_X,\end{aligned} \tag{3.32}$$

where $\mathrm{E}_c(V_t)$ represents the counterparty-level exposure of all derivatives in the portfolio. We now calculate the CDF of the MtM of the netted portfolio using Equations 2.57 and 3.31b. We now have the CDF of the counterparty-level exposure of the portfolio. The PFE is obtained using a root-finding algorithm similar to the other cases discussed.

Finally, the integration range and the COS support are acquired in the same way as explained for the netting-set-level exposure.

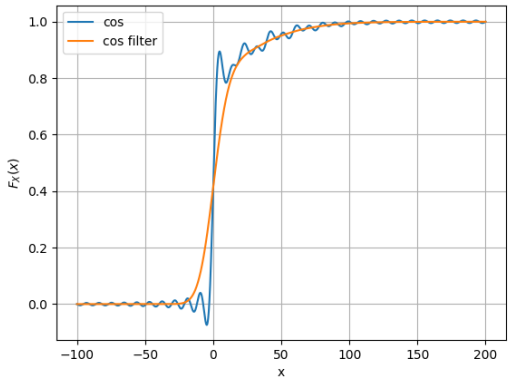

Figure 3.4: The CDF of a the counterparty-level exposure of a portfolio with 100 derivatives at $t = 14$ with a discontinuity at 0.

4

ERROR ANALYSIS

We have seen that an error is introduced in the derivation of the COS method. The error convergence will be studied for the COS approximation of the CDF of the exposure of a portfolio. The last section showed that depending on the type of exposure, it may be necessary to include a spectral filter in the COS method. Therefore, an error analysis will be performed for the situation with and without a spectral filter. Both situations have been studied extensively throughout the literature. First, the error analysis will be performed for the errors introduced in the derivation of the CDF without a spectral filter, as given in Equation 2.61. This will be followed by an investigation of the error introduced when applying a spectral filter to the COS approximation of the CDF, as shown in Expression 3.31b.

4.0.1. WITHOUT FILTERING

The COS method can be used without a spectral filter to approximate the CDF of the MtM value of a derivative or the netting-set level exposure of a portfolio. Two sources of errors are introduced in the derivation of Equation 2.61. These two sources are the series truncation of the Fourier cosine series expansion and the error related to approximating $A_k(x)$ by $F_k(x)$. Two more errors are introduced in the numerical integration step of the characteristic function. Truncation of the integration range gives rise to an error. Given the truncated integration range, the Clenshaw–Curtis quadrature introduces another error in the evaluation of the characteristic function. The propagation of the numerical integration errors will be studied rather than the numerical integration errors themselves, as they have been well studied in the literature. The first two error sources are well studied in [17] for the PDF approximation. The same approach is used for the error analysis of the CDF approximation.

The series truncation of the Fourier-cosine series on $[a,b]$ gives rise to the error:

$$\epsilon_1 = \frac{2}{b-a} \sum_{k=N+1}^{\infty} A_k \, \frac{b-a}{k\pi} \sin\left(k\pi \frac{x-a}{b-a}\right) \tag{4.1}$$

The substitution of the cosine series coefficients by the characteristic function approximation introduces the error:

$$\epsilon_2 = \frac{x-a}{b-a}\int_{\mathbb{R}\setminus[a,b]} f(x)dx + \sum_{k=1}^{N}\frac{b-a}{k\pi}\sin\left(\frac{k\pi(x-a)}{b-a}\right)\mathrm{Re}\left\{\int_{\mathbb{R}\setminus[a,b]} e^{\frac{ik\pi V(x)}{b-a}} f(x)dx e^{-i\frac{ka\pi}{b-a}}\right\} \tag{4.2}$$

The probability densities in this expression are, by fabrication, standard normally distributed as explained in Chapter 3.

To classify the errors from Expressions 4.1 and 4.2, we will give the definitions of the convergence rate. The definitions will consider different function classes, as the convergence rate depends on the decay rate of the cosine coefficients. We will derive the convergence rate of ϵ_1 and ϵ_2 using the following definitions from [34].

We start by defining the algebraic and exponential indexes of convergence in the following definitions.

Definition 4.0.1 (Algebraic index of convergence)**.** *The algebraic index of convergence $n(\geq 0)$ is the largest number for which*

$$\lim_{k\to\infty} \mid A_k \mid k^n < \infty, \quad k \gg 1,$$

where the A_k are the coefficients of the series. An alternative definition is that if the coefficients of the series, A_k, decay asymptotically as

$$A_k \sim \mathcal{O}(1/k^n), \quad k \gg 1,$$

then n is the algebraic index of convergence.

Definition 4.0.2 (Exponential index of convergence)**.** *If the algebraic index of convergence $n(\geq 0)$ is unbounded – in other words, if the coefficients, A_k, decrease faster than $1/k^n$ for any finite n – the series is said to have exponential convergence. Alternatively, if*

$$A_k \sim \mathcal{O}(e^{-\gamma k^r}), \quad k \gg 1,$$

with γ, the constant, being the 'asymptotic rate of convergence', for some $r > 0$, then the series shows exponential convergence. The exponent r is the index of convergence.

For $r < 1$, the convergence is called subgeometric.

For $r = 1$, the convergence is either called supergeometric with

$$A_k \sim \mathcal{O}(k^{-n}e^{-(k/j)\ln(k)})$$

(for some $j > 0$) or geometric with

$$A_k \sim \mathcal{O}(k^{-n}e^{-\gamma k}) \tag{4.3}$$

The next two propositions show the behaviour of both the algebraically and geometrically converging series. They use the definition of the algebraic and exponential index of convergence, respectively.

Proposition 4.0.3 (Series truncation error of algebraically converging series)**.** *It can be shown that the series truncation error of an algebraically converging series behaves like*

$$\sum_{k=N+1}^{\infty} \frac{1}{k^n} \sim \frac{1}{(n-1)N^{n-1}}.$$

The proof of this proposition is given in [41].

Proposition 4.0.4 (Series truncation error of geometrically converging series)**.** *If a series has geometric convergence, then the error after truncation of the expansion after* $(N+1)$ *terms,* $E_T(N)$*, reads*

$$E_T(N) \sim P^* e^{-N\nu}.$$

Here, constant $\nu > 0$ *is called the asymptotic rate of convergence of the series, which satisfies*

$$\nu = \lim_{n\to\infty} (-\log | E_T(n) | / n),$$

and P^* *denotes a factor which varies less than exponentially with* N*.*

Using the next proposition along with the previous propositions, we can analyse the convergence of errors ϵ_1 and ϵ_2.

Proposition 4.0.5 (Convergence of Fourier-cosine series)**.** *If* $g(x)$ *is infinitely differentiable with nonzero derivatives, then its Fourier-cosine series expansion on* $[a,b]$ *has geometric convergence. The constant* γ *in 4.3 is then determined by the location in the complex plane of the singularities nearest to the expansion interval. Exponent n is determined by the type and strength of the singularity.*

Otherwise, the convergence is algebraic. Integration by parts shows that the algebraic index of convergence, n, is at least as large as n'*, with* n' *denoting the highest order of derivative that exists or is nonzero.*

If the function $g(x)$ *has a discontinuity in* $[a,b]$*, say at* x_0*, then at the discontinuity, the series value converges to* $\frac{1}{2}(g(x_0^+) + g(x_0^-))$*, as the Fourier-cosine series has, in essence, the same properties as a Fourier series.*

The proof of this proposition is referred to in [34]. Moreover, Proposition 4.0.5 tells us that the approximation of the CDF will converge algebraically with low order in the case of a discontinuity. The low order of convergence is expected because of the Gibbs phenomenon observed in the case when a discontinuity is approximated using a Fourier series expansion.

We now have the theory needed to analyse the series truncation error and the error originating from the replacement of A_k by F_k. Applying the triangle inequality to the error coming from the truncation of the Fourier-cosine series gives us

$$\begin{aligned} \epsilon_1 &\leq \sum_{k=N+1}^{\infty} \left| A_k \cdot \frac{b-a}{k\pi} \right| \left| \sin\left(\frac{k\pi(x-a)}{b-a} \right) \right| \\ &\leq \sum_{k=N+1}^{\infty} \left| A_k \cdot \frac{b-a}{k\pi} \right| \\ &\leq C \sum_{k=N+1}^{\infty} |A_k| \end{aligned} \tag{4.4}$$

where C is a constant. In the last step, we used that $(b-a)/k\pi$ is decreasing for increasing k. Using propositions 4.0.3 and 4.0.4, we can formulate the following lemmas specifying the convergence for ϵ_1. The lemmas are taken from [17].

Lemma 4.0.6. *Error ϵ_1 converges exponentially in the case of density functions $g(x) \in \mathbb{C}^\infty([a,b])$ with nonzero derivatives:*

$$|\epsilon_1| < Pe^{-(N-1)\nu}, \tag{4.5}$$

where $\nu > 0$ is a constant, and P is a term that varies less than exponentially with N.

Lemma 4.0.7. *Error ϵ_1 for densities having discontinuous derivatives can be bounded as follows:*

$$|\epsilon_1| < \frac{\overline{P}}{(N-1)^{\beta-1}}, \tag{4.6}$$

where $\overline{P}$ is a constant and $\beta \geq 1$.

The next lemma gives a bound on error ϵ_2 and is taken from [17].

Lemma 4.0.8. *Error ϵ_2 consist of integration range truncation errors and can be bounded by*

$$|\epsilon_2| < Q\,|\epsilon_3| \tag{4.7}$$

where Q is some positive constant and

$$\epsilon_3 := \int_{\mathbb{R}\setminus[a,b]} f(x)\,dx.$$

The proof of this lemma is added in Appendix A.0.12.

An additional error is introduced by the propagation of the numerical integration error in the calculation of the characteristic function. A lower bound will be presented for the error propagated in the COS approximation. The lower bound is a loose bound taken from the working paper [42]. The error bound given in Lemma 4.0.9 holds for the COS approximation of the CDF both with and without the use of a spectral filter.

Lemma 4.0.9.

$$\tilde{F}_X^\sigma(x) = F_X^\sigma(x) + \mathcal{O}(\sqrt{K}) \cdot \epsilon(J, \mathrm{TOL}), \tag{4.8}$$

with $\epsilon(J,\mathrm{TOL})$ is an error term arising from the Clenshaw–Curtis quadrature rule and converging to 0 as $J \to \infty$ and $\mathrm{TOL} \to 0$. J is the number of points adopted in the Clenshaw–Curtis quadrature rule, and TOL is the integration truncation error.

The proof of this lemma is given in Appendix A.0.13. Here, it is also shown that the lemma also holds for the COS approximation without a spectral filter.

Using the results from 4.0.8, 4.0.6, 4.0.7 and 4.0.9, we can formulate a bound for the total error of the COS approximation to the CDF. Considering a high accuracy level in the characteristic function, that is, a sufficiently large amount of quadrature points on a wide

integration range, the total error either converges exponentially or algebraically. The total error converges exponentially whenever the density function has nonzero derivatives, belonging to $\mathbb{C}^{\infty}([a,b]) \subset \mathbb{R}$, that is,

$$|\epsilon| < Pe^{-(N-1)\nu} + C|\epsilon_3|. \tag{4.9}$$

or algebraically whenever one of the derivatives has a discontinuity, that is,

$$|\epsilon| < \frac{\overline{P}}{(N-1)^{B-1}} + C|\epsilon_3|. \tag{4.10}$$

The probability density function in the definition of ϵ_3 is standard normal. Therefore this error will converge exponentially. The convergence rate of the total error therefore depends on the distribution of the approximated cumulative density function. For a simple log-normal distribution we know that the density function belongs to $\mathbb{C}^{\infty}([a,b])$. Hence, it will show exponential convergence. The distribution of the other interest rate derivatives is a a linear combination of log-normal distributions, which has no known analytical expression. Hcine and Bouallegue showed in [43] that the distribution of a linear combination of log-normal random variables can be approximated by a skew log-normal distribution. Consequently, we expect the convergence rate to be exponential. However, a formal analysis of this error is left for future research.

4.0.2. With filtering

We add a spectral filter to the Fourier-cosine expansion whenever approximating the CDF of the counterparty-level exposure of a portfolio. It was presented in [39] that the application of spectral filters can restore the convergence of the Fourier series approximation of piecewise smooth functions. The convergence rate can even be restored to exponential convergence for functions with known discontinuities.

The convergence rate of a Fourier series approximation of a piecewise smooth function making use of a spectral filter turns out to be dependent on the order of the spectral filter. This behaviour was formulated in a theorem by Fang et al. [42], based on the findings by [39] and [40].

Theorem 4.0.10. *Let $f(y)$ be a piecewise p-times continuously differentiable $C^p([-\pi,\pi])$ function with one point discontinuity η; and $c_k = (1/2\pi)\int_{\pi}^{\pi} f(y)\exp\left(-ky\right)dy$ is the k-th Fourier coefficient. $\sigma(k/N)$ is a filter of order p. Then, if $y \neq \eta$, it holds that*

$$\left|f_N^{\sigma}(y) - f(y)\right| \sim \mathcal{O}(K^{1-p}),$$

where $f(y)$ is the filtered partial sum of a Fourier series, that is,

$$f_N^{\sigma}(y) = \sum_{|k|\leq N} c_k \sigma(k/N) e^{iky}.$$

This theorem states that the filtered Fourier expansion $f_N^{\sigma}(y)$ converges to the PDF $f(y)$. Using the integration relation between the PDF and CDF, we find that the filter Fourier series expansion $F_N^{\sigma}(x)$ given in Equation 3.31b converges to the CDF $F(x)$. Hence, Theorem 4.0.10 can be applied to find a bound on the convergence rate of F_N^{σ}.

As mentioned in [42], the bound is to be understood as a lower bound because [39] observed numerical evidence of faster convergence. However, no theoretical proof was given. The lower bound of the convergence rate of F_N^σ is given in Lemma 4.0.11.

Lemma 4.0.11. *If the CDF $F(x)$ is continuous at x, the absolute difference between $F_N^\sigma(x)$ given in 3.31b and $F(x)$ converges as follows:*

$$\left|F_N^\sigma(y) - F(y)\right| \sim \mathcal{O}(K^{1-p}),$$

where N is the number of Fourier series terms, and p is the order of the spectral filter.

The filtered Fourier series requires an expression for the characteristic function. The characteristic function is obtained using numerical integration. The numeric integration error is propagated in the filtered Fourier series. Lemma 4.0.9 gives an error bound for this additional propagated error.

If we consider a high accuracy level in the characteristic function, that is, a sufficiently large amount of quadrature points on a wide integration range, then the bound of the convergence rate of the filtered Fourier series is obtained from Lemma 4.0.11. We therefore expect to see an exponential convergence rate.

5

NUMERICAL RESULTS

This chapter includes the results of the numerical tests evaluating the efficiency and convergence of the COS method for calculating PFEs. The methodology of the performed numerical tests has been discussed in the previous chapter 3. The overview per section is given below.

The first section covers the numerical results of recovering CDF and calculating PFE using the COS method for cases involving only one risk factor. It starts with the sensitivity analysis of a simple log-normal PDF for the four control parameters of the COS method, which are the number of expansion terms, the number of quadrature points, the COS support and the integration range. These tests are followed by the sensitivity analysis of the MtM distribution of a ZCB, which is also log-normally distributed. The last numerical results check the performance of the COS based approximation of the exposure of an RFS. The accuracy of using the transformation 3.8 for the exposure are examined, followed by tests on the PFE profile of an RFS. Moreover, the importance of a dynamic COS support is demonstrated.

In the second section, the numerical results of PFE calculations using the COS method for cases involving three risk factors are presented and analyzed. This again follows the methodology set out in Chapter 3. The first result shows the impact of the number of quadrature points on the overall error of the COS method. The next results verify the accuracy of COS-recovered PFE profile of both the FX forward and the XCS. Finally, comparisons are made between the COS method and the MC method regarding the calculation speed and accuracy of PFEs on both the netting-set and counterparty level, whereby all tests are conducted for a portfolio with 100 derivatives.

5.1. ONE-DIMENSIONAL RESULTS

5.1.1. CONVERGENCE TESTS FOR LOG-NORMAL MODEL

In this subsection, a few sets of convergence tests are performed for a simple log-normal distribution with mean $\mu = 0.01$ and standard deviation $\sigma = 0.007$ using the methodol-

ogy described in 3.2.1.

As discussed earlier, when focusing on the error coming from the number of COS terms, the value of other variables are chosen as accurately are assigned conservative values such that other errors than the COS error are suppressed to an negligible level. Therefore, 2000 quadrature points are chosen on the truncated integration range $[l, u] = [-0.55, 0.57]$, obtained by taking the ppf of a normal distribution at an error tolerance level of $1e-15$. In practice, taking 400 quadrature points already achieves an accuracy of 10^{-9}. The support is chosen as $[a, b] = [0.62, 1.65]$, resulting from the ppf of a log-normal distribution with an error tolerance of 10^{-12}.

The accuracy of the COS approximations of the log-normal PDF is illustrated in Figures 5.1 and 5.2. The figures show the convergence of the approximation in both the L^1, L^2 norms. Logarithmic scaling is used for the y-axis in both plots, for the ease of observing the exponential convergence rate in Fourier-cosine series expansion w.r.t. the number of cosine terms. Figure 5.1 is based on 400 quadrature terms. The plot shows that increasing the number of expansion terms after 64 increases the total error. The reason is as follows. The numerical integration error originating from the calculation of the characteristic function adds to the total error via each cosine series coefficient. Therefore, the more expansion terms, the more times the numerical integration error is aggregated up. Using 2000 quadrature points increases the accuracy of the numeric integration and thereby alleviates the problem of a propagated numeric integration error, as shown in Figure 5.2. This confirms our theoretical error analysis in the previous chapter. The residual error in both figures comes from one of the other three control parameters or from the error introduced by the numeric integration in general.

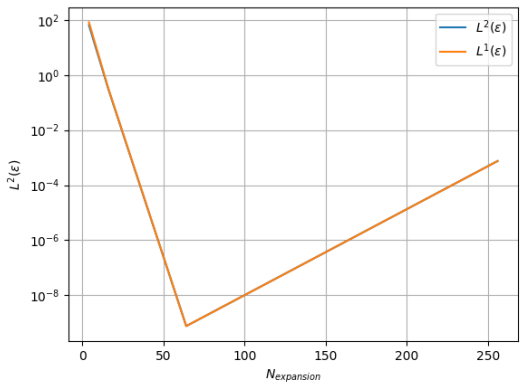

Figure 5.1: Approximating the log-normal PDF with $\mu = 0.01$, $\sigma = 0.007$ using 400 Clenshaw–Curtis quadrature points and varying the number of expansion terms.

Next, we further analyse the impact of the number of quadrature points on the accuracy of the COS method. The characteristic function of a log-normal variable has no closed-form expression; therefore, the exact PDF of the log-normal is compared to the approximation using the COS method. To ensure that the error is not coming from the

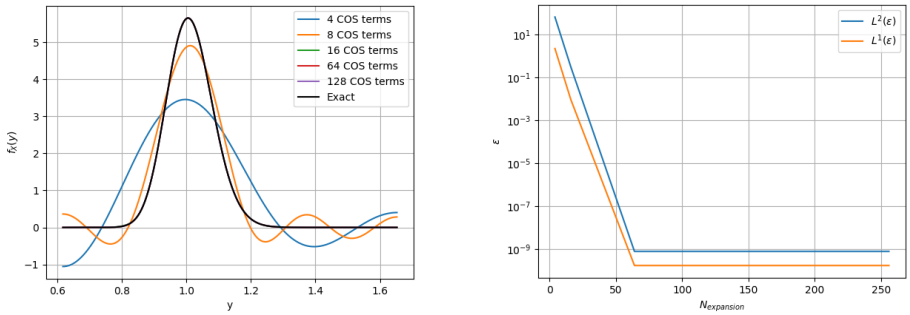

(a) Approximated log-normal density function for multiple COS expansion terms.

(b) Convergence of log-normal PDF in the L^1 and L^2 norm as a function of the number of expansion terms.

Figure 5.2: Approximating the log-normal PDF with $\mu = 0.01$, $\sigma = 0.007$ using 2000 Clenshaw–Curtis quadrature points and varying the number of expansion terms.

5

number of expansion terms, we take 128 expansion terms in this set of tests. The integration range and the COS support are determined the same way as before. The results of approximating the log-normal PDF by varying the number of quadrature points are summarized in Figure 5.3.

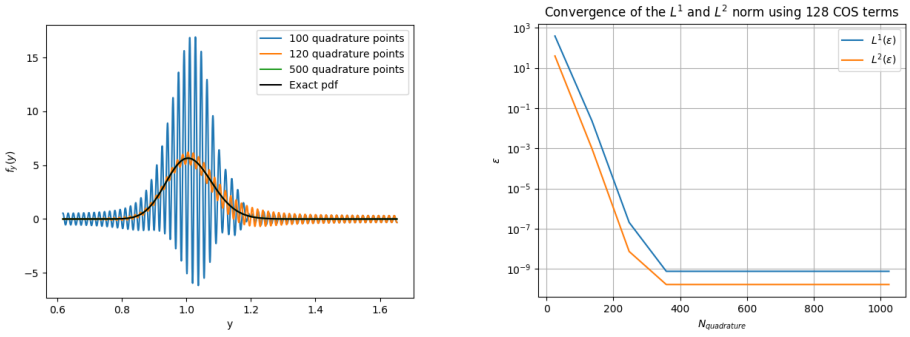

(a) Approximated log-normal density function for different numbers of quadrature points.

(b) Convergence of log-normal PDF in the L^1 and L^2 norm.

Figure 5.3: Approximating the log-normal PDF with $\mu = 0.01$, $\sigma = 0.007$ using 128 expansion terms and varying the number of quadrature points.

Subfigure 5.3b indicates an exponential convergence rate of the COS method in the number of quadrature points. Similar to the convergence plot of the number of expansion terms, the curve flattens after 400 quadrature points, the residual error coming from other control parameters. Recall that we have already observed the same level of remaining errors in the convergence tests for the number of expansion terms, and thus, it can be concluded that the residual error comes either from the truncation of the integration range or from the chosen COS support.

Figure 5.3a shows that the approximations of the PDF of a log-normal are very oscillatory for a low number of quadrature points. These fluctuations give rise to the large error of the COS method. The fluctuations in the approximation of the log-normal PDF are a result of the resonation of the fluctuations of the characteristic function, as shown in B.1. Increasing the number of quadrature points dampens the fluctuations in the characteristic function for higher frequencies and thereby increases the convergence.

As a third set of tests, the integration range is varied to analyse the impact of the integration range on the accuracy of the COS approximation. The number of expansion terms and the number of quadrature points are fixed at 128 and 500, respectively. The error tolerance level of the COS support is the same as before. The error tolerance level of the integration range is tuned, thereby the width of the integration range is varied. The results are presented in Figure 5.4. Figure 5.4b suggests that the error converges exponentially w.r.t. the width of the integration range, measured in terms of L_1 and L_2 norms. The same behaviour is observed as for the sensitivity analysis of the number of expansion terms and the number of quadrature points. The curve flattens when the tolerance is larger than 10^{-12}, giving the integration range $[l,u] = [-0.48, 0.50]$. The error of the COS approximation of the log-normal PDF is 10−9, like before. The residual error must be either from Fourier-cosine series truncation error, the COS support truncation error, or from the Clenshaw–Curtis quadrature.

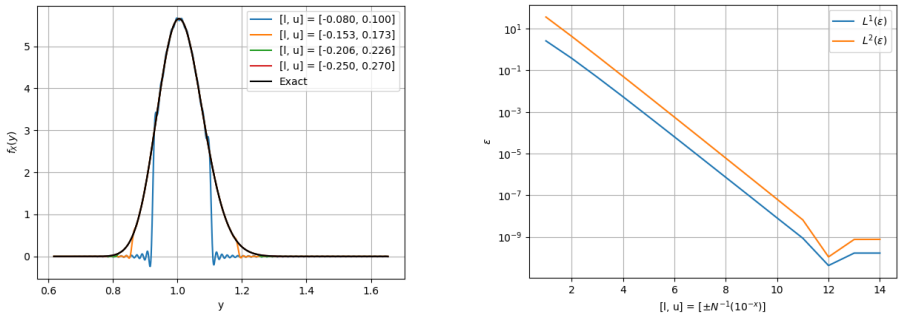

(a) Approximated log-normal density function for different numbers of quadrature points.

(b) Convergence of log-normal PDF in the L^1 and L^2 norm.

Figure 5.4: Approximating the log-normal PDF with $\mu = 0.01$, $\sigma = 0.007$ using 128 expansion terms and 400 quadrature points. The integration range is varied.

Finally, the impact of the COS support on the approximation of the PDF of a log-normal distribution is shown in Figure 5.5. Figure 5.5a indicates that the approximation of the PDF is accurate away from the boundaries of the domain of the COS support. This means that if one wants an approximation that is accurate on the domain $[a_1, b_1]$, then the COS support should be chosen at least 5% larger. Additionally, the graph shows that the approximation of the PDF using the Fourier-cosine expansion gives back an even function, which is aligned with the fact that Fourier-cosine series expansion is derived from the Fourier series expansion of an even-ed copy of the original function. This is even more

clearly visible in Figure 5.5b. The beginning of the COS support is fixed at $a = 0.6$, and the end point b is variable. The graph shows clearly that the function is even in the point b. If the Fourier-sine expansion were used to approximate the PDF instead of the Fourier-cosine expansion, then the approximation would be odd in the boundaries as shown in B.2.

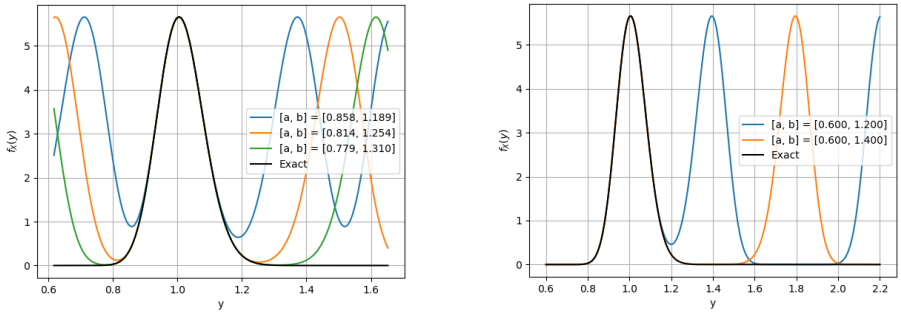

(a) Approximated log-normal density function for different numbers of quadrature points.

(b) Convergence of log-normal PDF in the L^1 and L^2 norm.

Figure 5.5: Approximating the log-normal PDF with $\mu = 0.01$, $\sigma = 0.007$ using 128 expansion terms and 400 quadrature points. The COS support is varied.

In the end, the goal is to calculate the potential future exposure. This risk quantification measure can be quickly retrieved from the CDF. The calculation of the CDF is analogous to the PDF, as shown in the previous chapter; the only difference is the basis functions used in the Fourier expansion. A convergence plot for the CDF of a log-normal distribution w.r.t. the number of expansion terms is presented in Figure 5.6. The other control parameters are set the same way as in the corresponding convergence tests for PDF.

Figure 5.6 shows that the COS approximation of the CDF converges faster than the COS approximation of the PDF in Figure 5.2, which is not surprising since the CDF is by definition one order higher differentiable than PDF and the Fourier series expansion convergence speed is determined by the smoothness of the original function. Similar to the approximation of the PDF, the convergence is exponential until 64 expansion terms, and the error curve flattens out afterwards. The residual error is from the same roots as we have seen for all considered convergence plots for the PDF tests but is of a lower level. This suggests that the CDF is easier to approximate using a Fourier expansion, which aligns with the fact that the CDF is by definition one order higher differentiable than the PDF.

During the sensitivity analysis, the observation was made that the COS method has an inherent difficulty in approximating the distribution of a log-normal distribution for a large standard deviation. Especially for $\sigma > 0.5$, the COS method needs significantly more expansion terms to approximate the CDF of a log-normal distribution. This behaviour is depicted for $\sigma = 0.5$ and $\sigma = 1$ in Figures B.3 and B.4, respectively. Additionally, Figure B.3 shows that whenever the number of expansion terms becomes very large,

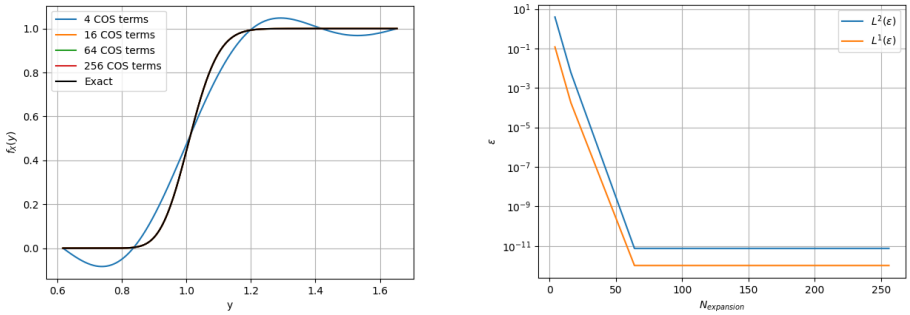

(a) Approximated log-normal density function for multiple COS expansion terms.

(b) Convergence of log-normal PDF in the L^1 and L^2 norm as a function of the number of expansion terms.

Figure 5.6: Approximating the log-normal PDF with $\mu = 0.01$, $\sigma = 0.007$ using 2000 Clenshaw–Curtis quadrature points and varying the number of expansion terms.

that is, > 1024, the error made in the quadrature is blown-up, increasing the overall error. This can be solved by adding more quadrature points, thereby increasing the accuracy of the calculated characteristic function. This is again another topic for future research.

5.1.2. COS-RECOVERED CDF AND PFE

In this subsection, we test the performance of the COS method in recovering the CDF of single trades as well as of a portfolio, and in turn, the performance of the COS method in calculating the corresponding PFEs.

ZERO-COUPON BOND

From Subsection 3.2.2, we know that a ZCB has a log-normal distribution. This enables us to compare the exact distribution to the approximation using the COS method.

The convergence of the COS method is checked w.r.t. both the number of expansion terms and the number of quadrature points. The distribution of the ZCB in the $G1++$ is given by Expression 2.46 with the A, B parameters given by Expression 2.47. The numerical results are obtained using the same setup as used by Pitterbarg [37] and by Oosterlee and Grzelak [38]. The values of the mean-reversion coefficient, volatility and the ZCB using this setup are

$$a = 1\%, \quad \sigma = 0.7\%, \quad P^M(0,T) = e^{-0.02T}.$$

The number of expansion terms and quadrature points used in the numerical test for the ZCB are 64, 500, respectively. These numbers are used because the previous sensitivity analysis showed that these values are conservative enough to ensure a high level of accuracy. The integration range and the COS support are defined in the same way as before, i.e. using their respective per cent point functions and an error tolerance level close to machine precision, resulting in the ranges $[l,u] = [-3.96, 3.98]$ and $[a,b] = [0.03, 34.03]$. The testing ZCB has a maturity of 10 years, a notional of 1000 Euro and the PFE is studied at the point of 3.5 years in the future. The error convergence of the

COS method w.r.t. both the number of expansion terms and the number of quadrature points are plotted in Figure 5.7.

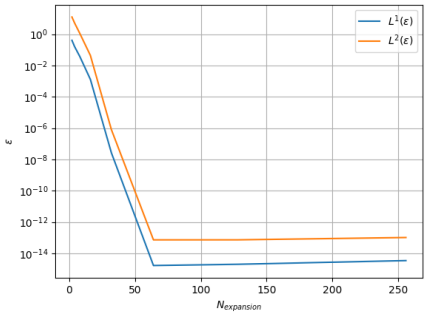

(a) Convergence of the CDF approximation of the ZCB in the L^1 and L^2 norm as a function of the number of expansion terms.

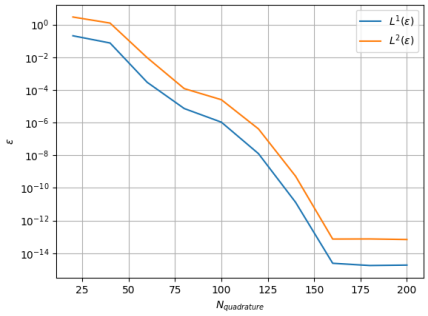

(b) Convergence of the CDF approximation of the ZCB in the L^1 and L^2 norm as a function of the number of quadrature points.

Figure 5.7: Approximating the CDF of a ZCB with $a = 1\%$, $\sigma = 0.7\%$. The number of quadrature points and expansion terms are 500, 64, respectively, for their corresponding graphs.

Figure 5.7a shows that the approximation of the CDF of a ZCB converges exponentially. The curve flattens after 64 expansion terms at the level of 10^{-14}. This behaviour is in agreement with the behaviour observed for a simple log-normal distribution. Using more than 64 expansion terms does not increase accuracy. The residual error comes from the inherent error of the Clenshaw–Curtis quadrature, which resonates through the series expansion. Analogously, the convergence plot shown in Figure 5.7b also suggests exponential convergence with respect to the number of quadrature points used. However, using only 160 quadrature points is already enough to get an error of order 10^{-14}, whereas 400 were needed for the simple log-normal distribution. The mean and standard deviation of the log-normal ZCB, $\log(A(t,T)) \approx 0.86$, $B(t,T)\sigma \approx 0.09$, are more favourable to approximate using the COS method than we have seen for the previous log-normal distribution.

INTEREST RATE SWAP

The PFE profile of a single receiver interest-rate swap calculated using the COS method is compared to the PFE acquired using the benchmark Monte Carlo simulation. The PFE profile is obtained by finding the 97.5% quantile for each point in time. The same values for the variables are used as in the tests for the ZCB. As an initial guess for the COS support, we chose the notional $\frac{N}{2}$ of the RFS with $N = \$1000, -$. Therefore, the COS support is $[a,b] = [\pm 500]$. The considered RFS has 10 payment dates starting one year from now and ending after 10 years. The fixed rate K is chosen to be 0.01. Based on the results of the previous analysis, we deem 64 expansion terms and 500 quadrature points sufficient to ensure a high level of accuracy. The PFE results of the MC method are generated for both 10,000 and 100,000 paths representing the possible scenarios of the interest rate.

Figure 5.8 illustrates the typical profile of a PFE term structure of an interest rate swap. The PFE falls at each payment date because the amount owed by the counterparty drops each time a coupon is just paid out, thereby decreasing the counterparty credit risk. All curves have zero PFE at $t = 0$, a PFE of $N \cdot K$ at $t = T_b = 10$ and, naturally a PFE of zero for $t > T_b$. Moreover, the graph shows that the PFE profiles calculated using the Monte Carlo simulations fluctuate around the PFE acquired using the COS method. Increasing the number of simulated interest-rate paths improves the accuracy of the MC method and thus MC based PFEs converge to the PFEs from the COS method.

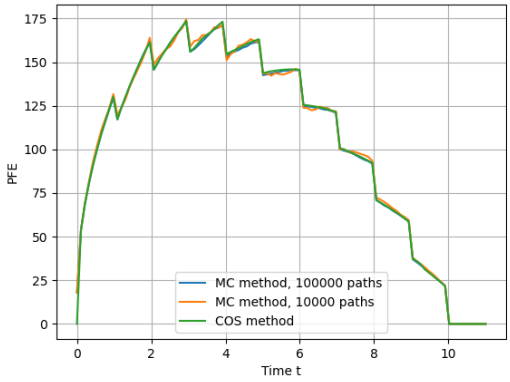

Figure 5.8: The PFE profile of a single RFS with 10 payments between $T_a = 1$ and $T_b = 10$.

Table 5.1 compares the computational time and error between COS and MC in more detail. The reference values are calculated using the COS method with very conservative parameters: 2000 quadrature points and 256 expansion terms, and 20 discretised time points. The error of both methods is the time average of the calculated PFEs at 20 different time points, expressed as a percentage of the total notional at $t = 0$. The table shows that the COS method, calculated using 100 quadrature points and 64 expansion terms, is more than 40 times faster than the MC method using $0.5 \cdot 10^5$ paths yet with a much lower error. The table also indicates that MC method converges w.r.t. the number of simulations. It is clear from the table that reaching the accuracy of the COS method would require many more simulations and, thus, much more time.

Table 5.1: Comparing the computational time and accuracy of calculating the PFE for different numbers of MC paths and the COS method. The error is averaged over the 20 considered time points and is expressed as a percentage of the total notional.

Method	CPU Time (seconds)	Time-averaged Error (%)
MC $(0.5 \cdot 10^5)$	38.3	0.043
MC (10^6)	54.2	0.033
MC $(2 \cdot 10^6)$	113.3	0.029
COS	0.9	0.006

The COS support used in Figure 5.8 is initialised as $[a,b] = [\pm 500]$. However, the PFE decreases as the RFS approaches maturity. As a result, the rise of the CDF happens on a very small interval of the initially chosen COS support. Graphically, this makes the CDF look like a step function on the wide interval, a step-function being a function with a discontinuity. At the place of the discontinuity, the Fourier-expansion approximation shows the Gibbs phenomenon, thereby making the PFE results inaccurate and unreliable. Theoretically, this behaviour can be explained by the fact that whenever the COS support is chosen too large, a large number of expansion terms is needed to capture the important cosine basis functions. The importance of the basis functions is determined by the weight of the cosine coefficients. The observed problem could be solved by either adding more expansion terms or shrinking the COS support. We chose to update the COS support dynamically to maintain a high level of efficiency. Figure 5.9a shows the approximated CDF of an IRS for a wide COS support $[a,b] = [\pm 300]$ and for a smaller interval $[a,b] = [0, 50]$. It is clear that when the COS support is chosen too large, the CDF will look like a step-function, and the resulting CDF approximation has the Gibbs phenomenon near the jump. Choosing a smaller COS support solves this problem and gives an accurate CDF. Figure 5.9b compares a static with a dynamically chosen COS support to calculate the PFE profile of a single RFS. We can see that the statically chosen COS support has a large error when the evaluation times are close to the maturity $9 < t < 10$. The difference between the results are substantial; not changing the COS support gives PFE results 450% larger than with the updated COS support. Changing the COS support for $t > 9$ to a smaller interval again gives the accurate approximation.

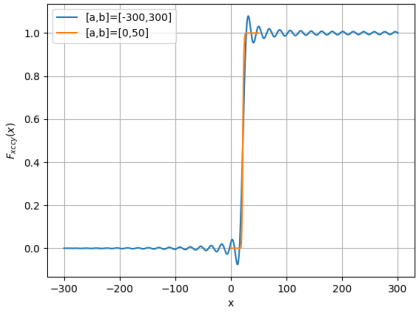

(a) Comparison of the approximated CDF of an IRS at time $t = 9$ close to maturity $T = 10$ for two sizes of the COS support.

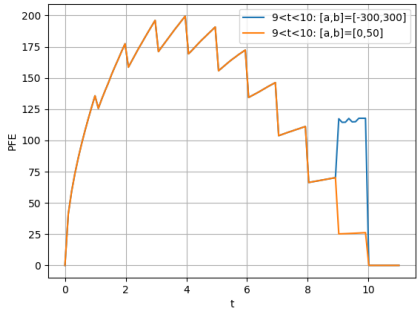

(b) Comparison of the static and dynamically chosen COS support to acquire the PFE profile of a single RFS.

Figure 5.9: The observed behaviour in the situation that the COS support is chosen too large for a single RFS with 10 payments between $T_a = 1$ and $T_b = 10$.

EXPOSURE

Exposure is defined as the maximum of the MtM value of a derivative and 0, as defined by Definition 2.1.1. The Gibbs phenomenon will present itself when we approximate a function with a discontinuity using the COS method. The fluctuations significantly

decrease the accuracy and reliability of the approximation. Subsection 3.2.2 discussed the possibility of using a transformation on the CDF of the continuous MtM distribution to obtain the CDF of the exposure. Figure 5.10a demonstrates the presence of the Gibbs phenomenon when we try to approximate the CDF of the exposure of an RFS directly. Figure 5.10b plots the resulting CDF of the exposure using a transformation: the Gibbs phenomenon disappears and the level of accuracy is much higher.

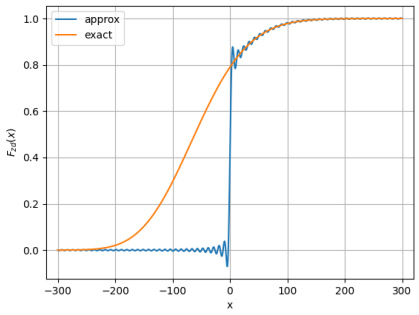

(a) Calculating the exposure of an RFS directly by employing a maximum in the integrand of the characteristic function.

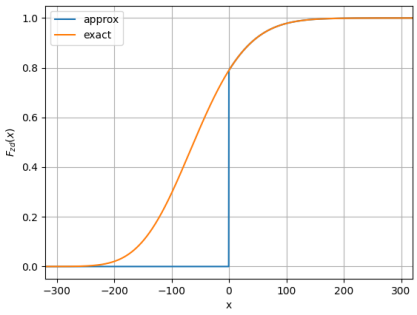

(b) Calculating the exposure of an RFS by employing a transformation of the MtM distribution of the RFS.

Figure 5.10: A comparison between calculating the exposure of an RFS directly using the characteristic function and transforming the MtM distribution.

5.2. THREE-DIMENSIONAL RESULTS

The numerical results for the three-risk-factor cases are again based on the same setup as by Pitterbarg [37] and Grzelak and Oosterlee [38]. To this extent, we define the functions for the ZCB by $P_d^M(0,T) = \exp(-0.02T)$ and $P_f^M(0,T) = \exp(-0.05T)$. The coefficients used to study the sensitivity of the COS method w.r.t. the number of quadrature points are

$$\sigma_d = 0.7\%, \sigma_f = 1.2\%, \sigma_X = 0.02\%, a_d = 1\%, a_f = 5\%, \mu_X = 0.008.$$

The correlation parameters as found in the correlation matrix 3.13 are

$$\rho_{df} = 25.00\%, \rho_{dX} = -15.00\%, \rho_{fX} = -15.00\%.$$

Furthermore, the initial spot FX rate (yen per dollar) is chosen to be 105.00.

5.2.1. CONVERGENCE TESTS FOR LOG-NORMAL MODEL

The sensitivity analysis is performed for the analytic distribution given in 3.20. The CDF of the MtM of this expression has a log-normal distribution, which can be compared to the COS-recovered CDF. The expression has three risk factors; therefore, the characteristic function is defined as the integral over three state variables. It thus requires a three-dimensional Clenshaw–Curtis quadrature to calculate the characteristic function.

The quadrature part is the only part changed from the one-dimensional setup, and thus, we will only analyze the impact of the number of quadrature points on the error of the COS approximation.

The foreign ZCB used in the sensitivity analysis has a maturity of 11 and we analyse the MtM value at $t = 4$ years. The integration ranges $[l, u]$ for the state variables $\tilde{z}_d, \tilde{z}_f, \tilde{z}_X$ are identical and defined as the 10^{-15} quantiles of the standard normal distribution giving $[l, u] = [\pm 7.94]$. The COS support $[a, b]$ can be analytically calculated and is chosen as the 10^{-10} quantiles of the distribution given in 3.21. The number of quadrature points ranges from 10 to 120 in all three directions. Further, 64 COS terms are used to reproduce the CDF of Expression 3.21. In Figure 5.11, the difference between the calculated and analytical CDF is measured in both the L^1 and L^2-norm. The plot uses a logarithmic y-scaling.

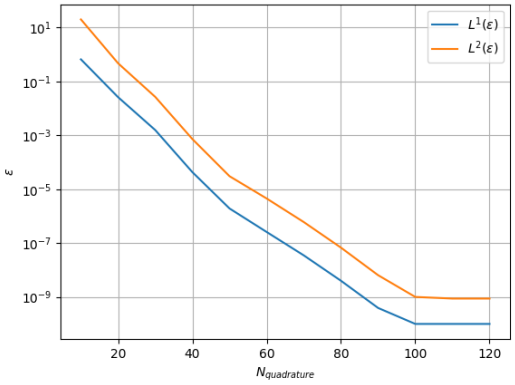

Figure 5.11: Exponential convergence results for the log-normally distributed CDF of a foreign ZCB exchanged to domestic currency in L^1, L^2-norm. The ZCB has a maturity of 11 years and is considered at $t = 4$.

The convergence plot shows exponential convergence w.r.t. the number of quadrature points. There is no increase in accuracy after 100 quadrature points in all directions. This behaviour is comparable to the one-dimensional case. The residual error is resulted from the Clenshaw–Curtis quadrature, which resonates to the final approximation error.

5.2.2. COS-RECOVERED CDF AND PFE

FX FORWARD

The parameters are the same as in the previous section. This is also true for the integration range $[l, u]$. Based on the convergence plot 5.11, we choose 60 quadrature points for a balance between high accuracy and a reasonable computation time. The COS support cannot be chosen as a quantile of the analytical distribution and is, therefore, set manually as $[a, b] = [\pm N_d/2] = [\pm 500]$, following our rule-of-thumb. The number of expansion terms remains 64.

Figure 5.12 shows a comparison of the PFE profiles of an FX Forward with a maturity of 11 years generated by the COS method and the MC simulation. The plot indicates that

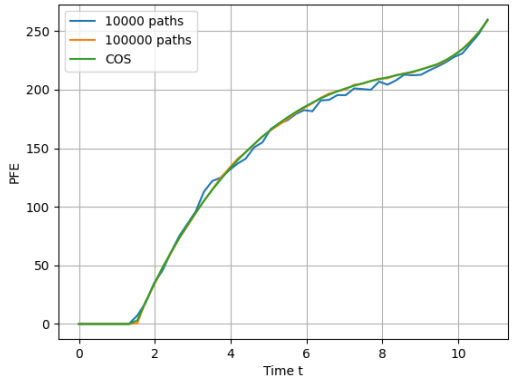

Figure 5.12: A comparison of the PFE profiles of an FX forward with maturity $T = 11$ created using the COS method and the MC simulation.

MC results with the lower amount of MC paths deviate further from the other two profiles. This behaviour is as expected due the fact that the accuracy of the MC method is lower as we go further to the right detail of the distribution due to fewer number of relevant scenarios in the details. The orange curve from the 100,000 path simulation is only faintly visible, meaning that PFE profiles from the COS method and the MC simulation with 100,000 simulations are nearly the same for all times t.

CROSS-CURRENCY SWAP

For the tests for the Cross-currency swaps, the parameters used in the MC simulation and the COS method are the same as in Section 3.5.1. Moreover, the testing XCCY swap starts at date $T_\alpha = 1$ year and ends at $T_\beta = 10$ years, with 10 payments between the start and end date. The constant rate K is chosen in such a way that the XCCY swap is fair valued at $t = 0$, giving $K = 0.02$. The integration ranges $[l_i, u_i]$ for all state variables are also the same, and 60 quadrature points are used to discretize the integral of each dimension. Similar to the calculation of the PFE profile of a FX Forward, the COS support cannot be chosen as a quantile of an analytical distribution and is, therefore, set manually, using our rule-of-thumb: The COS support $[a, b]$ is chosen to be $[\pm N_d/2] = [\pm 500]$ for $t \leq 9$ years and $[0, 50]$ for $9 < t < 10$.

Figure 5.13 compares the PFE profile from the MC simulation and that from the COS method. The MC simulation is done for 10,000 and 100,000 paths, where the PFE profile of the latter shows better alignment with the PFE profile of the COS method, as expected. To acquire the PFE profile using the COS method, the COS support must be updated for $t \geq 9$ years to maintain accuracy, as is explained in Subsection 5.1.2. The PFE profile of the XCCY swap has the classical form with 0 at $t = 0$, and $N \cdot K \cdot \tau = 20$ at $t = T_\beta = 10$ with a rise and fall in between. After each coupon payment, the PFE first drops and then starts to rise again as the uncertainty of the next coupon payment grows.

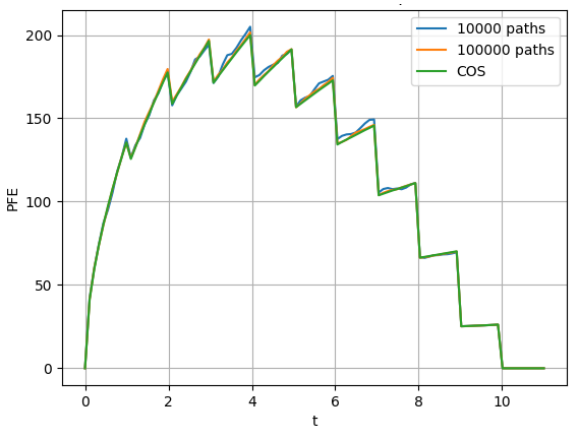

Figure 5.13: A comparison of the PFE profiles of an XCS swap between the COS method and MC simulation. The XCS has 10 payments between $T_\alpha = 1$ year and $T_\beta = 10$ years and considers a constant rate of $K = 0.02$.

NETTING-SET-LEVEL EXPOSURE

The coefficients for the $G1++$ model are the same as in the preceding subsections. A testing portfolios are generated as follows: Using a Python script, different derivatives are created with a random currency, fixed rate, tenor and maturity. The portfolios are attached in Appendix C. For replicability, the tables show year-count fractions based on Act360 day-count convention instead of dates. For the tests of netting-set level PFE calculations, the MtM value of the portfolio is the sum of the value of each derivative, reflecting the netting-set definition. The derivatives in the portfolio have different maturities, with the longest being $T = 14.7$ years.

The convergence is analysed for $t = 9.87$ years. First, the CDF of the exposure is approximated using conservative parameters, 130 quadrature points for all state variables and 200 expansion terms. The COS support is $[a,b] = [-2000, 2500]$. The results are compared to approximations that vary the number of expansion terms while keeping the number of quadrature points constant and vice versa. Figure 5.14 shows the results of the convergence analysis. Figure 5.14a shows that the error converges exponentially until 32 expansion terms are used. Using more does not decrease the error. Similarly, Figure 5.14b shows exponential convergence with respect to the number of quadrature points.

Figure 5.15a shows the PFE of the netting-set-level exposure of the portfolio attached in the appendix. The PFE profile consists of 101 equidistant time points between today, $t = 0$, and the longest maturity date, $T = 14.7$ years. The COS support is preset at $[a,b] = [-3000, 15000]$ and is changed to $[a,b] = [-1000, 2000]$ whenever the calculated PFE at the previous time point is below 1500.0. In the Monte Carlo simulation, 100,000 is considered. The figure shows that the potential future exposure is initially high and starts decreasing after 4.5 years. The decrease can be explained by an increasing number of matured derivatives. These matured derivatives have no inherent risk and, thus, do not add to the PFE.

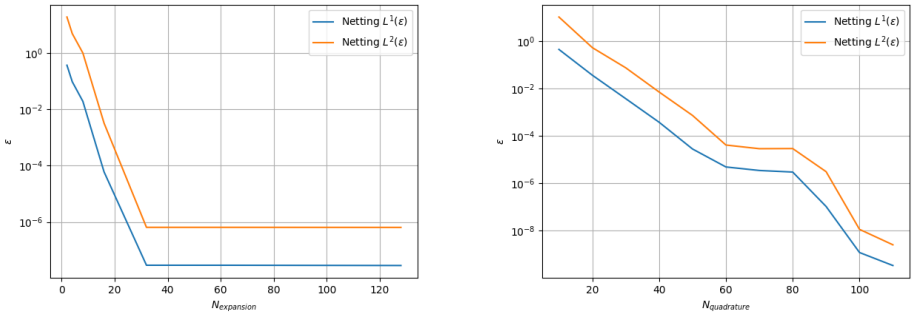

(a) Convergence of the CDF approximation as a function of the number of expansion terms.

(b) Convergence of the CDF approximation as a function of the number of quadrature points.

Figure 5.14: Convergence of the CDF approximation of the netting-set-level exposure using a COS benchmark with 100 quadrature points and 200 expansion terms.

The PFE results for the Monte Carlo algorithm and the COS method show identical profiles and results that are nearly the same. Figure 5.15b shows the relative difference between the PFE acquired using COS and MC as a percentage of the benchmark MC results. The plot shows that the relative difference is below 1% for the first 8 years and starts increasing with spikes after these 8 years. The width of the COS support is the reason for the increasing error after 8 years. The CDF of the netting set will reach the 97.5% quantile at values far smaller than the upper bound of the COS support, even though the COS support is already changed to account for this. Whenever the COS support is too broad, the CDF begins to look like a step function, as explained in the previous subsection for Figure 5.9. As the PFE is decreasing and the COS support remains the same, the COS method is increasingly inaccurate. However, an actual trading institution has a constant flux of trades, thereby maintaining exposure levels. In that case, the inaccuracy problems are not an issue.
In addition to the accuracy, it is important to analyse the time it takes to compute the PFE for both the COS method and the Monte Carlo algorithm. Three portfolios of different sizes are considered. The portfolio used in the error analysis consists of 100 derivatives and the other two consist of 64 and 32 derivatives, respectively. The portfolios are added in Appendix C. The PFE is calculated for 20 equidistant points in time ranging from today's date $t = 0$ until the maturity of the longest running derivative T. The benchmark PFE is calculated using the COS method with conservative parameters, 200 expansion terms and 130 quadrature points for every state variable. Analysis of the computational time is done using the 'cProfile' package, which shows both the total computation time and the computation time per function in the code. The time-averaged error is the difference between the benchmark PFE results and the PFE of the considered method. It is expressed as a percentage of the total notional at $t = 0$ of the corresponding portfolio. The total notional of the portfolios containing 100, 64 and 32 derivatives are, respectively, \$154,166.80, \$97,812.29 and \$46,368.27.

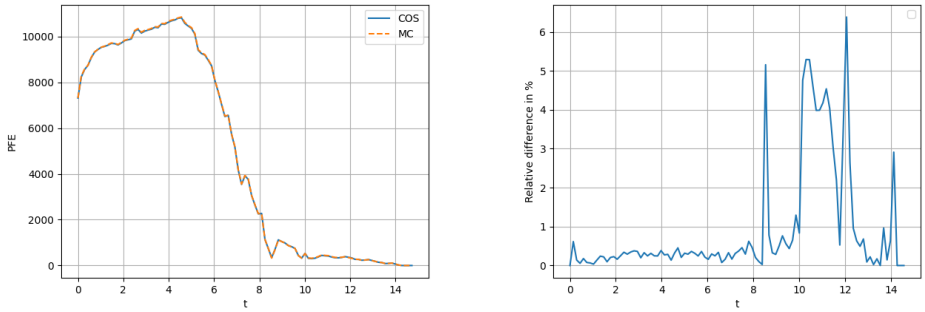

(a) PFE profile of netting-set-level exposure of a random portfolio.

(b) Relative difference of the calculated PFE expressed as a percentage of MC.

Figure 5.15: The PFE profile of the netting-set-level exposure of a randomly generated portfolio containing 100 derivatives for both MC and COS.

Tables 5.2, 5.3 and 5.4 compare the accuracy and computational time required to calculate the PFE of a portfolio with different numbers of derivatives. The tables show no apparent convergence for the number of MC simulations increasing from $0.5 \cdot 10^6$ to $2 \cdot 10^6$. The computational time of the MC simulation approximately doubles when the number of simulations is doubled. Moreover, the COS method is much faster and more accurate for all considered portfolios. It would take far more simulations in the Monte Carlo method to reach the level of accuracy of the COS method.

Table 5.2: The accuracy and computational time required to calculate the PFE of netting-set-level exposure of a portfolio with 100 derivatives. The error is averaged over the 20 considered time points and is expressed as a percentage of the total notional.

Method	CPU Time (seconds)	Time-averaged Error (%)
MC $(0.5 \cdot 10^6)$	91.6	0.021
MC (10^6)	179.6	0.019
MC $(2 \cdot 10^6)$	371.0	0.022
COS	11.5	0.002

Table 5.3: The accuracy and computational time required to calculate the PFE of netting-set-level exposure of a portfolio with 64 derivatives. The error is averaged over the 20 considered time points and is expressed as a percentage of the total notional.

Method	CPU Time (seconds)	Time-averaged Error (%)
MC $(0.5 \cdot 10^6)$	50.1	0.033
MC (10^6)	96.8	0.032
MC $(2 \cdot 10^6)$	193.2	0.034
COS	11.0	0.001

Table 5.4: The accuracy and computational time required to calculate the PFE of netting-set-level exposure of a portfolio with 32 derivatives. The error is averaged over the 20 considered time points and is expressed as a percentage of the total notional.

Method	CPU Time (seconds)	Time-averaged Error (%)
MC $(0.5 \cdot 10^6)$	29.2	0.014
MC (10^6)	57.5	0.014
MC $(2 \cdot 10^6)$	126.6	0.014
COS	10.5	0.002

Another interesting result is that increasing the number of derivatives has little effect on the computation time of the COS method but a large effect on the computation time of the Monte Carlo algorithm. The computation time of the Monte Carlo method increases whenever the number of derivatives in a portfolio increases. The MC method takes almost twice as long for a portfolio with 100 derivatives compared to a portfolio with 64 derivatives. This behavior can be explained by the computational complexity of the two methods: for the COS method the computation per time point is dominated by the numerical integration, i.e. the computational complexity is $\mathcal{O}(N_{cos}N_{quad}^d)$; the MC method on the other hand has the computational complexity linear in the number of trades per time point, i.e. $\mathcal{O}(N_{sim})N_{trade}$. And this is confirmed by a profile analysis using the Python package 'cProfile', which shows the time spend in each function of the code. The MC algorithm evaluates the pricing functions that are linear combinations of ZCBs for each path. Adding more derivatives will increase the number of ZCBs that need to be evaluated at all paths. Because the number of paths is large, this takes a long time. The COS method, in contrast, must only evaluate the ZCBs at the quadrature points and so evaluates 60 for each state variable, which does not take much time.

In addition to the effect of the number of derivatives in a portfolio, we will analyse the effect of the number of time points used in the PFE calculation on the computational time. We have not seen a sign of convergence for the number of simulations; therefore, the computational times will be studied using $0.5 \cdot 10^6$ paths. Three different numbers of timesteps are considered. To be more precise, we consider 20, 50 and 100 timesteps. Table 5.5 shows average computation times over five measurements[1] for three different portfolios and for increasing numbers of timesteps.

Table 5.5: Comparison of the computational times (in seconds) needed to compute the PFE for a netting-set portfolio with, respectively, 20, 50 and 100 time steps.

Number of Derivatives	MC	COS	MC	COS	MC	COS
32	28.6	10.8	73.1	26.0	151.5	51.9
64	47.6	11.2	119.4	26.6	241.0	53.6
100	94.1	11.9	233.5	28.4	469.5	56.8

Again, the analysis of the computational time is done using the 'cProfile' package. The table shows that there is a direct relation between the computation time and the number

[1] All measurements are added to the tables in Appendix B.2.

of timesteps. Whenever the number of timesteps increases, the computation time also increases. This relationship is almost linear. Using the analysis from the cProfile package, we can see that almost all computation time in the COS method comes from the discrete cosine transform. This transform is used to obtain the weights for the Fourier-cosine expansion. Obtaining the weights must be redone for each timestep and so scales linearly with the number of timesteps, independent of the number of derivatives.

COUNTERPARTY-LEVEL EXPOSURE

In this section, we test the performance of the COS method for counterparty level PFE calculations. It is demonstrated that the COS method has the potential to serve as a much faster alternative of the MC method for PFE calculations of real portfolios.

The model coefficients used in the counterparty level PFE calculations are the same as in the case of the netting-set-level. The same portfolio containing 100 derivatives is used.

First, we will analyse the statement by Ruijter et al. about the relation between the convergence rate and the distance from the discontinuity. The reference values of the CDF of the counterparty-level exposure of the portfolio are approximated using the COS method with very conservative parameters: 130 quadrature points for all state variables and 150 expansion terms. The convergence of the COS-recovered CDF is verified via varying first the number of quadrature points and then the number of expansion terms. For both reference value generation and the convergence tests we use the same COS support $[a,b] = [-100, 2500]$ and consider the CDF at $t = 9.87$ years. The errors for the EE and PFE, obtained from both CDFs, are studied in terms of L^1-norm, which is shown in Figure 5.16. Indeed, the absolute error in the L^1-norm is higher for the EE than for PFE. This is expected because, by definition, the EE is smaller than the PFE and, thus, closer to the discontinuity at 0.

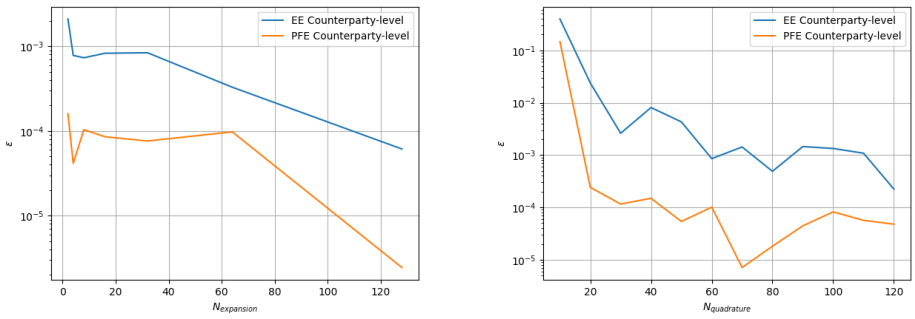

(a) Convergence of the CDF approximation as a function of the number of expansion terms.

(b) Convergence of the CDF approximation as a function of the number of quadrature points.

Figure 5.16: Error convergence of the filtered COS method in the L^1 observed in the EE and PFE.

In the same way, we examine the convergence rate of the entire CDF using the L^1 and L^2-norms. Figure 5.17 indicates that the filtered COS method still converges exponentially, as the y-axis is in log-scale, only that the slope is not as sharp as in the netting-set level

calculations. Moreover, the magnitude of the errors is three orders larger than the errors observed for the netting-set-level calculations. This difference in convergence rate is caused by the smoothness of the true CDFs. The CDF of the counterparty-level exposure directly approximates the exposure having a discontinuity at 0, whereas the CDF of the netting-set-level exposure is acquired by approximating the CDF of the MtM price of the portfolio, which is a smooth function, and then using the transformation in 3.8. The COS method converges faster for smooth functions [17].

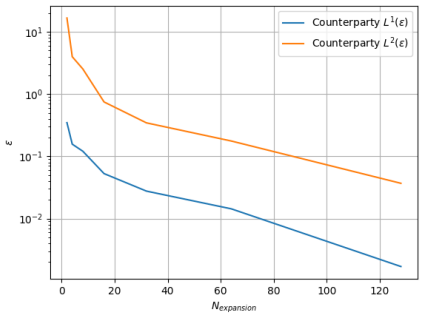

(a) Convergence of the CDF approximation as a function of the number of expansion terms.

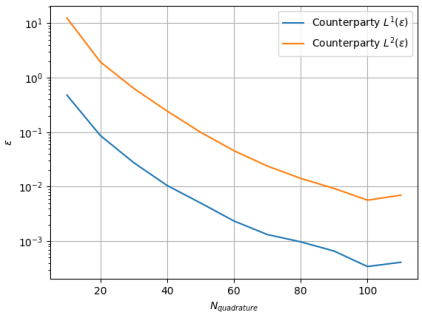

(b) Convergence of the CDF approximation as a function of the number of quadrature points.

Figure 5.17: Error convergence of the filtered COS method in the L^1 and L^2-norms

The PFE profile of the counterparty-level exposure of a portfolio containing 100 derivatives is plotted in Figure 5.18. The COS support is initialised as $[a,b] = [-100, 15,000]$ and changed to $[a,b] = [-100, 2000]$ if the previous PFE is below 1500. The numerical results are attained using the COS method with a second-order exponential filter as described in 3.5.2.

A comparison between the PFE profile using the COS method and that using a MC method is made in Figure 5.18. The graph shows that the PFE profile of the MC simulation closely match that of the COS method.

Figure 5.19 presents the plots between the absolute and relative difference of the PFEs calculated using the MC simulation and the PFEs from the COS method without a filter. The absolute difference between the two methods fluctuates around 40 euros on a maximal PFE of 12,300. The relative difference for the first 10 years stays below 0.5%. After 10 years, most derivatives have matured, and PFE decreases. If the absolute difference remains the same and the PFE decreases, then the relative difference logically increases. Initially, the changed COS support lowers the absolute difference near $t = 8.5$, although as the PFE keeps increasing, both the absolute difference and the relative difference increase. In practice, the portfolio is always be filled with derivatives that have not expired; therefore, it will most likely be in the situation of the first 6 years.

Analogous to the netting-set-level tests, Tables 5.6, 5.7 and 5.8 summarize the computational time and accuracy of three portfolio of different sizes. The PFE is calculated for 20 equidistant points in time ranging from today's date $t = 0$ until the maturity of the longest running derivative T. The reference value of the PFE is calculated using

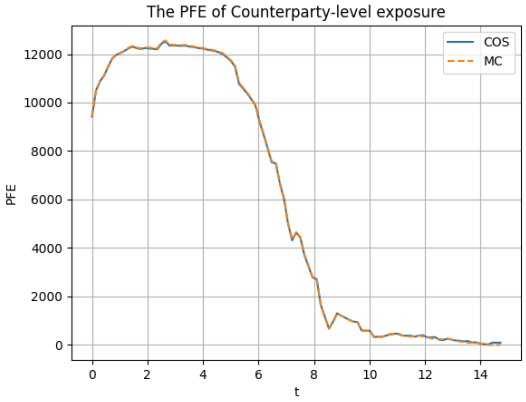

Figure 5.18: A comparison of the PFE profiles of counterparty-level exposure of a portfolio with 100 derivatives for the MC method and the COS method with and without a filter.

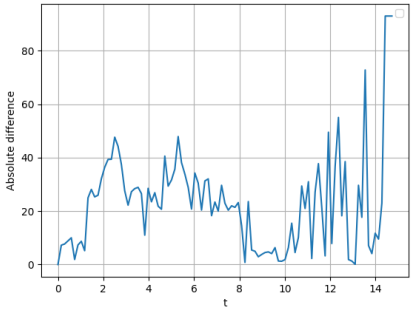

(a) Absolute difference of the PFE between the MC simulation and the COS method.

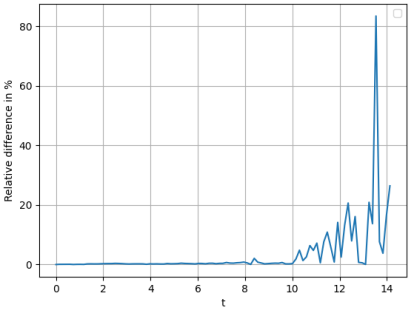

(b) Relative difference of the calculated PFE expressed as a percentage of MC.

Figure 5.19: The absolute and relative difference between the PFEs of counterparty-level exposure of a portfolio created by the MC simulation and the COS method.

the COS method with conservative parameters: 200 expansion terms and 130 quadrature points for every state variable. We again use the 'cProfile' package, to analyze both the total computation time and the computation time per function in the code. The time-averaged error is the average of the differences between the reference value and the tested PFEs across all time points. It is expressed as a percentage of the total notional at $t = 0$ of the corresponding portfolio. The total notionals of the portfolios containing 100, 64 and 32 derivatives are, respectively, \$154,166.80, \$97,812.29 and \$46,368.27.
Again, convergence in MC method is hardly observed by increasing the number of simulations from $0.5 \cdot 10^6$ to $2 \cdot 10^6$. The CPU times are similar to those observed for the netting-set-level exposure calculations, which is as expected because the same number of calculations need to be done or, in other words, the computational complexity of the

Table 5.6: The accuracy and computational time required to calculate the PFE of counterparty-level exposure of a portfolio with 100 derivatives. The error is averaged over the 20 considered time points and is expressed as a percentage of the total notional.

Method	CPU Time (seconds)	Time-averaged Error (%)
MC $(0.5 \cdot 10^6)$	92.4	0.026
MC (10^6)	183.3	0.027
MC $(2 \cdot 10^6)$	370.5	0.028
COS	11.5	0.007

Table 5.7: The accuracy and computational time required to calculate the PFE of counterparty-level exposure of a portfolio with 64 derivatives. The error is averaged over the 20 considered time points and is expressed as a percentage of the total notional.

Method	CPU Time (seconds)	Time-averaged Error (%)
MC $(0.5 \cdot 10^6)$	48.0	0.035
MC (10^6)	96.4	0.035
MC $(2 \cdot 10^6)$	196.5	0.030
COS	11.0	0.003

Table 5.8: The accuracy and computational time required to calculate the PFE of counterparty-level exposure of a portfolio with 32 derivatives. The error is averaged over the 20 considered time points and is expressed as a percentage of the total notional.

Method	CPU Time (seconds)	Time-averaged Error (%)
MC $(0.5 \cdot 10^6)$	28.8	0.019
MC (10^6)	58.8	0.019
MC $(2 \cdot 10^6)$	127.3	0.019
COS	10.5	0.003

MC method is the same as for netting-set level calculations. Hence, very similar results are observed for MC method considering the computational time: as we have previously seen, the computational time doubles whenever the number of paths is doubled, and the computational time almost doubles when comparing 64 to 100 derivatives.

The time-averaged error is higher for all considered portfolios compared to the netting-set-level exposure calculations. From the tables, it is clear that the COS method is much faster and more accurate. It would take far more simulations to reach the level of accuracy of the COS method.

Table 5.9 presents the impact of the number of timesteps used in the PFE calculations on the computational time. Theoretically, it is clear that the overall computational complexity 1) is linear in the number of time steps for both MC method and the COS method, 2) grows linearly in the number of derivatives for the MC method, while 3) stays unaffected by the number of derivatives for the COS method. Like before, we test these relations for three different portfolio sizes. We consider $0.5 \cdot 10^6$ paths for this analysis, as we did not observe an improved accuracy when increasing the number of MC simulations. The analysis was done in the same way as for the netting-level case, using the

'cProfile' module of Python. The computation times in the table are averages of five runs, which are added in Appendix B.3. Table 5.9 suggests that the computation time of the Monte Carlo method increases linearly in the number of derivatives. The increase in computation time for an increasing number of derivatives is much smaller for the COS method. The reason is the same as before for the netting-level exposure. For the MC simulation, the derivatives must be priced for all paths, which takes most of the computation time. The computation of the COS method stems mainly from the retrieval of the weights of the Fourier-cosine series and the large matrix multiplications. Because the number of quadrature points is constant, this does not increase for increasing number of derivatives. This is also the reason that the computation times grow almost linearly when increasing the number of timesteps for the COS method. The COS method is more efficient when considering a portfolio with a large number of derivatives.

Table 5.9: Comparison between the computational times (in seconds) needed to compute the PFE for a counterparty-level portfolio with, respectively, 20, 50 and 100 time steps.

Number of Derivatives	MC	COS	MC	COS	MC	COS
32	29.2	10.5	74.7	26.5	156.4	53.0
64	47.8	11.0	119.1	26.7	246.0	53.6
100	89.5	11.5	233.8	28.5	482.0	58.3

6

CONCLUSION

In this thesis, a new, semi-analytical method of calculating the PFE metric for CCR has been developed, tested and analyzed. The method is based on the Fourier-cosine expansion, and thus, is an extension of the COS method to the field of CCR quantification. This method aims to fulfill the need in the industry for fast and accurate PFE calculations in practice.

The research in this thesis focuses on the calculation of PFEs for liquid IR and FX portfolios involving up to three correlated risk-factors: a domestic and foreign short rate and the exchange rate of this currency pair. Both netting-set level and counterparty level PFEs are covered in our research. Regarding model choices, the short rates are modelled under the Hull–White model and for the exchange rates we assume they follow geometric Brownian motion. Note that, even though not directly tested, other model choices can be incorporated to the COS method as well.

The COS method is based on the key insight that the Fourier series coefficients of the CDF (and of the PDF) of the total exposure of the portfolio are readily available from the characteristic function. Once the model choices are made regarding interest rates and FX rates, the characteristic function of the total exposure can be solved numerically via quadrature rules, such as the Clenshaw–Curtis quadrature rule. The risk metrics, in our case, the PFE, can be attained once the CDF is reconstructed using the Fourier series.

A small adjustment is needed to the Fourier series coefficients when it comes to the counterparty level PFE calculations, since the CDF of the counterparty-level exposure of a portfolio has a discontinuity at 0. Fourier series expansion on such functions gives rise to the problem of the Gibbs phenomenon. To alleviate this problem, a well-studied spectral filter method is applied, which is simply to multiply the original series coefficients by a filter and thus requires no additional computation costs.

Our theoretical error analysis predicts stable convergence of the COS method and that the spectral filter restores the high convergence rate.

The numerical tests indeed confirm our theoretical analysis and we have observed exponential convergence of the COS method for both netting-set and counterparty level PFEs.

Additionally, the industry-standard MC simulation is compared to the COS method. For three artificial portfolios of different sizes, it was observed that the COS method is at least five times more accurate but takes only one-tenth of the CPU time of the MC method. Especially for portfolios with a large number of derivatives, the COS method is demonstrated to be at least one order of magnitude faster while reaching a higher accuracy. We conclude that the COS method is a much more efficient alternative for MC method, at least for portfolios involving three risk factors.
The limitation of applying the COS method for risk management purposes lies in the characteristic function calculation. The required numerical integration suffers from the 'curse of dimension' when more risk factors are added. Hence, the team already picks up the research topics on dimension reduction techniques, such as the canonical polyadic decomposition (CPD) method, or the recent machine learning integration methods.

Another possible way to speed up the COS method is to identify and exclude unimportant Fourier series terms (i.e. the terms with very small series coefficients). The idea is to find the principal basis functions somehow, e.g. by decomposing the marginal distribution of each risk factor. Basis functions with a small series coefficient are not important for the approximation, and thus, leaving them out could greatly reduce the computational complexity while having little impact on accuracy.

Furthermore, a rule of thumb is currently used for the initial choice of the COS support. It was observed that a too-large COS support leads to a poor representation of the important basis functions, and thus low accuracy if we do not increase the number of expansion terms. Hence, another future research topic is to define the COS support properly for portfolios.

BIBLIOGRAPHY

[1] I. ISDA, *Key trends in the size and composition of otc derivatives markets in the second half of 2020*, 2020.

[2] K. Glau, R. Pachon, and C. Pötz, "Speed-up credit exposure calculations for pricing and risk management," *Quantitative Finance*, vol. 21, no. 3, pp. 481–499, 2021.

[3] R. R. Bliss and G. G. Kaufman, "Derivatives and systemic risk: Netting, collateral, and closeout," *Journal of Financial Stability*, vol. 2, no. 1, pp. 55–70, 2006.

[4] J. Gregory, *The XVA Challenge: Counterparty Risk, Funding, Collateral, Capital and Initial Margin*. John Wiley & Sons, 2020.

[5] D. Tavella and C. Randall, *Pricing financial instruments: The finite difference method*. John Wiley & Sons, 2000, vol. 13.

[6] F. Qian, "Advanced estimation of credit valuation adjustment," Ph.D. dissertation, PhD thesis, Technische Universiteit Delft, 2017.

[7] C. S. De Graaf, Q. Feng, D. Kandhai, and C. W. Oosterlee, "Efficient computation of exposure profiles for counterparty credit risk," *International Journal of Theoretical and Applied Finance*, vol. 17, no. 04, p. 1 450 024, 2014.

[8] C. de Graaf, D. Kandhai, and P. Sloot, "Efficient estimation of sensitivities for counterparty credit risk with the finite difference monte carlo method," *Journal of Computational Finance, Forthcoming*, 2016.

[9] R. Schöftner, "On the estimation of credit exposures using regression-based monte carlo simulation," *The Journal of Credit Risk*, vol. 4, no. 4, pp. 37–62, 2008.

[10] Y. Krepkiy, A. Lakhany, and A. Zhang, "Efficient least squares monte-carlo technique for pfe/ee calculations," *arXiv preprint arXiv:2105.07061*, 2021.

[11] S. Ghamami and B. Zhang, "Efficient monte carlo counterparty credit risk pricing and measurement," *Journal of Credit Risk*, vol. 10, no. 3, 2014.

[12] S. Jain and C. W. Oosterlee, "The stochastic grid bundling method: Efficient pricing of bermudan options and their greeks," *Applied Mathematics and Computation*, vol. 269, pp. 412–431, 2015.

[13] P. Karlsson, S. Jain, and C. W. Oosterlee, "Counterparty credit exposures for interest rate derivatives using the stochastic grid bundling method," *Applied Mathematical Finance*, vol. 23, no. 3, pp. 175–196, 2016.

[14] Q. Feng, S. Jain, P. Karlsson, D. Kandhai, and C. W. Oosterlee, "Efficient computation of exposure profiles on real-world and risk-neutral scenarios for bermudan swaptions," *Available at SSRN 2790874*, 2016.

[15] K. Glau, M. Mahlstedt, and C. Pötz, "A new approach for american option pricing: The dynamic chebyshev method," *SIAM Journal on Scientific Computing*, vol. 41, no. 1, B153–B180, 2019.

[16] Y. Shen, J. A. Van Der Weide, and J. H. Anderluh, "A benchmark approach of counterparty credit exposure of bermudan option under lévy process: The monte carlo-cos method," *Procedia Computer Science*, vol. 18, pp. 1163–1171, 2013.

[17] F. Fang and C. W. Oosterlee, "A novel pricing method for european options based on fourier-cosine series expansions," *SIAM Journal on Scientific Computing*, vol. 31, no. 2, pp. 826–848, 2009.

[18] C. W. Oosterlee and L. A. Grzelak, *Mathematical Modeling and Computation in Finance: With Exercises and Python and Matlab Computer Codes*. World Scientific, 2019.

[19] P. Mörters and Y. Peres, *Brownian motion*. Cambridge University Press, 2010, vol. 30.

[20] J.-F. Le Gall, *Brownian motion, martingales, and stochastic calculus*. Springer, 2016.

[21] D. Brigo and F. Mercurio, *Interest rate models-theory and practice: with smile, inflation and credit*. Springer, 2006, vol. 2.

[22] J. M. Harrison and S. R. Pliska, "Martingales and stochastic integrals in the theory of continuous trading," *Stochastic Processes and Their Applications*, vol. 11, no. 3, pp. 215–260, 1981.

[23] C. Kenyon, A. D. Green, and M. Berrahoui, "Which measure for pfe? the risk appetite measure a," *The Risk Appetite Measure A (December 15, 2015)*, 2015.

[24] H. Geman, N. El Karoui, and J.-C. Rochet, "Changes of numeraire, changes of probability measure and option pricing," *Journal of Applied Probability*, vol. 32, no. 2, pp. 443–458, 1995.

[25] I. J. Clark, *Foreign exchange option pricing: A Practitioner's guide*. John Wiley & Sons, 2011.

[26] U. Wystup, *FX options and structured products*. John Wiley & Sons, 2017.

[27] O. Vasicek, "An equilibrium characterization of the term structure," *Journal of Financial Economics*, vol. 5, no. 2, pp. 177–188, 1977.

[28] L. U. Dothan, "On the term structure of interest rates," *Journal of Financial Economics*, vol. 6, no. 1, pp. 59–69, 1978.

[29] J. C. Cox, J. E. Ingersoll Jr, and S. A. Ross, "An intertemporal general equilibrium model of asset prices," *Econometrica: Journal of the Econometric Society*, pp. 363–384, 1985.

[30] J. Hull and A. White, "Pricing interest-rate-derivative securities," *The Review of Financial Studies*, vol. 3, no. 4, pp. 573–592, 1990.

[31] M. Di Francesco, "A general gaussian interest rate model consistent with the current term structure," *International Scholarly Research Notices*, vol. 2012, 2012.

[32] P. Boyle, M. Broadie, and P. Glasserman, "Monte carlo methods for security pricing," *Journal of Economic Dynamics and Control*, vol. 21, no. 8-9, pp. 1267–1321, 1997.

[33] F. Fang and C. W. Oosterlee, "Pricing early-exercise and discrete barrier options by fourier-cosine series expansions," *Numerische Mathematik*, vol. 114, no. 1, pp. 27–62, 2009.

[34] J. P. Boyd, *Chebyshev and Fourier spectral methods*. Courier Corporation, 2001.

[35] L. N. Trefethen, "Is gauss quadrature better than clenshaw–curtis?" *SIAM review*, vol. 50, no. 1, pp. 67–87, 2008.

[36] R. udiger Frey and D. Sommer, "A systematic approach to pricing and hedging of international derivatives with interest rate risk," 1995.

[37] V. Piterbarg, *A multi-currency model with fx volatility skew*, 2005.

[38] L. A. Grzelak and C. W. Oosterlee, "On cross-currency models with stochastic volatility and correlated interest rates," *Applied Mathematical Finance*, vol. 19, no. 1, pp. 1–35, 2012.

[39] M. Ruijter, M. Versteegh, and C. W. Oosterlee, "On the application of spectral filters in a fourier option pricing technique," *Journal of Computational Finance*, vol. 19, no. 1, pp. 75–106, 2015.

[40] D. Gottlieb and C.-W. Shu, "On the gibbs phenomenon and its resolution," *SIAM review*, vol. 39, no. 4, pp. 644–668, 1997.

[41] C. M. Bender, S. Orszag, and S. A. Orszag, *Advanced mathematical methods for scientists and engineers I: Asymptotic methods and perturbation theory*. Springer Science & Business Media, 1999, vol. 1.

[42] F. Fang, X. Shen, and C. Qiu, "A new and efficient fourier method for risk quantification and allocation of credit portfolios," *Available at SSRN 4153482*, 2022.

[43] M. B. Hcine and R. Bouallegue, "On the approximation of the sum of lognormals by a log skew normal distribution," *arXiv preprint arXiv:1502.03619*, 2015.

A

MATHEMATICAL DEFINITIONS AND PROOFS

Definition A.0.1 (Local martingale)**.** *A process M is called a local martingale if there exists an increasing sequence of stopping times ($\tau_n \nearrow \infty$ almost surely), such that the stopped process*

$$M^{\tau_n} = (M_t^{\tau_n})_{t\geq 0} \text{ with } M_t^{\tau_n}(\omega) := M_{\tau_n(\omega)\wedge t}(\omega)$$

is a martingale.

Definition A.0.2 (Finite variation)**.** *A process A has finite variation if for every $\omega \in \Omega$, the path of $t \mapsto A_t(\omega)$ has finite variation for each finite $[0,t]$; that is,*

$$V_{A(\omega)}[0,t] := \sup\left\{ \sum_{k=1}^{\tau} \mid A_{t_k}(\omega) - A_{t_{k-1}}(\omega) \mid : 0 \leq t_0 < t_1 < \cdots < t_r \leq t \right\} < \infty$$

Definition A.0.3 (Self-financing)**.** *A trading strategy ϕ is self-financing if $V(\phi) \geq 0$, and*

$$V_t(\phi) = V_0(\phi) + G_t(\phi), \quad 0 \leq t < T.$$

Definition A.0.4 (Equivalent martingale measure)**.** *An equivalent martingale measure $\mathbb{Q}$ is a probability measure on space $(\Omega, \mathscr{F})$ such that*

1. *$\mathbb{Q}_0$ and $\mathbb{Q}$ are equivalent measures, that is, $\mathbb{Q}_0(A) = 0$ if and only if $\mathbb{Q} = 0$, for every $A \in \mathscr{F}$;*
2. *the Radon–Nikodym derivative $d\mathbb{Q}/d\mathbb{Q}_0$ belongs to $L^2(\Omega, \mathscr{F}, \mathbb{Q}_0)$.*
3. *the 'discounted asset price' process $D(0,\cdot)S$ is an $(\mathbb{F}, \mathbb{Q})$-martingale; that is, $\mathbb{E}\left(D(0,t)S_t^k \mid \mathscr{F}_u\right) = D(0,u)S_u^k$, for all $k = 0, 1, \ldots, K$ and all $0 \leq u \leq t \leq T$, with E denoting expectation under $\mathbb{Q}$.*

Theorem A.0.5 (Itô isometry)**.** *Let W(t) be a Brownian motion defined up to time $T > 0$ for any stochastic process $g(t)$ satisfying regularity conditions. Then the following relation holds:*

$$\mathbb{E}^{\mathbb{Q}}\left[\left(\int_0^T g(t)dW(t)\right)^2\right] = \int_0^T \mathbb{E}^{\mathbb{Q}}\left[g^2(t)\right]dt$$

Proposition A.0.6. *For all $f \in L^2[0,1]$, the process $\left\{\int_0^t f(s)dW(s) : 0 \le t \le 1\right\}$ is a Gaussian process.*

Proof. First, we note that $(W(t_i^{(n)}) - W(t_{i-1}^{(n)}))$ is normally distributed with zero expectation and variance $t_i^{(n)} - t_{i-1}^{(n)}$. $I(\mathscr{S}_n, f)$ is defined as the finite sum of normal distributions and is, therefore, also normally distributed. We calculate the expectation as follows:

$$\begin{aligned}
\mathbb{E}(I(\mathscr{S}_n, f)) &= \mathbb{E}(\sum_{i=1}^{k(n)} f(t_{i-1}^{(n)})(W(t_i^{(n)}) - W(t_{i-1}^{(n)}))) \\
&= \sum_{i=1}^{k(n)} \mathbb{E}(f(t_{i-1}^{(n)})(W(t_i^{(n)}) - W(t_{i-1}^{(n)}))) \\
&= \sum_{i=1}^{k(n)} f(t_{i-1}^{(n)})\mathbb{E}(W(t_i^{(n)}) - W(t_{i-1}^{(n)})) \\
&= \sum_{i=1}^{k(n)} f(t_{i-1}^{(n)}) \cdot 0 = 0
\end{aligned}$$

where we used the linearity of the sum and the fact that $(W(t_i^{(n)}) - W(t_{i-1}^{(n)}))$ is normally distributed with zero expectation and variance $t_i^{(n)} - t_{i-1}^{(n)}$.

Similarly, we calculate the variance:

$$\begin{aligned}
\mathrm{Var}\left(I(\mathscr{S}_n, f)\right) &= \mathrm{Var}\left(\sum_{i=1}^{k(n)} f(t_{i-1}^{(n)})(W(t_i^{(n)}) - W(t_{i-1}^{(n)}))\right) \\
&= \sum_{i=1}^{k(n)} f^2(t_{i-1}^{(n)}) Var(W(t_i^{(n)}) - W(t_{i-1}^{(n)})) \\
&= \sum_{i=1}^{k(n)} f^2(t_{i-1}^{(n)})(t_i^{(n)} - t_{i-1}^{(n)}) = \sigma^2(\mathscr{S}_n, f)
\end{aligned}$$

where we again used the linearity to switch the variance and the summation and took out $f(t_{i-1}^{(n)})$ using the calculation rules of the variance for constants. In the third equality, we used that $(W(t_i^{(n)}) - W(t_{i-1}^{(n)}))$ is normally distributed with zero expectation and variance $t_i^{(n)} - t_{i-1}^{(n)}$.

Now we define, for $0 \le t \le 1$ and $f \in L^2([0,1])$: $\int_0^t f(s)dW(s) = I(f \times 1[0,t])$ where I(f) is the Paley–Wiener integral defined as $I(f) = \lim_{n\to\infty} I(\mathscr{S}_n, f)$, and $I(\mathscr{S}_n, f)$ is the Paley–Wiener sum defined as $I(\mathscr{S}_n, f) = \sum_{i=1}^{k(n)} f(t_{i-1}^{(n)})\left(W(t_i^{(n)} - W(t_{i-1}^{(n)})\right)$.

For a Gaussian process, we must have that for all vector $v \in \mathbb{R}^n$ holds $< v, (X_{t_1}, \ldots, X_{t_n}) >= \sum_{i=1}^n v_i X_{t_i}$ is normally distributed. $I(f)$ is normally distributed with zero expectation and a variance of $\int_0^1 f(s)^2 ds$. Similarly, we see that $I(f \times 1[0, t_i])$ is normally distributed with expectation 0 and variance $\int_0^{t_i} f(s)^2 ds$. Thus we have:

$$\begin{aligned}\sum_{i=1}^n v_i X_{t_i} &= \sum_{i=1}^n v_i \int_0^{t_i} f(s) dW(s) \\ &= (\sum_{i=0}^n v_i) \int_0^{t_1} f(s) dW(s) + (\sum_{i=2}^n v_i) \int_{t_1}^{t_2} f(s) dW(s) + \ldots + (\sum_{i=n}^n v_i) \int_{t_{n-1}}^{t_n} f(s) dW(s)\end{aligned}$$

We see that these are all independent increments, which are, therefore, also normally distributed. The sum of a finite number of normal distributions is again normally distributed, so the defined process is Gaussian. □

Proposition A.0.7. *The drift parameter $\theta(t)$ in the Hull–White model to calibrate the model to the observed market is given by*

$$\theta(t) = \frac{\partial f^M(0,t)}{\partial T} + a f^M(0,t) + \frac{\sigma^2}{2a}\left(1 - e^{-2at}\right).$$

Proof. We start from the Hull–White dynamics, given as

$$dr(t) = (\theta(t) - a r(t)) dt + \sigma dW(t).$$

Furthermore, we observe that

$$\begin{aligned}d\left(e^{at} r(t)\right) &= a e^{at} r(t) dt + e^{at} dr(t) \\ &= a e^{at} r(t) dt e^{at} \left[(\theta(t) - a r(t)) dt + \sigma dW(t)\right] \\ &= e^{at} \theta(t) dt + \sigma dW(t).\end{aligned}$$

Next, we observe that for any $v \geq t$, we can integrate both sides of the equation above to get

$$r(v) = e^{-a(v-t)} r(t) + e^{-av} \left[\int_t^v e^{a(s-v)} \theta(s) ds + \int_t^v e^{a(s-v)} \sigma dW(s)\right].$$

For $0 \leq t \leq T$, we know that the ZCB is defined as in Definition 2.4.2. If we fill in the

solution to the short rate from above, we get

$$\begin{aligned}
P(t,T) &= \mathbb{E}^{\mathbb{Q}}\left(e^{-\int_t^T r_v dv} \mid \mathscr{F}_t\right) \\
&= \mathbb{E}^{\mathbb{Q}}\left[\exp\left(\int_t^T \left\{e^{a(t-v)}r(t) + \int_t^v e^{a(s-v)}\theta(s)ds + \int_t^v e^{a(s-v)}\sigma dW(s)\right\} dv\right) \mid \mathscr{F}_t\right] \\
&= e^{-r(t)B(t,T)}\mathbb{E}^{\mathbb{Q}}\left[\exp\left(-\int_t^T\int_t^v e^{a(s-v)}\theta(s)dsdv - \int_t^T\int_t^v e^{a(s-v)}\sigma dW(s)dv\right) \mid \mathscr{F}_t\right] \\
&= e^{-r(t)B(t,T)}\mathbb{E}^{\mathbb{Q}}\left[\exp\left(-\int_t^T\int_s^T e^{a(s-v)}\theta(s)dvds - \int_t^T\int_s^T \sigma e^{a(s-v)}dvdW(s)\right) \mid \mathscr{F}_t\right] \\
&= e^{-r(t)B(t,T)}\mathbb{E}^{\mathbb{Q}}\left[\exp\left(-\int_t^T \theta(s)B(s,T)ds - \int_t^T \sigma B(s,T)dW(s)\right) \mid \mathscr{F}_t\right] \\
&= e^{-r(t)B(t,T)}e^{-\int_t^T \theta(s)B(s,T)ds}\mathbb{E}^{\mathbb{Q}}\left[e^{-\int_t^T \sigma B(s,T)dW(s)} \mid \mathscr{F}_t\right] \\
&= e^{-r(t)B(t,T)-\int_t^T \theta(s)B(s,T)ds + V(t,T)/2}.
\end{aligned}$$

In the last expression, the moment-generating function of a normal distribution is used. Because an Itô integral is a martingale, it will have zero mean. The variance is denoted by V(t,T). The full expression, together with the expression of B(t,T), is given below. These parameters were defined to decrease the amount of notation.

$$B(t,T) = \int_t^T e^{a(t-v)}dv = \frac{1}{a}\left(e^{a(t-T)} - 1\right),$$

$$V(t,T) = \int_t^T \sigma^2 B^2(s,T)ds = \mathrm{Var}\left(\int_t^T \sigma B(s,T)dW(s)|\mathscr{F}_t\right).$$

The Itô isometry, defined in A.0.5, is used to calculate the expression of the variance V(t,T). Furthermore, we can use the definition of the market instantaneous forward rate to get

$$\begin{aligned}
f^M(0,t) &= -\frac{\partial}{\partial t}\ln\left(P^M(0,t)\right) \\
&= r(0)\frac{\partial}{\partial t}B(0,t) + \theta(t)B(t,t) + \int_0^t \theta(s)\frac{\partial}{\partial t}B(s,t)ds - \frac{1}{2}\partial V(0,t) \\
&= r(0)e^{-at} + \int_0^t \theta(s)e^{a(s-t)}ds - \frac{1}{2}\frac{\partial}{\partial t}V(0,t),
\end{aligned}$$

$$\begin{aligned}
\frac{\partial}{\partial t}f^M(0,t) &= -ar(0)e^{-at} + \theta(t) - a\int_0^t \theta(s)e^{a(s-t)}ds - \frac{1}{2}\frac{\partial^2}{\partial t^2}V(0,t) \\
&= -a\left(f^M(0,t) + \frac{1}{2}\frac{\partial}{\partial t}V(0,t)\right) + \theta(t) - \frac{1}{2}\frac{\partial^2}{\partial t^2}V(0,t).
\end{aligned}$$

Combining these expressions and reshuffling the variables gives us the expression,

$$\begin{aligned}
\theta(t) &= \frac{\partial}{\partial}f^M(0,t) + af^M(0,t) + \frac{1}{2}\left(\frac{\partial^2}{\partial t^2}V(0,t) + a\frac{\partial}{\partial t}V(0,t)\right) \\
&= \frac{\partial f^M(0,t)}{\partial T} + af^M(0,t) + \frac{\sigma^2}{2a}\left(1 - e^{-2at}\right).
\end{aligned}$$

□

Proposition A.0.8. *The price of a ZCB for the G1++ model can be expressed in the form,*

$$P(t,T) = A(t,T)e^{-B(t,T)x(t)},$$

where

$$B(t,T) = \frac{1}{a}\left[1-e^{-a(T-t)}\right],$$
$$A(t,T) = \frac{P^M(0,T)}{P^M(0,t)}e^{1/2[V(t,T)-V(0,T)+V(0,t)]}.$$

Here, $V(t,T)$ is the variance of $\int_t^T x(s)$ conditional on $\mathscr{F}_t$ given by

$$V(t,T) = \frac{\sigma^2}{a^2}\left(T-t-2\frac{1-e^{-a(T-t)}}{a}+\frac{1-e^{-2a(T-t)}}{2a}\right).$$

Proof. In the end, we want to obtain an expression for the ZCB defined by

$$P(t,T) = \mathbb{E}^{\mathbb{Q}}\left(e^{-\int_t^T r(s)ds} \mid \mathscr{F}_t\right).$$

Furthermore, we must have for all maturities T that it holds that $P(0,T) = P^M(0,T)$ because then the ZCB from the model exactly fits the market. We calculate the above expectation to find $P(0,T)$. First, we take the integral over the instantaneous short rate r(t), $\int_0^T r(s)ds$. It is known that the process x(t) is normally distributed conditional on $\mathscr{F}_0$ by the nature of its Ornstein–Uhlenbeck SDE. Then, $\int_0^T x(t)dt$ is also normally distributed. Indeed,

$$\begin{aligned}\int_0^T x(t)dt &= \int_0^T\int_0^t \sigma e^{-a(t-u)}dW(u)dt \\ &\overset{Fubini}{=} \sigma\int_0^t\int_u^T e^{-at}dtdW(u) \\ &= \frac{\sigma}{a}\int_0^T\left(1-e^{-a(t-u)}\right)dW(u).\end{aligned} \tag{A.2}$$

From the result of A.0.6, we know this is again normally distributed. From the fact that it is an Itô integral, we can immediately deduce that it has zero mean. The variance can be defined as

$$\begin{aligned}V(0,T) &= \mathrm{Var}\left(\int_0^T x(t) \mid \mathscr{F}_0\right) \\ &= \frac{\sigma^2}{a^2}\int_0^T\left(1-e^{-a(T-u)}\right)^2 du \\ &= \frac{\sigma^2}{a^2}\left(T-2\frac{1-e^{-aT}}{a}+\frac{1-e^{-2aT}}{2a}\right).\end{aligned}$$

From the moment generating function of a normal distribution defined as $\mathcal{N}(\mu, \sigma^2)$, we know that $\mathbb{E}(e^z) = e^{\mu_z + 1/2\sigma_z^2}$. Using this, we find

$$\begin{aligned} P(0,T) &= \mathbb{E}^{\mathbb{Q}}\left(e^{-\int_0^T r(s)ds} \mid \mathscr{F}_0\right) \\ &= \mathbb{E}^{\mathbb{Q}}\left(e^{-\int_0^T x(s)ds - \int_0^T \beta(s)ds} \mid \mathscr{F}_0\right) \\ &= e^{-\int_0^T \beta(s)ds}\mathbb{E}^{\mathbb{Q}}\left(e^{-\int_0^T x(s)ds} \mid \mathscr{F}_0\right) \\ &= e^{-\int_0^T \beta(s)ds} e^{1/2V(0,T)}. \end{aligned}$$

Because we must have $P^M(0,T) = P(0,T)$ for all maturities $T > 0$ for the model to be perfectly fitted to the market, we must have

$$P^M(0,T) = e^{-\int_0^T \beta(s)ds} e^{1/2V(0,T)}.$$

Taking into consideration the definition of the market instantaneous forward rate,

$$P^M(0,T) = e^{-\int_0^T f^M(0,s)ds}$$

we can rewrite the expression above to the form

$$e^{-\int_0^T f^M(0,s)ds} = e^{-\int_0^T \beta(s)ds} e^{1/2V(0,T)}.$$

The exponents can be removed on all sides. Then, by differentiation, we find

$$\begin{aligned} \beta(T) &= f^M(0,T) + \frac{\sigma^2}{a}\int_0^T \left(1 - e^{-a(T-u)}\right) e^{-a(T-u)} du \\ &= f^M(0,T) + \frac{\sigma^2}{2a^2}\left(1 - e^{-aT}\right)^2. \end{aligned}$$

The same steps can be done for $P(t,T)$, which does not need the entire β curve. Therefore, we have

$$\int_t^T x(s)ds = x(t)\frac{1 - e^{-a(T-t)}}{a} + \frac{\sigma}{a}\int_t^T \left(1 - e^{-a(T-u)}\right) dW(u).$$

Using a similar argument as before, we find that the integral conditional on $\mathscr{F}_t$ is normally distributed with mean and variance given by

$$\begin{aligned} \mathbb{E}^{\mathbb{Q}}\left[\int_t^T x(s)ds \mid \mathscr{F}_t\right] &= x(t)\frac{1 - e^{-a(T-t)}}{a}, \\ \mathrm{Var}\left(\int_t^T x(s)ds \mid \mathscr{F}_t\right) &= \frac{\sigma^2}{a^2}\int_t^T \left(1 - e^{-a(T-u)}\right)^2 du \\ &= \frac{\sigma^2}{a^2}\left(T - t - 2\frac{1 - e^{-a(T-t)}}{a} + \frac{1 - e^{-2a(T-t)}}{2a}\right) = V(t,T). \end{aligned}$$

Using the found expressions, we can formulate a new expression for the ZCB $P(t,T)$ given by

$$\begin{aligned}
P(t,T) &= \mathbb{E}^{\mathbb{Q}}\left(e^{-\int_t^T r(s)ds} \mid \mathscr{F}_t\right) \\
&= \mathbb{E}^{\mathbb{Q}}\left(e^{-\int_t^T x(s)ds - \int_t^T \beta(s)ds} \mid \mathscr{F}_t\right) \\
&= e^{-\int_t^T \beta(s)ds}\mathbb{E}^{\mathbb{Q}}\left[e^{\int_t^T x(s)ds}\right] \\
&= e^{-\int_0^T \beta(s)ds} e^{-\int_0^t \beta(s)ds} e^{-(1-e^{-a(T-t)})x(t)/a} e^{V(t,T)/2} \\
&= \frac{P^M(0,T)}{P^M(0,t)} e^{(V(t,T)-V(0,T)+V(0,t))/2} e^{-B(t,T)x(t)},
\end{aligned}$$

where

$$\begin{aligned}
A(t,T) &= \frac{P^M(0,T)}{P^M(0,t)} e^{[V(t,T)-V(0,T)+V(0,t)]/2} \\
B(t,T) &= \frac{1-e^{-a(T-t)}}{a}.
\end{aligned}$$

□

Theorem A.0.9. *The probability distribution function can be retrieved using the COS method using the following expressions:*

$$f(x) = \sum_{k=0}^{\infty}{}' A_K \cdot \cos\left(k\pi\frac{x-a}{b-a}\right),$$

$$A_k = \frac{2}{b-a}\int_a^b f(x)\cos\left(k\pi\frac{x-a}{b-a}\right)dx,$$

Proof. [1] The proof starts from the definition of the Fourier expansion of a function $f(x)$ on an interval $[-1,1]$. This is defined as

$$f(\theta) = \sum_{k=0}^{\infty}{}' \overline{A}_k \cos(k\pi\theta) + \sum_{k=1}^{\infty} B_k \sin(k\pi\theta),$$

where the prime at the sum, $\sum'$, denotes that the first term in the summation must be halved. The coefficients A_k, B_k are given by

$$\overline{A}_k = \int_{-1}^{1} f(\theta)\cos(k\pi\theta)\,d\theta, \quad B_k = \int_{-1}^{1} f(\theta)\sin(k\pi\theta)\,d\theta.$$

To obtain the Fourier cosine expansion, we set $B_k = 0$. The cosine expansion can represent even functions around $\theta = 0$ exactly. To express a function $f(x)$ as a cosine expansion, we need the function to be even. Any function $f : [0,\pi] \to \mathbb{R}$ can be made even on $[-\pi,\pi]$, as follows:

$$\overline{f}(\theta) = \begin{cases} f(\theta), & \theta \geq 0 \\ f(-\theta). & \theta < 0 \end{cases}$$

[1] This proof is adopted from [18].

Now that the function $f(x)$ is made even, the cosine expansion supported on $[-\pi,\pi]$ reads

$$\overline{f}(\theta) = \sum_{k=0}^{\infty}{}' \overline{A}_k \cos(k\theta),$$

with

$$\overline{A}_k = \frac{1}{\pi}\int_{-\pi}^{\pi} \overline{f}(\theta)\cos(k\theta)\,\mathrm{d}\theta = \frac{2}{\pi}\int_0^{\pi} f(\theta)\cos(k\theta)\,\mathrm{d}\theta.$$

A change of variables is required to change the support from $[-\pi,\pi]$ on which the cosine expansion is originally defined to any arbitrary support $[a,b]$. That is,

$$\theta := \frac{x-a}{b-a}\pi, \quad x = \frac{b-a}{\pi}\theta + a.$$

The cosine expansion on the support $[a,b]$ is then given by

$$f(x) = \sum_{k=0}^{\infty}{}' \overline{A}_k \cdot \cos\left(k\pi\frac{x-a}{b-a}\right),$$

with

$$\overline{A}_k = \frac{2}{b-a}\int_a^b f(x)\cos\left(k\pi\frac{x-a}{b-a}\right)\mathrm{d}x.$$

□

Proposition A.0.10. *The stochastic process for the FX rate $X(t)$ is defined as*

$$dX(t) = \mu X(t)dt + \sigma X(t)dW^{\mathbb{P}}(t).$$

Under the domestic risk-neutral measure $\mathbb{Q}^d$, the dynamics will be transformed to

$$dX(t) = \left(r_d(t) - r_f(t)\right)X(t)dt + \sigma_X X(t)dW_X^{\mathbb{Q}^d}.$$

Here, the subscripts d, f indicate whether the interest rate is domestic or foreign, respectively. The dynamics under the foreign risk-neutral measure $\mathbb{Q}^f$ are obtained by switching the subscripts d, f

Proof. Consider the FX rate $X(t)$ indicating the amount of domestic currency per unit of foreign currency. It has the dynamics defined as

$$dX(t) = \mu X(t)dt + \sigma X(t)dW^{\mathbb{P}}(t).$$

A money-savings account in the foreign market $B_f(t)$ can be expressed in the domestic currency using the exchange rate. So, in the domestic currency, the foreign-money savings account is worth $X(t)B_f(t)$. In the domestic risk-neutral measure $\mathbb{Q}^d$, any asset discounted by the domestic savings account as the numeraire is a martingale. Thus, $Y(t) = X(t)\dfrac{B_f(t)}{B_d(t)}$ is a martingale under the domestic risk-neutral measure. Itô's Lemma

gives,

$$\begin{aligned} dY(t) &= \big(r_f(t) - r_d(t)\big)\frac{B_f(t)}{B_d(t)}X(t)dt + \frac{B_f(t)}{B_d(t)}dX(t) \\ &= \big(r_f(t) - r_d(t)\big)\frac{B_f(t)}{B_d(t)}X(t)dt + \mu X(t)\frac{B_f(t)}{B_d(t)}dt + \sigma_X\frac{B_f(t)}{B_d(t)}X(t)dW_X^{\mathbb{P}} \\ &= \big(r_f(t) - r_d(t)\big)dt + \mu dt + \sigma_X dW_X^{\mathbb{P}}. \end{aligned}$$

The process $Y(t)$ is a martingale whenever the dynamics are free of drift. This can only hold whenever we have

$$dW_X^{\mathbb{Q}^d} = \frac{r_f(t) - r_d(t) + \mu}{\sigma_X} + dW_X^{\mathbb{P}}.$$

Incorporating this into the dynamics of the FX rate, we get the dynamics under the domestic risk-neutral measure,

$$dX(t) = \big(r_d(t) - r_f(t)\big)X(t)dt + \sigma_X X(t)dW_X^{\mathbb{Q}^d}.$$

Analogously to the above derivation, one could define the FX rate $X(t)$ as the amount of foreign currency per unit of domestic currency. Following the same steps, one would obtain the dynamics under the foreign risk-neutral measure $\mathbb{Q}^f$. The dynamics are the same as the one shown above, with the subscripts d, f switched. □

Proposition A.0.11. *The foreign interest rate under the domestic risk-neutral measure in the Gaussian one-factor model is given by*

$$dr_f(t) = \big[-a_f r_f(t) + \sigma_f\sigma_X\rho_{fx}\big]dt + \sigma_f dW_f^{\mathbb{Q}^d}.$$

Proof. We start by defining the dynamics for the foreign interest rate $r_f(t)$ and the FX rate $X(t)$. $X(t)$ specifies the amount of foreign currency that is exchanged for one unit of domestic currency.

$$dX(t) = \big(r_f(t) - r_d(t)\big)X(t) + \sigma_X dW_X^{\mathbb{Q}},$$

$$dr_f(t) = -a_f r_f(t)dt + \sigma_f dW_f^{\mathbb{Q}^f}.$$

Using the fundamental theorem of asset pricing, we find the Radon–Nikodym derivative defined as

$$\frac{d\mathbb{Q}^d}{d\mathbb{Q}^f} = \frac{B^d(T)X(T)}{X(0)B^f(T)},$$

where $B^d(T), B^f(T)$ are the money-savings accounts at time T in the domestic and foreign currency, respectively. To use Girsanov's theorem, we want to fill in the expressions for $B^d(T), B^f(T), X(T)$. For a money savings account, we can solve the dynamics easily; that is,

$$B^f(T) = B^f(0)e^{\int_0^T r^f(s)ds}$$

$$B^d(T) = B^d(0)e^{\int_0^T r^d(s)ds}$$

We will find an expression for $X(T)$ by defining the function $g(X(t)) = \log(X(t))$. Using Itô's formula, we find

$$\begin{aligned} g(t) &= g(0) + \int_0^t \frac{\partial g}{\partial t} dt + \int_0^t \frac{\partial g}{\partial x} dx + \frac{1}{2}\int_0^t \frac{\partial^2 g}{\partial x^2}[dx] \\ &= \log(X(0)) + \int_0^t (r^f(s) - r^d(s) - \frac{1}{2}\sigma_X^2)ds + \int_0^t \sigma_X dW^f(s). \end{aligned}$$

Taking the exponent on both sides, we get the result for $X(T)$:

$$X(T) = X(0)e^{\int_0^T (r^f(s) - r^d(s) - \frac{1}{2}\sigma_X^2)ds + \int_0^T \sigma_X dW^f(s)}.$$

Using the expressions found above, the Radon–Nikodym derivative is

$$\begin{aligned} \frac{d\mathbb{Q}^d}{d\mathbb{Q}^f} &= \frac{B^d(T)X(T)}{X(0)B^f(T)} \\ &= e^{\int_0^T (r^f(s) - r^d(s) - \frac{1}{2}\sigma_X^2)ds + \int_0^T \sigma_X dW^f(s)} e^{\int_0^T r^d(s) - r^f(s) ds} \\ &= e^{\frac{1}{2}\sigma_X^2 T - \sigma_X W^f(T)} \end{aligned}$$

Thus, we find $\mathscr{E}(L)_t$ where $L^t = \sigma_X W_X^{\mathbb{Q}}(t)$. From Girsanov's theorem follows that the Brownian motion under the domestic risk-neutral measure is given by

$$\begin{aligned} dW_f^{\mathbb{Q}^d} &= dW_f^{\mathbb{Q}^f} - \langle dW_f^{\mathbb{Q}^f}, \sigma_X dW_X^{\mathbb{Q}^f} \rangle \\ &= dW_f^{\mathbb{Q}^f} - \sigma_x \rho_{xf} dt. \end{aligned}$$

Here, the correlation between the Brownian motion of the foreign currency and the FX rate used is ρ_{xf}. Filling in the above expression in the dynamics for the foreign currency, the result from the proposition follows. □

Lemma A.0.12. *Error ϵ_2 consists of integration range truncation errors and can be bounded by*

$$|\epsilon_2| < C|\epsilon_3| \tag{A.6}$$

where C is some positive constant, and

$$\epsilon_3 := \int_{\mathbb{R}\setminus[a,b]} f(x)dx$$

Proof. [2] We first assume $f(x)$ to be a real function. As we will only work with normal densities, this assumption will hold true in our problems. This enables us to rewrite 4.2 as

$$\epsilon_2 = \frac{x-a}{b-a}\int_{\mathbb{R}\setminus[a,b]} f(x)dx + \sum_{k=1}^{N} \frac{b-a}{k\pi} \sin\left(\frac{k\pi(x-a)}{b-a}\right) \int_{\mathbb{R}\setminus[a,b]} \cos\left(\frac{ik\pi(V(x)-a)}{b-a}\right) f(x)dx$$

[2] This proof is adapted from [17].

We apply the triangle inequality twice to the equation above. This gives us

$$\epsilon_2 \leq C_1 \left| \int_{\mathbb{R}\setminus[a,b]} f(x)dx \right| + \sum_{k=1}^{N} \left| \frac{b-a}{k\pi} \right| \left| \sin\left(\frac{k\pi(x-a)}{b-a} \right) \right| \left| \int_{\mathbb{R}\setminus[a,b]} \cos\left(\frac{ik\pi(V(x)-a)}{b-a} \right) f(x)dx \right|$$

$$\leq C_1 \left| \int_{\mathbb{R}\setminus[a,b]} f(x)dx \right| + \sum_{k=1}^{N} \left| \frac{b-a}{k\pi} \right| \int_{\mathbb{R}\setminus[a,b]} \left| \cos\left(\frac{ik\pi(V(x)-a)}{b-a} \right) \right| \left| f(x)dx \right|$$

where C_1 is a positive constant, and we have used that $|\sin(t)| \leq 1$. Also, $|\sin(t)| \leq 1$, and $f(x)geq0$, which enables us to write:

$$\epsilon_2 \leq C_1 \left| \int_{\mathbb{R}\setminus[a,b]} f(x)dx \right| + \epsilon_3 \cdot \sum_{k=1}^{N} \left| \frac{b-a}{k\pi} \right|$$

where $\epsilon_3 = \int_{\mathbb{R}\setminus[a,b]} f(x)dx$. The magnitude of this error depends on the size of $[a,b]$. Moreover, $\frac{b-a}{k\pi}$ is algebraically converging. It is easy to see that the summation is bounded; that is,

$$\sum_{k=1}^{N} \left| \frac{b-a}{k\pi} \right| \leq C_2$$

where C_2 is again a positive constant. It then follows that error ϵ_2 can be written as

$$|\epsilon_2| < C\,|\epsilon_3|$$

□

Lemma A.0.13.

$$\tilde{F}_X^{\sigma}(x) = F_X^{\sigma}(x) + \mathcal{O}(\sqrt{K}) \cdot \epsilon(J, \mathrm{TOL}),$$

with $\epsilon(J,\mathrm{TOL})$ *is an error term arising from the Clenshaw–Curtis quadrature rule and converges to 0 as* $J \to \infty$ *and* $\mathrm{TOL} \to 0$. J *is the number of points adopted in the Clenshaw–Curtis quadrature rule, and* TOL *is the integration truncation error.*

Proof. [3] The COS approximation of the CDF without the integration error in A_k is given by

$$F_X^{\sigma}(x) = \frac{A_0}{2} \cdot (x-a) + \sum_{k=1}^{\infty} A_k \frac{b-a}{k\pi} \sin\left(k\pi \frac{x-a}{b-a} \right).$$

Introducing the numerical integration error to A_k, we get

$$\tilde{F}_X^{\sigma}(x) = \frac{A_0 + \epsilon(J,\mathrm{TOL},0)}{2} x + \sum_{k=1}^{N} \left(A_k + \epsilon(J,\mathrm{TOL},k) \right) \sigma\left(\frac{k}{N} \right) \frac{b-a}{k\pi} \sin\left(k\pi \frac{x-a}{b-a} \right)$$

where $\epsilon(J,\mathrm{TOL},k)$ refers to the difference between F_k in 2.57 and A_k in 2.55b; that is $\epsilon(J,\mathrm{TOL},k) = F_k - A_k$.

$\{\epsilon(J,\mathrm{TOL},k),\ k \geq 0\}$ has a uniform bound. This can be shown by observing the approximation of $\phi(\omega)$ by $\phi(\omega)$. The latter is the numerical integration of the integrand

[3] This proof is adapted from [42].

$\exp(i\omega V(x))\,f(x)$, where $V(x)$ is the pricing function, and $f(x)$ is the density of the risk-factor.

The Clenshaw–Curtis quadrature evaluates the integrand at the selected Chebyshev points and sums the values at the evaluated points. Notice that the integrand includes a complex exponential; therefore, we have $|\exp(i\omega V(x))| \leq 1$ for all $\omega = k\pi/(b-a),\ k \geq 0$. Using this bound, we see that the integrand is independent of k. Hence, there is a uniform bound denoted by $\epsilon(J,\mathrm{TOL})$.

Using that $\epsilon(J,\mathrm{TOL})$ bounds each $\epsilon(J,\mathrm{TOL},k)$, we find

$$\begin{aligned}\left|\tilde{F}_X^{\sigma}(x) - F_X^{\sigma}(x)\right| &= \left|\frac{\epsilon(J,\mathrm{TOL},0)}{2}x + \sum_{k=1}^{N}\epsilon(J,\mathrm{TOL},k)\sigma(k/N)\frac{b-a}{k\pi}\sin\left(k\pi\frac{x-a}{b-a}\right)\right| \\ &\leq \left((K+1)\epsilon(J,\mathrm{TOL})^2\left(\frac{x^2}{4} + \sum_{k=1}^{N}\sigma(k/N)^2\frac{(b-a)^2}{k^2\pi^2}\sin\left(k\pi\frac{x-a}{b-a}\right)^2\right)\right)^{\frac{1}{2}} \\ &\leq \left((K+1)\epsilon(J,\mathrm{TOL})^2\left(\frac{x^2}{4} + \bar{\sigma}^2\sum_{k=1}^{N}\frac{1}{k^2}\right)\right)^{\frac{1}{2}},\end{aligned}$$

where $bar\sigma$ is the maximum of the spectral filter function on the interval $[0,1]$. Notice that the same can be done whenever we take $\sigma(k/N) = 1$, which gives back the COS approximation of the CDF without a spectral filter.

Using

$$\sum_{k=1}^{N}\frac{1}{k^2} < \sum_{k=1}^{\infty}\frac{1}{k^2} = \frac{\pi^2}{6},$$

we find the error bound

$$\left|\tilde{F}_X^{\sigma}(x) - F_X^{\sigma}(x)\right| < C\sqrt{K}\epsilon(J,\mathrm{TOL})$$

where the constant C is asymptotically independent of K. □

B

FIGURES

B.1. LOG-NORMAL APPROXIMATION USING COS

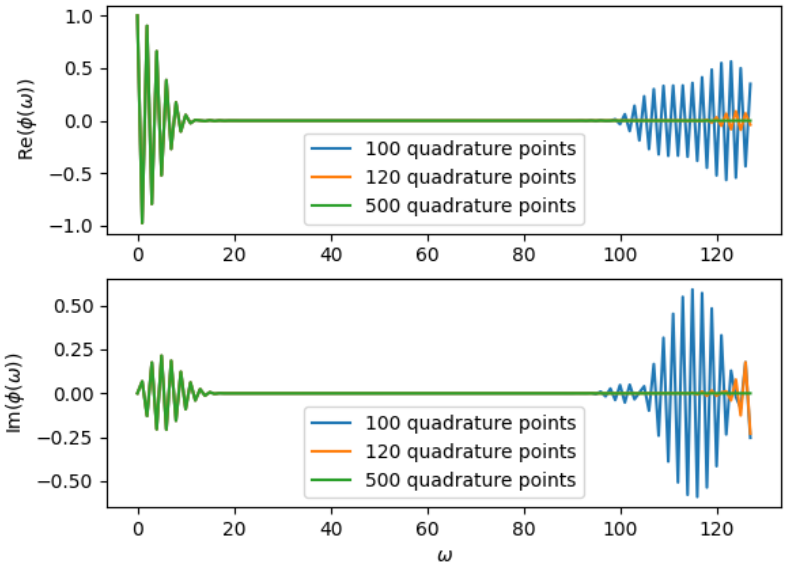

Figure B.1: The characteristic function of a log-normal(0.01, 0.007) variable is recovered using a Clenshaw–Curtis quadrature for various quadrature terms on $[l, u] = [0.55, 0.57]$.

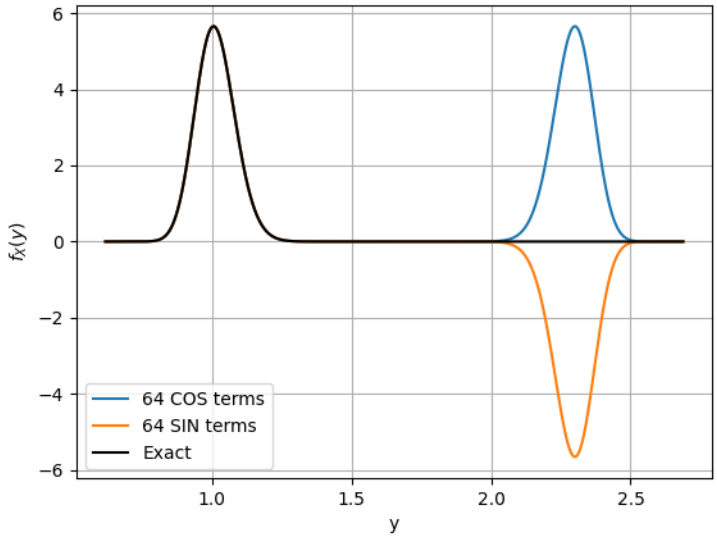

Figure B.2: Approximation of the log-normal PDF with $\mu = 0.01$, $\sigma = 0.007$ using the COS and SIN method on the support $[0.62, 1.65]$. The characteristic function is acquired using 500 quadrature points on $[-0.55, 0.57]$.

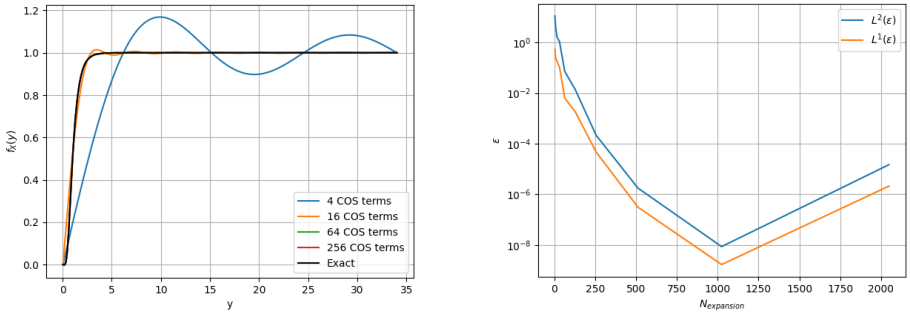

(a) Approximated log-normal density function for multiple COS expansion terms.

(b) Convergence of log-normal PDF in the L^1 and L^2 norm as a function of the number of expansion terms.

Figure B.3: Approximating the log-normal PDF with $\mu = 0.01$, $\sigma = 0.5$ using 2000 Clenshaw–Curtis quadrature points and varying the number of expansion terms.

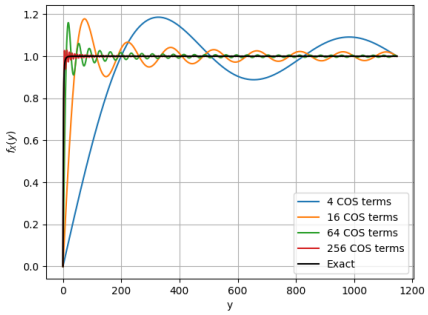

(a) Approximated log-normal density function for multiple COS expansion terms.

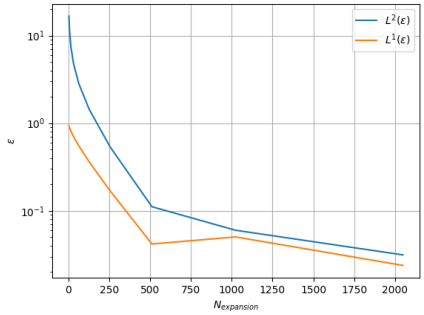

(b) Convergence of log-normal PDF in the L^1 and L^2 norm as a function of the number of expansion terms.

Figure B.4: Approximating the log-normal PDF with $\mu = 0.01$, $\sigma = 1.0$ using 2000 Clenshaw–Curtis quadrature points and varying the number of expansion terms.

B.2. COMPUTATION TIME NETTING-SET LEVEL

Table B.1: Computational times of the PFE using a Monte Carlo algorithm for a netting-set portfolio with a different number of derivatives using 20 timesteps. The measurement is repeated five times, and the average is computed.

Number of Derivatives	1	2	3	4	5	Average
32	29.059	28.905	28.214	28.534	28.445	28.631
64	47.462	47.424	47.307	48.309	47.455	47.591
100	94.700	94.534	96.099	93.318	91.760	94.082

Table B.2: Computational times of the PFE using the COS method for a netting-set portfolio with a different number of derivatives using 20 timesteps. The measurement is repeated five times, and the average is computed.

Number of Derivatives	1	2	3	4	5	Average
32	10.543	10.86	10.495	11.078	10.903	10.776
64	11.224	11.607	11.126	10.753	11.517	11.245
100	11.947	11.619	11.642	11.747	12.339	11.859

Table B.3: Computational times of the PFE using a Monte Carlo algorithm for a netting-set portfolio with a different number of derivatives using 50 timesteps. The measurement is repeated five times, and the average is computed.

Number of Derivatives	1	2	3	4	5	Average
32	73.23	73.190	73.279	72.527	73.199	73.085
64	119.592	118.927	120.041	119.350	119.297	119.441
100	232.661	236.560	231.518	233.690	233.041	233.494

Table B.4: Computational times of the PFE using the COS method for a netting-set portfolio with a different number of derivatives using 50 timesteps. The measurement is repeated five times, and the average is computed.

Number of Derivatives	1	2	3	4	5	Average
32	26.868	25.859	25.679	25.820	25.936	26.032
64	26.744	26.748	26.561	26.432	26.606	26.618
100	28.067	28.307	28.503	28.690	28.456	28.405

Table B.5: Computational times of the PFE using a Monte Carlo algorithm for a netting-set portfolio with a different number of derivatives using 100 timesteps. The measurement is repeated five times, and the average is computed.

Number of Derivatives	1	2	3	4	5	Average
32	154.534	148.577	152.258	151.926	150.087	151.476
64	240.352	241.685	240.314	240.371	242.087	240.962
100	469.514	475.465	466.663	470.005	466.005	469.530

Table B.6: Computational times of the PFE using the COS method for a netting-set portfolio with a different number of derivatives using 100 timesteps. The measurement is repeated five times, and the average is computed.

Number of Derivatives	1	2	3	4	5	Average
32	52.258	51.771	52.149	51.431	52.084	51.939
64	53.109	52.418	56.255	52.990	53.353	53.625
100	56.043	58.360	57.275	56.223	56.315	56.843

B.3. COMPUTATION TIME COUNTERPARTY-LEVEL

Table B.7: Computational times of the PFE using a Monte Carlo algorithm for a counterparty-level portfolio with a different number of derivatives using 20 timesteps. The measurement is repeated five times, and the average is computed.

Number of Derivatives	1	2	3	4	5	Average
32	28.846	27.394	29.262	29.251	31.233	29.197
64	47.955	47.892	47.547	47.837	47.970	47.840
100	92.357	93.965	85.295	88.014	87.695	89.465

Table B.8: Computational times of the PFE using the COS method for a counterparty-level portfolio with a different number of derivatives using 20 timesteps. The measurement is repeated five times, and the average is computed.

Number of Derivatives	1	2	3	4	5	Average
32	10.505	10.580	10.449	10.600	10.473	10.521
64	10.837	11.272	11.347	10.679	10.659	10.959
100	11.494	11.604	11.218	11.916	11.505	11.547

Table B.9: Computational times of the PFE using a Monte Carlo algorithm for a counterparty-level portfolio with a different number of derivatives using 50 timesteps. The measurement is repeated five times, and the average is computed.

Number of Derivatives	1	2	3	4	5	Average
32	75.446	74.907	74.237	74.292	73.329	74.721
64	119.59	118.745	118.584	119.401	118.992	119.08
100	236.056	231.859	233.928	237.403	236.001	234.812

Table B.10: Computational times of the PFE using the COS method for a counterparty-level portfolio with a different number of derivatives using 50 timesteps. The measurement is repeated five times, and the average is computed.

Number of Derivatives	1	2	3	4	5	Average
32	26.208	26.344	26.381	26.249	27.207	26.478
64	26.597	26.847	26.539	26.795	26.752	26.706
100	28.470	28.664	28.119	28.472	28.705	28.486

Table B.11: Computational times of the PFE using a Monte Carlo algorithm for a counterparty-level portfolio with a different number of derivatives using 100 timesteps. The measurement is repeated five times, and the average is computed.

Number of Derivatives	1	2	3	4	5	Average
32	160.341	154.442	151.848	160.006	155.182	156.364
64	249.556	242.359	251.907	244.103	242.292	246.043
100	482.565	480.340	485.284	481.421	480.199	481.962

Table B.12: Computational times of the PFE using the COS method for a counterparty-level portfolio with a different number of derivatives using 100 timesteps. The measurement is repeated five times, and the average is computed.

Number of Derivatives	1	2	3	4	5	Average
32	53.431	53.601	52.701	52.386	52.664	52.957
64	53.649	53.550	53.797	53.484	53.572	53.610
100	57.517	57.173	60.192	58.632	57.736	58.250

C

PORTFOLIOS

The next sections will include the portfolios used throughout the thesis. The first section shows the portfolio with 100 derivatives, the second with 64 derivatives and the last shows the 32-derivative portfolios. The derivatives have unique trade ids. The derivatives have properties belonging to their product type, which is specified in the second column. All derivatives consist of two legs, the paying and receiving leg. These can have different currencies. The notional value of the legs is either the same if the legs have the same currency, or if they do not, a factor difference of 105 signifies the initial spot rate. Furthermore, the legs can be fixed or floating, which in turn has an effect on the 'Coupon' column. The fixed rate will be a number, and 'IBOR' signifies the floating rate. The start date and maturity of the derivatives are given in a year-count fraction based on Act360. This signifies the number of years from today $t = 0$. The coupon frequency represents the number of months between each payment date. To make coding easier, the number-of-coupons column was added to show the total number of coupons for each derivative. These columns are omitted for the FRAs and FX forwards, as they are not applicable.

C.1. PORTFOLIO WITH 100 DERIVATIVES

TradeId	ProductType	PayOrReceive	Ccy	Notional	IsFixed	StartDate	Coupon	CouponFrequency	NumberOfCoupons	Maturity
0	FRA	-1	USD	968	FALSE	0.255555556	IBOR			1.777777778
0	FRA	1	USD	968	TRUE	0.255555556	0.011			1.777777778
1	FRA	-1	USD	2160	FALSE	1.438888889	IBOR			7.019444444
1	FRA	1	USD	2160	TRUE	1.438888889	0.033			7.019444444
2	FRA	-1	JPY	68563	FALSE	0.511111111	IBOR			5.072222222
2	FRA	1	JPY	68563	TRUE	0.511111111	0.023			5.072222222
3	FRA	-1	JPY	106856	TRUE	0.086111111	0.012			8.713888889
3	FRA	1	JPY	106856	FALSE	0.086111111	IBOR			8.713888889
4	FRA	-1	USD	1910	TRUE	1.525	0.054			6.6
4	FRA	1	USD	1910	FALSE	1.525	IBOR			6.6
5	FRA	1	JPY	244011	FALSE	0.341666667	IBOR			2.372222222
5	FRA	-1	JPY	244011	TRUE	0.341666667	0.043			2.372222222
6	FRA	-1	JPY	110295	TRUE	0.761111111	0.021			9.894444444
6	FRA	1	JPY	110295	FALSE	0.761111111	IBOR			9.894444444
7	FRA	-1	JPY	154244	TRUE	0.172222222	0.005			7.275
7	FRA	1	JPY	154244	FALSE	0.172222222	IBOR			7.275
8	FRA	-1	JPY	198682	FALSE	0.341666667	IBOR			5.919444444
8	FRA	1	JPY	198682	TRUE	0.341666667	0.012			5.919444444
9	FRA	-1	USD	1591	TRUE	0.425	0.033			8.033333333
9	FRA	1	USD	1591	FALSE	0.425	IBOR			8.033333333
10	FRA	1	JPY	148287	TRUE	0.425	0.016			6.005555556
10	FRA	-1	JPY	148287	FALSE	0.425	IBOR			6.005555556
11	FRA	-1	JPY	245248	TRUE	0.761111111	0.018			1.777777778
11	FRA	1	JPY	245248	FALSE	0.761111111	IBOR			1.777777778
12	FRA	1	JPY	101599	TRUE	0.425	0.023			4.483333333
12	FRA	-1	JPY	101599	FALSE	0.425	IBOR			4.483333333
13	FRA	-1	USD	811	FALSE	1.186111111	IBOR			6.763888889
13	FRA	1	USD	811	TRUE	1.186111111	0.048			6.763888889
14	FRA	1	JPY	94341	FALSE	0.341666667	IBOR			0.844444444
14	FRA	-1	JPY	94341	TRUE	0.341666667	0.028			0.844444444
15	FRA	1	JPY	75371	TRUE	1.438888889	0.026			4.988888889
15	FRA	-1	JPY	75371	FALSE	1.438888889	IBOR			4.988888889
16	FRA	1	USD	1791	TRUE	1.013888889	0.043			1.525
16	FRA	-1	USD	1791	FALSE	1.013888889	IBOR			1.525
17	FRA	1	USD	2459	TRUE	0.675	0.048			5.244444444
17	FRA	-1	USD	2459	FALSE	0.675	IBOR			5.244444444
18	FRA	1	JPY	105362	FALSE	1.438888889	IBOR			4.483333333
18	FRA	-1	JPY	105362	TRUE	1.438888889	0.031			4.483333333
19	FRA	-1	USD	658	TRUE	0.341666667	0.022			7.444444444
19	FRA	1	USD	658	FALSE	0.341666667	IBOR			7.444444444
20	FRA	-1	USD	1936	FALSE	1.1	IBOR			8.713888889
20	FRA	1	USD	1936	TRUE	1.1	0.008			8.713888889
21	FRA	-1	JPY	229981	FALSE	1.186111111	IBOR			2.705555556
21	FRA	1	JPY	229981	TRUE	1.186111111	0.054			2.705555556
22	FRA	1	USD	1479	TRUE	1.013888889	0.05			8.116666667
22	FRA	-1	USD	1479	FALSE	1.013888889	IBOR			8.116666667
23	FRA	1	USD	2455	TRUE	1.691666667	0.007			4.733333333
23	FRA	-1	USD	2455	FALSE	1.691666667	IBOR			4.733333333
24	FRA	1	JPY	196459	FALSE	0.675	IBOR			7.275
24	FRA	-1	JPY	196459	TRUE	0.675	0.043			7.275
25	FRA	1	USD	689	FALSE	0.675	IBOR			7.275
25	FRA	-1	USD	689	TRUE	0.675	0.036			7.275
26	FRA	-1	JPY	169941	TRUE	1.611111111	0.034			2.627777778
26	FRA	1	JPY	169941	FALSE	1.611111111	IBOR			2.627777778
27	FRA	1	USD	1948	FALSE	0.172222222	IBOR			8.791666667
27	FRA	-1	USD	1948	TRUE	0.172222222	0.034			8.791666667
28	FRA	1	JPY	211128	FALSE	1.438888889	IBOR			8.541666667
28	FRA	-1	JPY	211128	TRUE	1.438888889	0.022			8.541666667
29	FRA	1	JPY	124135	TRUE	1.525	0.053			7.613888889
29	FRA	-1	JPY	124135	FALSE	1.525	IBOR			7.613888889
30	IRS	1	JPY	109990	FALSE	0.341666667	JPY_3M	3	7	1.861111111
30	IRS	-1	JPY	109990	TRUE	0.341666667	0.02	6	4	1.861111111
31	IRS	-1	USD	1214	FALSE	0.930555556	USD_3M	3	7	2.455555556
31	IRS	1	USD	1214	TRUE	0.930555556	0.048	3	7	2.455555556
32	IRS	-1	JPY	86571	TRUE	1.691666667	0.05	1	11	2.541666667
32	IRS	1	JPY	86571	FALSE	1.691666667	JPY_1M	1	11	2.541666667
33	IRS	-1	USD	1634	TRUE	0.930555556	0.014	1	5	1.269444444

33	IRS	1	USD	1634	FALSE	0.930555556	USD_1M	1	5	1.269444444
34	IRS	-1	USD	2149	FALSE	0.425	USD_6M	6	22	11.07777778
34	IRS	1	USD	2149	TRUE	0.425	0.016	6	22	11.07777778
35	IRS	-1	USD	2489	FALSE	0.597222222	USD_3M	3	5	1.611111111
35	IRS	1	USD	2489	TRUE	0.597222222	0.046	3	5	1.611111111
36	IRS	-1	JPY	210504	FALSE	1.611111111	JPY_1M	1	20	3.216666667
36	IRS	1	JPY	210504	TRUE	1.611111111	0.014	1	20	3.216666667
37	IRS	1	JPY	192237	FALSE	1.691666667	JPY_3M	3	20	6.513888889
37	IRS	-1	JPY	192237	TRUE	1.691666667	0.028	3	20	6.513888889
38	IRS	-1	JPY	185564	FALSE	1.438888889	JPY_6M	6	9	5.497222222
38	IRS	1	JPY	185564	TRUE	1.438888889	0.017	6	9	5.497222222
39	IRS	-1	USD	1045	TRUE	0.511111111	0.029	3	24	6.344444444
39	IRS	1	USD	1045	FALSE	0.511111111	USD_3M	3	24	6.344444444
40	IRS	-1	USD	1611	TRUE	1.013888889	0.04	6	12	6.6
40	IRS	1	USD	1611	FALSE	1.013888889	USD_6M	6	12	6.6
41	IRS	-1	USD	1163	TRUE	1.438888889	0.04	12	14	14.63055556
41	IRS	1	USD	1163	FALSE	1.438888889	USD_12M	12	14	14.63055556
42	IRS	-1	USD	1567	TRUE	0.425	0.036	6	21	10.57222222
42	IRS	1	USD	1567	FALSE	0.425	USD_3M	3	41	10.57222222
43	IRS	1	USD	2272	FALSE	1.525	USD_6M	6	27	14.71666667
43	IRS	-1	USD	2272	TRUE	1.525	0.025	12	14	14.71666667
44	IRS	1	USD	1217	TRUE	1.611111111	0.032	3	21	6.686111111
44	IRS	-1	USD	1217	FALSE	1.611111111	USD_3M	3	21	6.686111111
45	IRS	1	JPY	60121	FALSE	1.355555556	JPY_3M	3	11	3.888888889
45	IRS	-1	JPY	60121	TRUE	1.355555556	0.055	6	6	3.888888889
46	IRS	-1	USD	1982	TRUE	1.691666667	0.007	6	8	5.244444444
46	IRS	1	USD	1982	FALSE	1.691666667	USD_3M	3	15	5.244444444
47	IRS	-1	USD	744	FALSE	0.172222222	USD_6M	6	9	4.230555556
47	IRS	1	USD	744	TRUE	0.172222222	0.045	6	9	4.230555556
48	IRS	1	USD	2002	FALSE	1.611111111	USD_3M	3	20	6.430555556
48	IRS	-1	USD	2002	TRUE	1.611111111	0.041	3	20	6.430555556
49	IRS	1	USD	1687	TRUE	0.172222222	0.027	6	14	6.763888889
49	IRS	-1	USD	1687	FALSE	0.172222222	USD_6M	6	14	6.763888889
50	FX	-1	USD	1832	TRUE					2.541666667
50	FX	1	JPY	192360	TRUE					2.541666667
51	FX	-1	JPY	169451	TRUE					5.583333333
51	FX	1	USD	1613.819048	TRUE					5.583333333
52	FX	-1	USD	870	TRUE					9.641666667
52	FX	1	JPY	91350	TRUE					9.641666667
53	FX	1	JPY	201390	TRUE					2.541666667
53	FX	-1	USD	1918	TRUE					2.541666667
54	FX	-1	JPY	85705	TRUE					4.569444444
54	FX	1	USD	816.2380952	TRUE					4.569444444
55	FX	-1	USD	1158	TRUE					1.525
55	FX	1	JPY	121590	TRUE					1.525
56	FX	-1	USD	1895	TRUE					4.569444444
56	FX	1	JPY	198975	TRUE					4.569444444
57	FX	1	JPY	155295	TRUE					7.102777778
57	FX	-1	USD	1479	TRUE					7.102777778
58	FX	-1	USD	2439	TRUE					7.613888889
58	FX	1	JPY	256095	TRUE					7.613888889
59	FX	-1	USD	1457	TRUE					5.072222222
59	FX	1	JPY	152985	TRUE					5.072222222
60	FX	-1	JPY	192469	TRUE					3.555555556
60	FX	1	USD	1833.038095	TRUE					3.555555556
61	FX	-1	USD	2231	TRUE					4.569444444
61	FX	1	JPY	234255	TRUE					4.569444444
62	FX	-1	JPY	233123	TRUE					2.030555556
62	FX	1	USD	2220.219048	TRUE					2.030555556
63	FX	1	JPY	229005	TRUE					10.14722222
63	FX	-1	USD	2181	TRUE					10.14722222
64	FX	1	USD	819.6857143	TRUE					7.613888889
64	FX	-1	JPY	86067	TRUE					7.613888889
65	FX	-1	JPY	218258	TRUE					1.525
65	FX	1	USD	2078.647619	TRUE					1.525
66	FX	1	USD	1955.228571	TRUE					7.613888889
66	FX	-1	JPY	205299	TRUE					7.613888889
67	FX	1	USD	625.3714286	TRUE					4.058333333

67	FX		-1	JPY	65664	TRUE					4.058333333
68	FX		1	USD	1690.495238	TRUE					2.030555556
68	FX		-1	JPY	177502	TRUE					2.030555556
69	FX		1	JPY	194460	TRUE					4.569444444
69	FX		-1	USD	1852	TRUE					4.569444444
70	FX		-1	USD	1091	TRUE					9.641666667
70	FX		1	JPY	114555	TRUE					9.641666667
71	FX		-1	USD	2315	TRUE					8.627777778
71	FX		1	JPY	243075	TRUE					8.627777778
72	FX		-1	JPY	159930	TRUE					1.013888889
72	FX		1	USD	1523.142857	TRUE					1.013888889
73	FX		-1	JPY	121809	TRUE					1.013888889
73	FX		1	USD	1160.085714	TRUE					1.013888889
74	FX		1	JPY	88935	TRUE					7.613888889
74	FX		-1	USD	847	TRUE					7.613888889
75	FX		-1	JPY	139698	TRUE					7.102777778
75	FX		1	USD	1330.457143	TRUE					7.102777778
76	FX		1	USD	2094.028571	TRUE					0.511111111
76	FX		-1	JPY	219873	TRUE					0.511111111
77	FX		1	USD	2309.580952	TRUE					8.627777778
77	FX		-1	JPY	242506	TRUE					8.627777778
78	FX		1	USD	1728.952381	TRUE					8.627777778
78	FX		-1	JPY	181540	TRUE					8.627777778
79	FX		1	JPY	192570	TRUE					8.116666667
79	FX		-1	USD	1834	TRUE					8.116666667
80	XCS		1	USD	1742	TRUE	1.269444444	0.05	3	16	5.072222222
80	XCS		-1	JPY	182910	FALSE	1.269444444	JPY_3M	3	16	5.072222222
81	XCS		-1	JPY	79631	TRUE	0.172222222	0.033	12	15	14.37777778
81	XCS		1	USD	758.3904762	FALSE	0.172222222	USD_12M	12	15	14.37777778
82	XCS		-1	USD	2283	FALSE	1.1	USD_6M	6	20	10.74444444
82	XCS		1	JPY	239715	TRUE	1.1	0.006	6	20	10.74444444
83	XCS		-1	USD	1296	FALSE	0.341666667	USD_12M	12	6	5.413888889
83	XCS		1	JPY	136080	TRUE	0.341666667	0.043	6	11	5.413888889
84	XCS		-1	JPY	126486	FALSE	1.525	JPY_6M	6	7	4.569444444
84	XCS		1	USD	1204.628571	TRUE	1.525	0.044	3	13	4.569444444
85	XCS		-1	JPY	255527	TRUE	1.525	0.053	3	15	5.072222222
85	XCS		1	USD	2433.590476	FALSE	1.525	USD_3M	3	15	5.072222222
86	XCS		-1	USD	635	TRUE	0.172222222	0.052	3	25	6.261111111
86	XCS		1	JPY	66675	FALSE	0.172222222	JPY_3M	3	25	6.261111111
87	XCS		1	USD	2294.257143	FALSE	1.438888889	USD_3M	3	13	4.483333333
87	XCS		-1	JPY	240897	TRUE	1.438888889	0.011	3	13	4.483333333
88	XCS		-1	USD	738	TRUE	1.355555556	0.041	3	4	2.116666667
88	XCS		1	JPY	77490	FALSE	1.355555556	JPY_3M	3	4	2.116666667
89	XCS		-1	JPY	93759	FALSE	0.425	JPY_12M	12	10	9.555555556
89	XCS		1	USD	892.9428571	TRUE	0.425	0.054	12	10	9.555555556
90	XCS		-1	USD	528	FALSE	0.425	USD_3M	3	9	2.455555556
90	XCS		1	JPY	55440	TRUE	0.425	0.008	3	9	2.455555556
91	XCS		1	JPY	120540	FALSE	0.597222222	JPY_12M	12	8	7.7
91	XCS		-1	USD	1148	TRUE	0.597222222	0.007	12	8	7.7
92	XCS		1	JPY	168210	FALSE	0.172222222	JPY_6M	6	5	2.202777778
92	XCS		-1	USD	1602	TRUE	0.172222222	0.008	6	5	2.202777778
93	XCS		1	USD	1162.971429	FALSE	1.269444444	USD_1M	1	8	1.861111111
93	XCS		-1	JPY	122112	TRUE	1.269444444	0.014	1	8	1.861111111
94	XCS		-1	USD	1273	TRUE	1.186111111	0.042	3	15	4.733333333
94	XCS		1	JPY	133665	FALSE	1.186111111	JPY_3M	3	15	4.733333333
95	XCS		1	JPY	110040	TRUE	1.013888889	0.034	6	17	9.130555556
95	XCS		-1	USD	1048	FALSE	1.013888889	USD_6M	6	17	9.130555556
96	XCS		1	USD	531.0857143	FALSE	0.597222222	USD_3M	3	29	7.7
96	XCS		-1	JPY	55764	TRUE	0.597222222	0.05	6	15	7.7
97	XCS		1	JPY	240975	TRUE	1.611111111	0.014	12	8	8.713888889
97	XCS		-1	USD	2295	FALSE	1.611111111	USD_12M	12	8	8.713888889
98	XCS		1	JPY	252735	TRUE	1.186111111	0.051	3	25	7.275
98	XCS		-1	USD	2407	FALSE	1.186111111	USD_3M	3	25	7.275
99	XCS		-1	JPY	252329	TRUE	0.844444444	0.049	6	10	5.413888889
99	XCS		1	USD	2403.133333	FALSE	0.844444444	USD_3M	3	19	5.413888889

C.2. PORTFOLIO WITH 64 DERIVATIVES

TradeId	ProductType	PayOrReceive	Ccy	Notional	IsFixed	StartDate	Coupon	CouponFrequency	NumberOfCoupons	Maturity
0	FRA	-1	USD	2169	FALSE	1.525	IBOR			4.569444444
0	FRA	1	USD	2169	TRUE	1.525	0.046			4.569444444
1	FRA	1	JPY	140333	FALSE	1.186111111	IBOR			5.244444444
1	FRA	-1	JPY	140333	TRUE	1.186111111	0.032			5.244444444
2	FRA	-1	USD	906	FALSE	0.255555556	IBOR			9.386111111
2	FRA	1	USD	906	TRUE	0.255555556	0.013			9.386111111
3	FRA	-1	USD	925	TRUE	0.675	0.027			10.82222222
3	FRA	1	USD	925	FALSE	0.675	IBOR			10.82222222
4	FRA	-1	JPY	215695	TRUE	0.425	0.047			2.961111111
4	FRA	1	JPY	215695	FALSE	0.425	IBOR			2.961111111
5	FRA	-1	JPY	93817	TRUE	0.086111111	0.047			6.175
5	FRA	1	JPY	93817	FALSE	0.086111111	IBOR			6.175
6	FRA	-1	USD	1932	FALSE	1.186111111	IBOR			3.216666667
6	FRA	1	USD	1932	TRUE	1.186111111	0.044			3.216666667
7	FRA	-1	JPY	186182	FALSE	1.525	IBOR			2.541666667
7	FRA	1	JPY	186182	TRUE	1.525	0.009			2.541666667
8	FRA	-1	USD	2302	TRUE	1.611111111	0.009			5.669444444
8	FRA	1	USD	2302	FALSE	1.611111111	IBOR			5.669444444
9	FRA	1	JPY	71078	FALSE	1.611111111	IBOR			9.216666667
9	FRA	-1	JPY	71078	TRUE	1.611111111	0.012			9.216666667
10	FRA	1	JPY	87325	FALSE	0.511111111	IBOR			6.088888889
10	FRA	-1	JPY	87325	TRUE	0.511111111	0.01			6.088888889
11	FRA	1	USD	2157	TRUE	0.930555556	0.021			5.497222222
11	FRA	-1	USD	2157	FALSE	0.930555556	IBOR			5.497222222
12	FRA	-1	JPY	113859	TRUE	1.525	0.028			9.641666667
12	FRA	1	JPY	113859	FALSE	1.525	IBOR			9.641666667
13	FRA	-1	JPY	137938	TRUE	1.355555556	0.021			3.888888889
13	FRA	1	JPY	137938	FALSE	1.355555556	IBOR			3.888888889
14	FRA	-1	JPY	164900	FALSE	1.355555556	IBOR			5.919444444
14	FRA	1	JPY	164900	TRUE	1.355555556	0.052			5.919444444
15	FRA	-1	USD	1411	FALSE	0.255555556	IBOR			8.372222222
15	FRA	1	USD	1411	TRUE	0.255555556	0.018			8.372222222
16	FRA	-1	USD	650	FALSE	0.341666667	IBOR			4.4
16	FRA	1	USD	650	TRUE	0.341666667	0.014			4.4
17	FRA	-1	JPY	243114	FALSE	0.675	IBOR			3.216666667
17	FRA	1	JPY	243114	TRUE	0.675	0.054			3.216666667
18	FRA	1	USD	1941	TRUE	1.1	0.018			7.7
18	FRA	-1	USD	1941	FALSE	1.1	IBOR			7.7
19	FRA	1	USD	1859	FALSE	0.930555556	IBOR			6.513888889
19	FRA	-1	USD	1859	TRUE	0.930555556	0.03			6.513888889
20	IRS	-1	JPY	228406	TRUE	1.1	0.017	6	24	12.77222222
20	IRS	1	JPY	228406	FALSE	1.1	JPY_6M	6	24	12.77222222
21	IRS	1	JPY	161953	FALSE	0.511111111	JPY_1M	1	7	1.013888889
21	IRS	-1	JPY	161953	TRUE	0.511111111	0.03	1	7	1.013888889
22	IRS	-1	USD	1545	FALSE	1.355555556	USD_6M	6	18	9.977777778
22	IRS	1	USD	1545	TRUE	1.355555556	0.036	6	18	9.977777778
23	IRS	1	USD	621	FALSE	1.355555556	USD_12M	12	4	4.4
23	IRS	-1	USD	621	TRUE	1.355555556	0.043	12	4	4.4
24	IRS	1	JPY	110482	FALSE	1.1	JPY_3M	3	25	7.188888889
24	IRS	-1	JPY	110482	TRUE	1.1	0.025	3	25	7.188888889
25	IRS	-1	JPY	176998	FALSE	1.013888889	JPY_6M	6	15	8.116666667
25	IRS	1	JPY	176998	TRUE	1.013888889	0.024	6	15	8.116666667
26	IRS	-1	USD	714	TRUE	0.930555556	0.035	6	10	5.497222222
26	IRS	1	USD	714	FALSE	0.930555556	USD_6M	6	10	5.497222222
27	IRS	-1	USD	666	TRUE	0.425	0.04	3	23	6.005555556
27	IRS	1	USD	666	FALSE	0.425	USD_3M	3	23	6.005555556
28	IRS	-1	JPY	199543	TRUE	1.611111111	0.01	1	21	3.3
28	IRS	1	JPY	199543	FALSE	1.611111111	JPY_1M	1	21	3.3
29	IRS	-1	JPY	259297	FALSE	0.511111111	JPY_6M	6	10	5.072222222
29	IRS	1	JPY	259297	TRUE	0.511111111	0.005	6	10	5.072222222
30	IRS	-1	USD	2079	TRUE	0.255555556	0.013	12	14	13.44444444
30	IRS	1	USD	2079	FALSE	0.255555556	USD_12M	12	14	13.44444444
31	IRS	1	JPY	223790	FALSE	1.013888889	JPY_3M	3	8	2.791666667
31	IRS	-1	JPY	223790	TRUE	1.013888889	0.018	3	8	2.791666667
32	FX	-1	JPY	164355	TRUE					8.116666667
32	FX	1	USD	1565.285714	TRUE					8.116666667
33	FX	1	USD	2300.92381	TRUE					3.044444444

33	FX	-1	JPY	241597	TRUE					3.044444444
34	FX	-1	USD	585	TRUE					7.102777778
34	FX	1	JPY	61425	TRUE					7.102777778
35	FX	-1	USD	743	TRUE					3.044444444
35	FX	1	JPY	78015	TRUE					3.044444444
36	FX	1	JPY	133560	TRUE					4.058333333
36	FX	-1	USD	1272	TRUE					4.058333333
37	FX	-1	JPY	139367	TRUE					7.613888889
37	FX	1	USD	1327.304762	TRUE					7.613888889
38	FX	-1	JPY	190090	TRUE					3.555555556
38	FX	1	USD	1810.380952	TRUE					3.555555556
39	FX	-1	JPY	100466	TRUE					4.569444444
39	FX	1	USD	956.8190476	TRUE					4.569444444
40	FX	1	JPY	230265	TRUE					4.569444444
40	FX	-1	USD	2193	TRUE					4.569444444
41	FX	1	USD	2095.552381	TRUE					6.088888889
41	FX	-1	JPY	220033	TRUE					6.088888889
42	FX	1	USD	1858.780952	TRUE					4.569444444
42	FX	-1	JPY	195172	TRUE					4.569444444
43	FX	1	JPY	200865	TRUE					9.130555556
43	FX	-1	USD	1913	TRUE					9.130555556
44	FX	1	USD	822.1619048	TRUE					8.627777778
44	FX	-1	JPY	86327	TRUE					8.627777778
45	FX	-1	USD	1917	TRUE					1.525
45	FX	1	JPY	201285	TRUE					1.525
46	FX	-1	JPY	101898	TRUE					7.613888889
46	FX	1	USD	970.4571429	TRUE					7.613888889
47	FX	-1	USD	1368	TRUE					8.627777778
47	FX	1	JPY	143640	TRUE					8.627777778
48	FX	-1	JPY	148502	TRUE					4.058333333
48	FX	1	USD	1414.304762	TRUE					4.058333333
49	FX	-1	JPY	138407	TRUE					9.641666667
49	FX	1	USD	1318.161905	TRUE					9.641666667
50	FX	1	USD	2350.695238	TRUE					5.583333333
50	FX	-1	JPY	246823	TRUE					5.583333333
51	FX	1	JPY	183015	TRUE					9.641666667
51	FX	-1	USD	1743	TRUE					9.641666667
52	XCS	-1	JPY	123821	FALSE	1.1	JPY_3M	3	14	4.4
52	XCS	1	USD	1179.247619	TRUE	1.1	0.046	3	14	4.4
53	XCS	1	USD	2126.142857	FALSE	0.675	USD_6M	6	13	6.763888889
53	XCS	-1	JPY	223245	TRUE	0.675	0.05	6	13	6.763888889
54	XCS	-1	JPY	101904	FALSE	1.186111111	JPY_3M	3	21	6.261111111
54	XCS	1	USD	970.5142857	TRUE	1.186111111	0.054	3	21	6.261111111
55	XCS	1	USD	578.5619048	FALSE	0.511111111	USD_3M	3	16	4.313888889
55	XCS	-1	JPY	60749	TRUE	0.511111111	0.037	3	16	4.313888889
56	XCS	-1	JPY	159870	FALSE	1.438888889	JPY_12M	12	10	10.57222222
56	XCS	1	USD	1522.571429	TRUE	1.438888889	0.049	12	10	10.57222222
57	XCS	-1	USD	1491	TRUE	1.186111111	0.009	6	18	9.808333333
57	XCS	1	JPY	156555	FALSE	1.186111111	JPY_6M	6	18	9.808333333
58	XCS	-1	JPY	256214	FALSE	0.172222222	JPY_3M	3	11	2.705555556
58	XCS	1	USD	2440.133333	TRUE	0.172222222	0.052	3	11	2.705555556
59	XCS	-1	JPY	192705	FALSE	0.597222222	JPY_12M	12	6	5.669444444
59	XCS	1	USD	1835.285714	TRUE	0.597222222	0.049	12	6	5.669444444
60	XCS	-1	JPY	195997	TRUE	0.675	0.052	3	9	2.705555556
60	XCS	1	USD	1866.638095	FALSE	0.675	USD_3M	3	9	2.705555556
61	XCS	-1	JPY	196190	FALSE	1.438888889	JPY_6M	6	6	3.975
61	XCS	1	USD	1868.47619	TRUE	1.438888889	0.051	6	6	3.975
62	XCS	1	USD	1855.12381	FALSE	0.172222222	USD_12M	12	25	24.52222222
62	XCS	-1	JPY	194788	TRUE	0.172222222	0.035	12	25	24.52222222
63	XCS	-1	USD	870	TRUE	1.611111111	0.008	12	25	25.96111111
63	XCS	1	JPY	91350	FALSE	1.611111111	JPY_12M	12	25	25.96111111

C.3. PORTFOLIO WITH 32 DERIVATIVES

TradeId	ProductType	PayOrReceive	Ccy	Notional	IsFixed	StartDate	Coupon	CouponFrequency	NumberOfCoupons	Maturity
0	FRA	-1	JPY	184942	FALSE	0.341666667	IBOR			1.861111111
0	FRA	1	JPY	184942	TRUE	0.341666667	0.008			1.861111111
1	FRA	-1	USD	1441	TRUE	1.355555556	0.034			4.902777778
1	FRA	1	USD	1441	FALSE	1.355555556	IBOR			4.902777778
2	FRA	-1	JPY	166127	FALSE	1.186111111	IBOR			3.719444444
2	FRA	1	JPY	166127	TRUE	1.186111111	0.044			3.719444444
3	FRA	-1	JPY	126909	FALSE	0.086111111	IBOR			5.158333333
3	FRA	1	JPY	126909	TRUE	0.086111111	0.032			5.158333333
4	FRA	1	USD	2145	TRUE	1.525	0.006			9.130555556
4	FRA	-1	USD	2145	FALSE	1.525	IBOR			9.130555556
5	FRA	-1	JPY	60636	TRUE	1.691666667	0.034			7.275
5	FRA	1	JPY	60636	FALSE	1.691666667	IBOR			7.275
6	FRA	-1	USD	2300	TRUE	0.425	0.054			1.438888889
6	FRA	1	USD	2300	FALSE	0.425	IBOR			1.438888889
7	FRA	-1	JPY	167729	TRUE	0.844444444	0.014			2.372222222
7	FRA	1	JPY	167729	FALSE	0.844444444	IBOR			2.372222222
8	FRA	-1	JPY	182821	FALSE	1.186111111	IBOR			4.230555556
8	FRA	1	JPY	182821	TRUE	1.186111111	0.018			4.230555556
9	FRA	-1	USD	2140	FALSE	1.013888889	IBOR			5.072222222
9	FRA	1	USD	2140	TRUE	1.013888889	0.038			5.072222222
10	IRS	-1	USD	2298	TRUE	0.597222222	0.029	12	9	8.713888889
10	IRS	1	USD	2298	FALSE	0.597222222	USD_12.0M	12	9	8.713888889
11	IRS	-1	USD	1968	TRUE	0.255555556	0.031	12	8	7.358333333
11	IRS	1	USD	1968	FALSE	0.255555556	USD_12.0M	12	8	7.358333333
12	IRS	-1	JPY	150640	TRUE	0.255555556	0.053	3	4	1.013888889
12	IRS	1	JPY	150640	FALSE	0.255555556	JPY_3.0M	3	4	1.013888889
13	IRS	-1	JPY	118091	TRUE	0.675	0.052	12	23	22.99722222
13	IRS	1	JPY	118091	FALSE	0.675	JPY_12.0M	12	23	22.99722222
14	IRS	-1	JPY	147468	FALSE	0.086111111	JPY_3.0M	3	12	2.875
14	IRS	1	JPY	147468	TRUE	0.086111111	0.022	3	12	2.875
15	IRS	1	JPY	205801	FALSE	0.675	JPY_3.0M	3	25	6.763888889
15	IRS	-1	JPY	205801	TRUE	0.675	0.009	3	25	6.763888889
16	FX	-1	USD	845	TRUE					2.541666667
16	FX	1	JPY	88725	TRUE					2.541666667
17	FX	-1	JPY	191396	TRUE					3.044444444
17	FX	1	USD	1822.819048	TRUE					3.044444444
18	FX	-1	JPY	96292	TRUE					1.013888889
18	FX	1	USD	917.0666667	TRUE					1.013888889
19	FX	1	USD	1032.209524	TRUE					4.058333333
19	FX	-1	JPY	108382	TRUE					4.058333333
20	FX	-1	USD	567	TRUE					5.583333333
20	FX	1	JPY	59535	TRUE					5.583333333
21	FX	1	JPY	56490	TRUE					9.130555556
21	FX	-1	USD	538	TRUE					9.130555556
22	FX	-1	JPY	105026	TRUE					4.058333333
22	FX	1	USD	1000.247619	TRUE					4.058333333
23	FX	-1	USD	950	TRUE					9.641666667
23	FX	1	JPY	99750	TRUE					9.641666667
24	FX	-1	USD	802	TRUE					5.583333333
24	FX	1	JPY	84210	TRUE					5.583333333
25	FX	-1	USD	1632	TRUE					5.072222222
25	FX	1	JPY	171360	TRUE					5.072222222
26	XCS	-1	USD	2261	TRUE	1.355555556	0.052	6	11	6.430555556
26	XCS	1	JPY	237405	FALSE	1.355555556	JPY_6M	6	11	6.430555556
27	XCS	-1	USD	1579	TRUE	1.186111111	0.015	3	4	1.947222222
27	XCS	1	JPY	165795	FALSE	1.186111111	JPY_3M	3	4	1.947222222
28	XCS	-1	JPY	139008	FALSE	0.761111111	JPY_3M	3	21	5.836111111
28	XCS	1	USD	1323.885714	TRUE	0.761111111	0.043	3	21	5.836111111
29	XCS	-1	USD	2444	FALSE	1.269444444	USD_12M	12	5	5.327777778
29	XCS	1	JPY	256620	TRUE	1.269444444	0.019	12	5	5.327777778
30	XCS	1	JPY	66150	TRUE	0.341666667	0.032	12	22	21.64722222
30	XCS	-1	USD	630	FALSE	0.341666667	USD_12M	12	22	21.64722222
31	XCS	-1	USD	1340	FALSE	1.438888889	USD_6M	6	9	5.497222222
31	XCS	1	JPY	140700	TRUE	1.438888889	0.022	3	17	5.497222222